CHARACTERIZATION OF BILE SALT AGGREGATES USING SINGLET AND TRIPLET EXCITED PROBE MOLECULES

by

Changqing Ju
B.Sc., Peking University, Beijing, China, 1991

A Thesis Submitted in Partial Fulfillment of the
Requirements for the Degree of

MASTER OF SCIENCE

in the Department of Chemistry

We accept this thesis as conforming
to the required standard

[redacted]
Dr. C. Bohne, Supervisor (Department of Chemistry)

[redacted]
Dr. T. M. Fyles, Departmental Member (Department of Chemistry)

[redacted]
Dr. C. Qian, Departmental Member (Department of Chemistry)

[redacted]
Dr. M. J. Ashwood-Smith, Outside Member (Department of Biology)

[redacted]
Dr. B. J. Hawkins , External Examiner (Department of Biology)

University of Victoria

Supervisor: Dr. C. Bohne

Abstract

Bile salt aggregation was studied by employing photophysical techniques to better understand the mechanism for the aggregates formation.

Fluorescence of excited singlet probe molecules was used to investigate the location sites of the probes in the sodium cholate aggregates. Naphthalene, anthracene and pyrene were employed as the probes. Both steady-state and time-resolved quenching studies were performed to investigate the extent of protection of the incorporated probes in bile salt aggregates from aqueous quencher. The quenching rate constants of the probes in sodium cholate aggregates were ca. 20-50 times smaller than in water. The highest protection was observed for the smallest molecule, naphthalene, followed by pyrene and anthracene. The pattern of bile salt aggregation and the number of bile salt molecules necessary to solubilize each probe was suggested to be dependent on the size and the shape of the probe molecules.

Excited triplet probe molecules were employed to establish the dynamics of association and dissociation of the probes in bile salt aggregates. The entry/exit dynamics was studied by following the quenching of the excited triplet naphthalene and xanthone by nitrite or cupric ions. Excited triplet xanthone was quenched much faster in bile salt aggregates than excited triplet naphthalene. In addition, the association and dissociation rate constants of xanthone in sodium cholate aggregates were greater than naphthalene. This work established that dynamics of excited triplet probe molecules can be studied in bile salt aggregates and that the location of the probe incorporated in sodium cholate aggregates can be different.

Examiners:

_____

_____

istry)

_____

ry)

_____

Biology)

_____

gy)

Acknowledgments

I would like to express my sincere thanks to my supervisor, Dr. Cornelia Bohne for her enthusiastic and encouraging guidance throughout this work.

I would also like to take this chance to thank my colleagues in the group Luis Netter, Yuan Liao, Mark Kleinman, as well as Scott Murphy, Victor Tuomi and Alex Adronov.

Special thanks are due to Dr. Tom Fyles and Dr. Peter Wan for their helpful advice.

Table of Contents

List of Figures

List of Tables

List of Schemes

1. Introduction

1.1. Photophysics

1.1.1. Jablonski Diagram

The absorption of electromagnetic radiation results in the excitation of a molecule from a lower to a higher molecular quantum state. The electronically excited molecule may undergo a number of different possible physical de-excitation pathways and return to the ground state. The Jablonski diagram,[1] is a simplified energy level diagram, which summarizes various pathways available for excitation and de-excitation of a molecule (Figure 1.1).

The de-excitation pathways are classified into two categories: (1) radiative processes, which involve the emission of electromagnetic radiation by the excited molecule as it returns to lower energy states, and (2) nonradiative processes, in which the populations in the initially excited quantum states are transferred into other states without any accompanying emission.

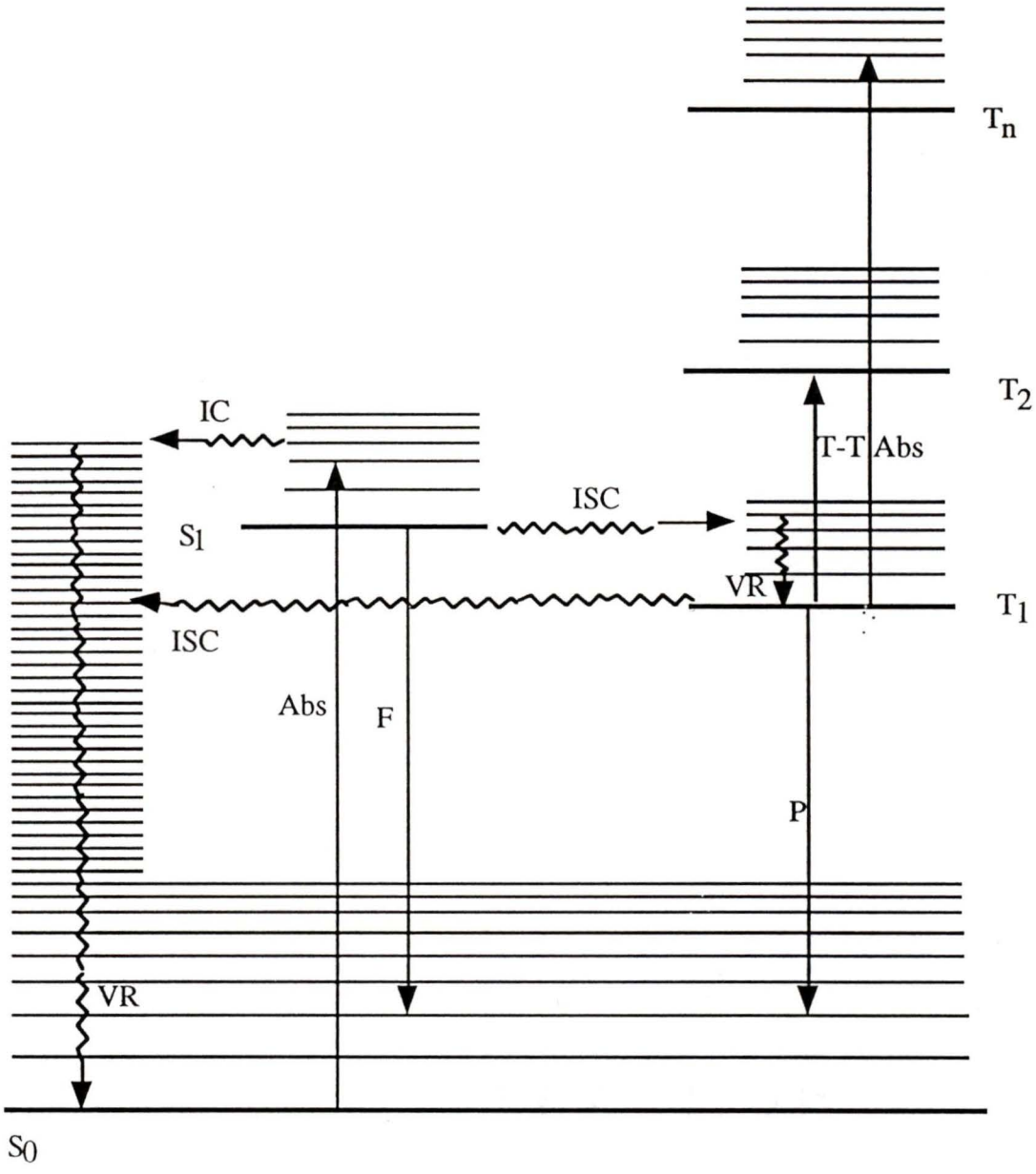

Figure 1.1: Jablonski energy-level diagram. IC, ISC and VR represent internal conversion, intersystem crossing and vibrational relaxation, respectively; Abs, F, P and T-T Abs represent absorption, fluorescence, phosphorescence and triplet-triplet absorption, respectively.

Nonradiative processes include internal conversion (IC), intersystem crossing (ISC) and vibrational relaxation (VR). IC refers to the nonradiative transition between electronic states of same spin multiplicity, e.g. $S_1 \rightarrow S_0$, and $S_2 \rightarrow S_1$. ISC is the nonradiative transition between electronic states with different spin multiplicities, e.g. $S_1 \rightarrow T_1$ and $T_1 \rightarrow S_0$. It is typically a forbidden process. VR is the transition between vibrational levels in the same electronic state. In solution phase, excess vibrational energy is rapidly ($<10^{-12}$ sec) removed by collisions with solvent molecules.

Fluorescence and phosphorescence are radiative processes of de-excitation. Fluorescence is the radiative emission between electronic states with the same spin multiplicity. The most common fluorescence emission involves the transition from the first excited singlet state (S_1) to the ground state (S_0), i.e. $S_1 \rightarrow S_0$ transition. Phosphorescence is the emission from an excited state to a lower electronic state with different spin multiplicities. $T_1 \rightarrow S_0 + h\upsilon$ is usually the most common form of phosphorescence. When the molecule in the low-lying triplet state (T_1) absorbs a second photon, excitation to higher triplet states occurs. This process is called triplet-triplet absorption, and it is the basis for the laser flash photolysis technique used in this study (vide infra).

Fluorescence does not involve a change of spin multiplicity. It is a quantum mechanically "allowed" transition and thus it occurs on relatively fast time scales. Typical time scales lie in the picosecond (10^{-12} s) to microsecond (10^{-6} s) range.[2] The fluorescence lifetime of a molecule can be defined in terms of the rate of depopulation of the first excited singlet state (i.e. $S_1 \rightarrow S_0$):[3]

$$\frac{d[^1M^*]}{dt} = -\frac{[^1M^*]}{\tau_0} \qquad (1\text{-}1)$$

where τ_0 is the molecular fluorescence lifetime. Upon integration, Eq 1-1 gives a fluorescence decay function of the form:

$$[^1M^*] = [^1M^*]_0 \, e^{-\frac{t}{\tau_0}} \qquad (1\text{-}2)$$

where $[^1M^*]$ and $[^1M^*]_0$ represent the excited state concentration at time t and t=0, respectively. From Eq 1-2, one can readily deduce that τ_0 is the time required for the concentration of the excited state to fall to 1/e (0.368) of the initial value.

The fluorescence lifetime of $^1M^*$ is given by:

$$\tau_0 = \frac{1}{k_r + k_{nr}} \qquad (1\text{-}3)$$

where k_r is the fluorescence rate constant, and k_{nr} is the sum of the rate constants of all nonradiative processes that depopulate the excited siglet state (Figure 1.1). Furthermore, the fluorescence quantum yield (Φ_{fluo}), which corresponds to the ratio of the number of photons emitted to the number absorbed, is equal to the fraction of fluorophores which decay through emission and is given by:

$$\Phi_{fluo} = \frac{k_r}{k_r + k_{nr}} = k_r \tau_0 \qquad (1\text{-}4)$$

1.1.2. Measurement of fluorescence

The fluorescence emission spectrum is the distribution of emission intensities as a function of wavelength. The emission spectrum is obtained by keeping the excitation wavelength constant and scanning the emission at various wavelengths. Fluorescence measurements involve the direct detection of photons emitted from excited molecules. For this reason, the measurement of fluorescence is a much more sensitive technique for the detection of molecular species than absorption spectrophotometry.

Fluorescence spectra are measured with a fluorescence spectrometer. The essential components are shown in Figure 1.2.

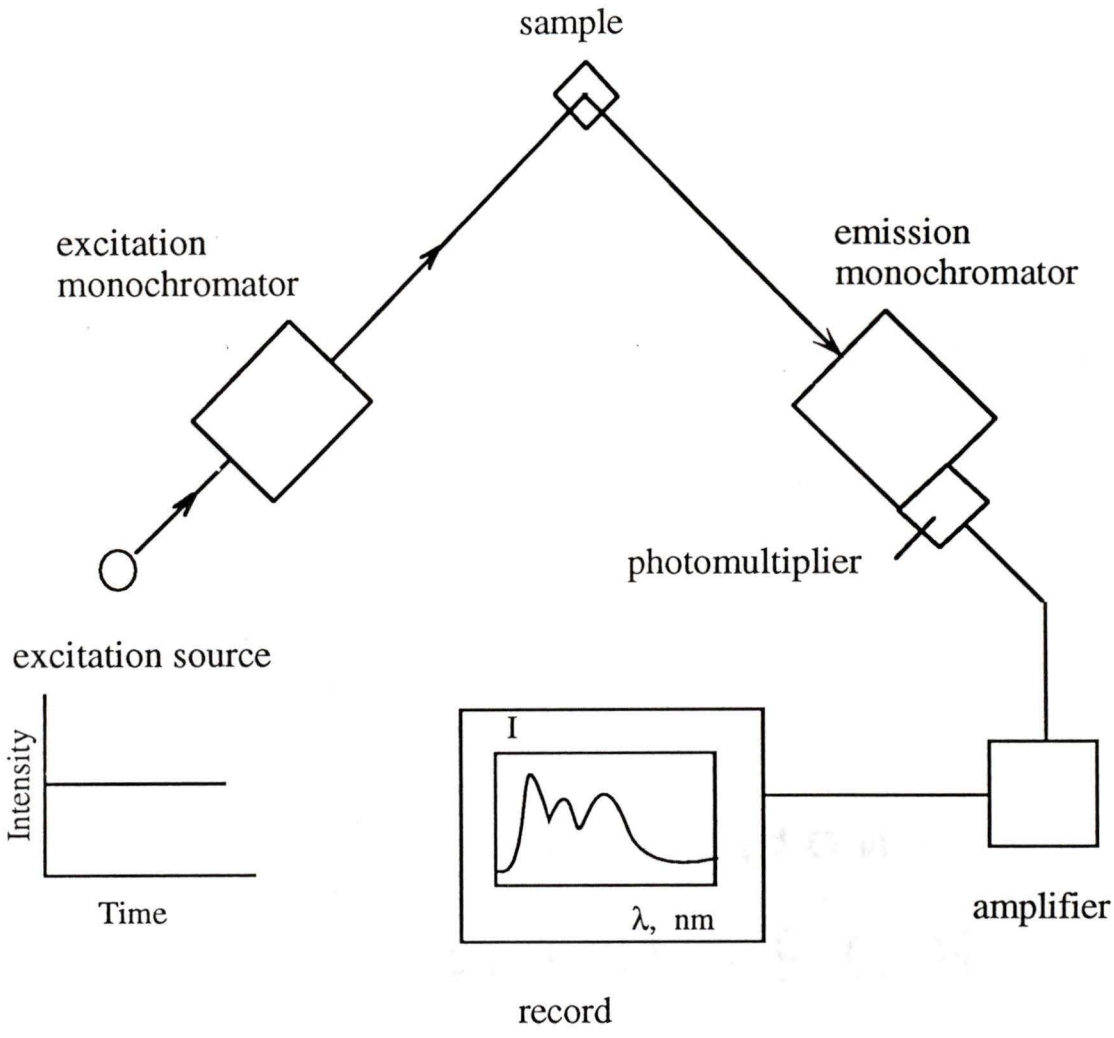

Figure 1.2: Simplified layout of a fluorescence spectrometer.

In a typical spectrofluorimeter the excitation source is a Xenon arc lamp which is a continuous source and gives constant intensity during the measurement. The fluorescence emission is detected at right angles to the incident excitation light in order to minimize the interference from scattered light.

The intensity of the absorbed light is given by the Beer-Lambert law:

$$I_{abs} = I_0 (1 - 10^{-\varepsilon lc}) \qquad (1\text{-}5)$$

where I_{abs} and I_0 are the intensities of absorbed and incident light, ε is the molar absorption coefficient ($M^{-1}cm^{-1}$), l is the pathlength (cm) and c is the molar concentration.

The fluorescence intensity I_{fluo} is given by:

$$I_{fluo} = I_{abs} \Phi_{fluo} \qquad (1\text{-}6)$$

Combining Eq 1-5 and Eq 1-6, the expression of I_{fluo} obtained is:

$$I_{fluo} = I_0 \Phi_{fluo} (1 - 10^{\varepsilon lc}) \qquad (1\text{-}7)$$

If $\varepsilon lc \leq 0.05$, Eq 1-7 can be simplified to:

$$I_{fluo} = 2.303\ I_0 \Phi_{fluo} \varepsilon lc \qquad (1\text{-}8)$$

According to Eq 1-8, the fluorescence intensity is proportional to the molar concentration of the solute. However, systematic errors are introduced by using this equation. In order to limit the measurement error to within 5%, the concentration of the solute should be kept low enough to meet $\varepsilon lc \leq 0.05$.

1.1.3. Time-correlated single photon counting

Time-correlated single photon counting (SPC) is a technique in which the fluorescence is measured as a function of time.[2-4] The combined features of high sensitivity and well-defined counting statistics make SPC the most widely used technique for the measurement of fluorescence decays.

Figure 1.3 is an illustration of a typical single photon counting apparatus. A pulsed light source, usually from a short pulsed flash lamp, generates multiphoton excitation pulses which excite the sample and cause the sample to emit light. The system contains two light detectors, which are photomultipliers (PMTs). The START PMT (Figure 1.3) is attached to the back of the housing which contains the lamp, and a signal is produced when it detects a pulse of light from the lamp. This signal triggers a time-to-amplitude converter (TAC in Figure 1.3). The TAC initiates a voltage ramp which increases steadily from zero. Emission from the sample is detected at right angles to the excitation light path by an extremely sensitive detector (STOP PMT in Figure 1.3). The STOP PMT is capable of responding to the detection of single photons, and it produces a signal and sends to the TAC which halts any further increase in the voltage ramp (Figure 1.4). Hence, the time difference between excitation of the sample and detection of an emitted photon is converted into a voltage. If no photon arrives before the voltage ramp has increased to its maximum value, the electronics are reset and the cycle begins again. The nature of the TAC operation is such as to only register the first "stop" pulse detected after a "start" pulse.

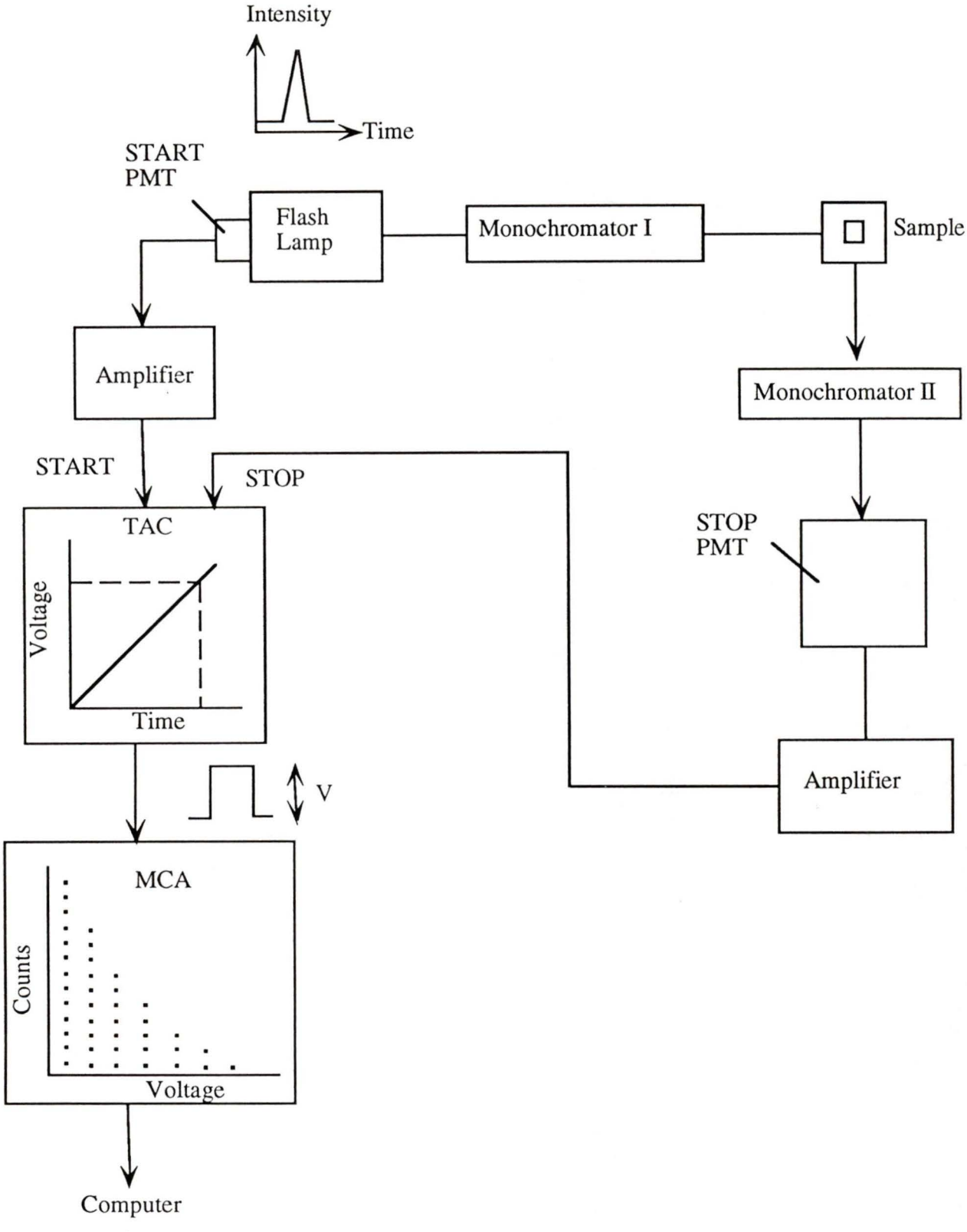

Figure 1.3: Simplified diagram of a time-correlated single-photon counting system.

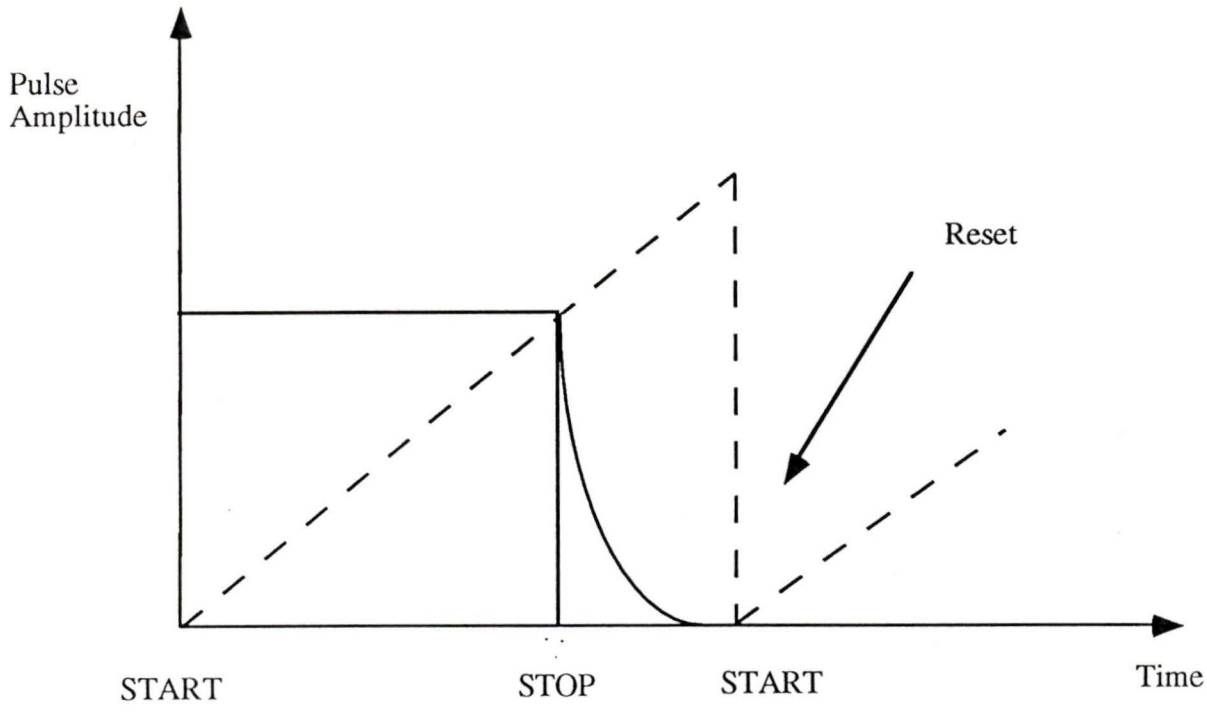

Figure 1.4: Voltage ramp generation by TAC.

The TAC is connected to a multichanal analyzer (MCA) which breaks the voltage range into a sequence of 500 channels. The MCA is calibrated and each of the channels corresponds to a certain time interval. Repeating the lamp flashes many times will ultimately lead to the detection of the fluorescence decay profile. In this work, 10,000 counts were accumulated in the channel with maximum counts since this number was considered to be sufficient for the data to be statistically meaningful.[5]

SPC traces are normally recorded using semilogarithmic graphics. The most versatile and commonly used analysis of the decay profiles is that of least squares fitting using an iterative reconvolution process. A variety of statistical tests exist for the examination of the compatibility between experimental and simulated decay profiles. The commonly used statistical tests for the fitting quality include the chi squared value (χ^2), plots of calculated residue and the auto correlation function, the Durbin-Watson parameter (DW), and the Z-test.[5,6] The criteria for a good fit are: (a) Chi squared. Acceptable values are between 0.8 and 1.3 for ideal Poisson distributed data. Low χ^2

values (≤ 0.75) mean that the data set is not sufficient for a meaningful fit, while high values (> 1.5) indicate significant deviation from the equation to which the data were fitted. (b) Residuals. Good fits should yield randomly distributed residuals centered about zero. (c) Autocorrelation. Random distribution around the zero point is desired. (d) Durbin-Watson parameter. This parameter is used to judge the fitting quality for multilinear models. For decays, DW values higher than 1.7, 1.75 and 1.8 indicate acceptable quality of fits (256 or 512 data channels) for single, double or triple exponential models, respectively. Lower DW values are symptoms of an incorrect fitting function or skewed data.[6] (e) Z-test. The residuals are generally considered to be random for $|Z| < 3$. When the Z value is within the [-2,2] interval there is a 95.44% probability that the residuals to the fit are random.[7]

1.1.4. Laser Flash Photolysis

LASER is an acronym for Light Amplification by the Stimulated Emission of Radiation.

According to the Boltzmann equation (Eq 1-7), under normal conditions, the distribution of the populations of atoms or molecules among their various energy states will be favored towards the ground state.

$$\frac{N_n}{N_m} = e^{-\Delta E_{nm}/kT} \qquad (1\text{-}9)$$

N_n and N_m are the population at the E_n and E_m states, ΔE_{nm} is the energy gap between these states and k is the Boltzmann constant.

Moderate excitation will give rise to an increase in the population of the excited state which will normally relax back to the original distribution through a combination of radiative and nonradiative de-excitation pathways. However, it is possible to provide a sample with a source of sufficiently intense excitation such that a significant proportion

of the molecules present are excited, thus a population inversion can be achieved. Under these circumstances, the interaction of a photon with an excited molecule can readily happen and stimulated emission becomes possible, releasing more photons which can trigger further stimulated emission. Figure 1.5 illustrates schematically the stimulated emission process.

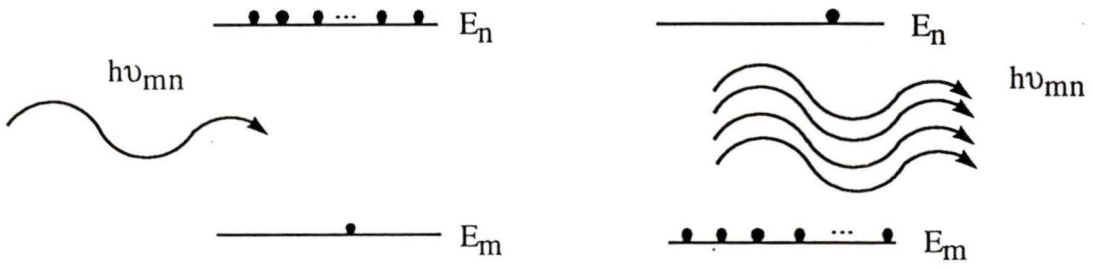

Figure 1.5: Energy level diagram showing the stimulated emission which builds up inside a laser.

A Nd:YAG laser was used in this work as the excitation source. The active medum is neodymium incorporated into a crystalline yttrium aluminum garnet (YAG) host. The Nd:YAG laser is a four-level laser. The main absorptions at 730 and 800 nm are usually pumped by a flashlamp. The laser transition is at 1064 nm. For electronic excitation, the 1064 nm laser is usually frequency doubled, tripled, or quadrupled to 532, 355, or 266 nm, respectively.

Laser flash photolysis is a technique developed in the late 1960s,[8,9] It provides a method to determine directly the absorption and kinetics of an excited state which has been generated by a short pulse of intense radiation of a laser. The short-lived intermediates in laser flash photolysis can be characterized through investigation of their primary photochemical or photophysical processes. The important components for a typical laser flash photolysis apparatus include the excitation source (laser), monitoring

source (lamp), sample cell, optical quality lenses and filters, detector, and analysis/output devices (digitizer/computer). A detailed description of the equipment used will be provided in Chapter 2 and a schematics diagram of the laser flash photolysis equipment is shown in Figure 2.1.

1.1.5. Quenching mechanisms

Quenching is the acceleration of the deactivation process of an excited state by a quencher.[10,11] Quenching reactions are easy to perform and can be applied to almost any system that has an intrinsic or extrinsic fluorescence or phosphorescence probe. The quenching reaction can be used to probe topographical features of a macromolecular assembly and to sense any structural changes that may be caused by varying conditions. The most common case is bimolecular deactivation of an excited-state by a quencher molecule. Quenching reactions can proceed by different mechanisms, such as energy transfer, charge transfer or electron transfer. These reactions can occur after the collision between the excited state and the quencher, at long-ranges when no contact between the reaction partners occurs,[12-14] or within complexes between the molecule and the quencher formed prior to the excitation process.

In general, there are two quenching mechanisms of an excited state probe to be considered: dynamic quenching and static quenching. Scheme 1.1 describes dynamic quenching.

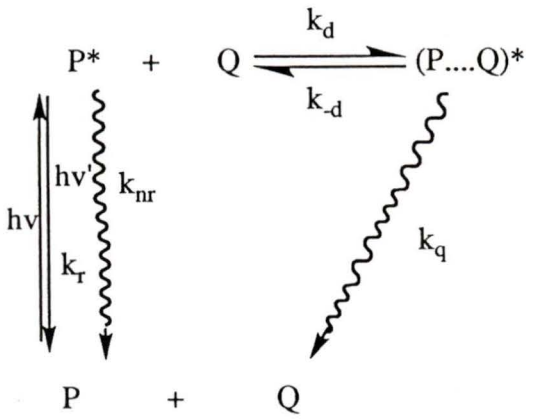

Scheme 1.1: Mechanism for dynamic quenching.

Here P is a probe molecule, which after being excited to the excited state (P*), can than emit a photon with rate constant k_r. The excited state P* may also return to the ground state by other nonradiative mechanisms, at a rate constant k_{nr}. In the presence of the solute quencher Q, the excited probe may collide with Q, at the diffusional rate constant k_d, to form an excited-state encounter complex, (P····Q)*. The complex will then undergo a quenching reaction with rate constant k_q. This quenching can be described by the Stern-Volmer equation:[10]

$$\frac{\tau_0}{\tau} = \frac{I_0}{I} = 1 + k_q \tau_0 [Q] = 1 + K_{SV}[Q] \qquad (1\text{-}10)$$

Where τ_0 and τ are lifetimes, I_0 and I are fluorescence intensities in the absence and presence of the quencher, respectively. The quenching rate constant is k_q and K_{SV} is the Stern-Volmer constant. If quenching occurs only by a dynamic mechanism, then the ratio τ_0/τ will be equal to the ratio of I_0/I.

The other quenching mechanism, static quenching, results from the formation of a ground state complex, (P····Q), (Scheme 1.2). Such a complex may also absorb a photon to form the excited-state encounter complex, (P····Q)*. The excited-state complex rapidly relaxes to ground state through nonradiative processes.

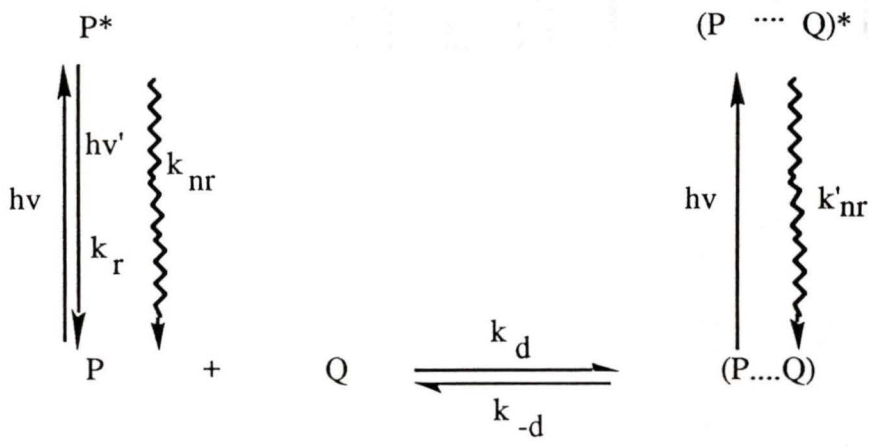

Scheme 1.2: Mechanism for static quenching.

In a static quenching mechanism, the concentration of the free probe molecule (P) is decreased by forming the ground-state complex with the quencher, and in turn, the fluorescence intensity is decreased. On the other hand, the fluorescence lifetime of the probe remains constant because only fluorescence coming from uncomplexed excited probe molecules is monitored. The quenching can be described by the following equations:[10]

$$\frac{I_0}{I} = 1 + K_{eq}[Q] \qquad (1\text{-}11)$$

$$\frac{\tau_0}{\tau} = 1 \qquad (1\text{-}12)$$

Where K_{eq} is the equilibrium constant of the ground-state complex.

In some cases when both static and dynamic quenching are involved, the total degree of quenching is thus a product of dynamic ($1+K_{SV}[Q]$) and static ($1+K_{eq}[Q]$) terms (Eq 1-11).[10]

$$\frac{I_0}{I} = (1 + K_{eq}[Q])(1 + K_{SV}[Q]) \qquad (1\text{-}13)$$

If the concentration of the quencher is low, Eq 1-13 can be simplified to Eq 1-14.

$$\frac{I_0}{I} = 1 + \left(K_{eq} + K_{SV} \right)[Q] \qquad (1\text{-}14)$$

1.2. Bile salts

Amphiphatic bile salts are the main products of cholesterol metabolism. Their structures determine their biological and physicochemical properties. In water, bile salts associate to form aggregates. The behavior of bile salt aggregates is quite different from micelles formed by conventional detergents. Bile salt aggregates are smaller, more rigid and of different structure than detergent micelles.[15] The main biological function of bile salt aggregates is to solubilize dietary lipids and thus greatly accelerate their absorption. The efficient performance of this function is facilitated by the concentrating effect of the gallbladder upon the bile secreted by the liver, the solubility of the bile salts under conditions prevailing in the small intestine, and their ability to form mixed aggregates to solubilized fatty acids and monoglycerides.[16] These mixed micelles incorporate appreciable amounts of insoluble molecules, such as fat-soluble vitamins and cholesterol, and thus solubilize them in such fluids as bile and intestinal lumenal content.[15]

1.2.1. Formation of bile acids

Bile salts are steroids and are formed by enzymatic modifications of cholesterol in the liver. Cholesterol is a 3β-monohydroxy C_{27} sterol with a steroid nucleus containing nineteen carbon atoms and a branched side chain containing eight carbon atoms. The molecule is completely saturated, except for a double bond at $C_{5\text{-}6}$, which makes the molecule nearly planar.[16] Formation of bile acids from cholesterol involves three major structural changes: (1) saturation of the double bond [bile acids are usually formed as 5β hydrogen(A/B cis)] and (2) epimerization of the hydroxyl group at C_3 from β to α configuration as well as (3) the addition of hydroxyl groups at the 7 and/or 12 positions

on the nucleus, and the side chain undergoes oxidative cleavage to form a carboxyl group at C_{24}. The structural changes in the biotransformation of cholesterol to bile acids are summarized in Figure 1.6.

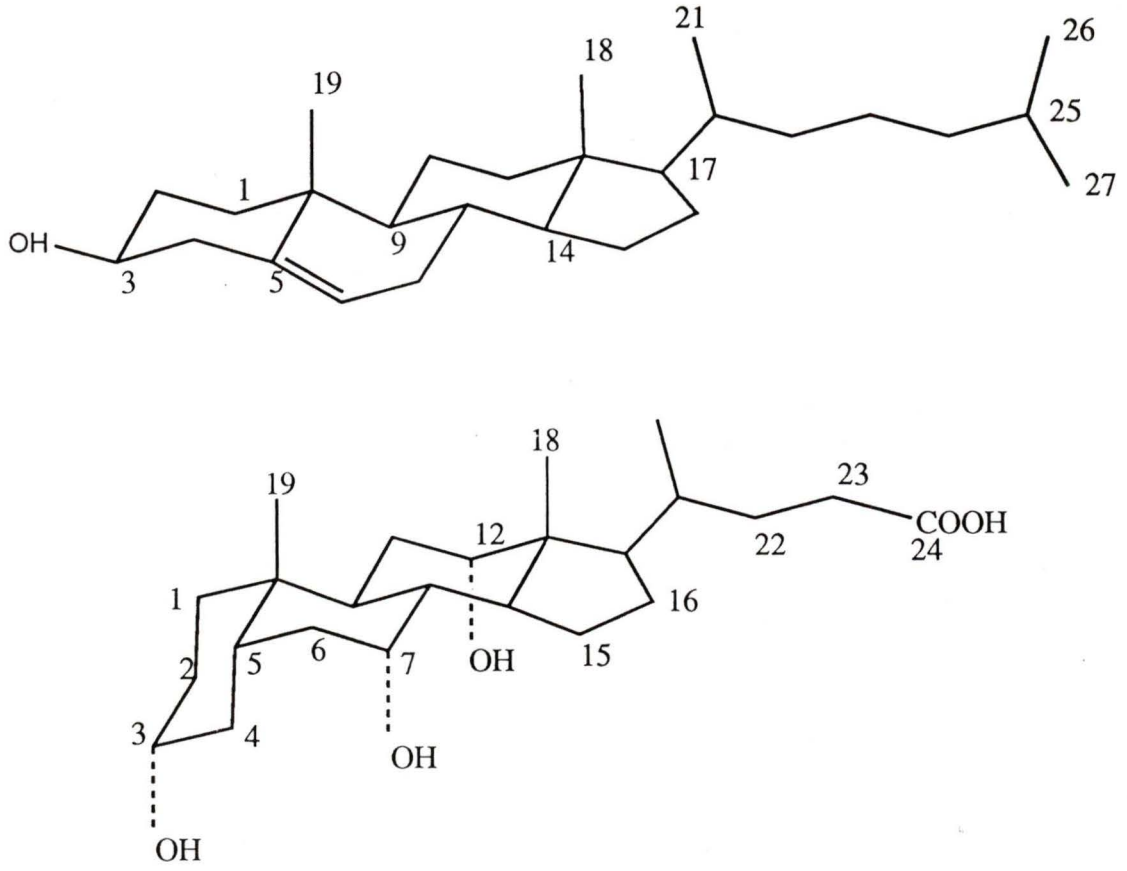

Figure 1.6: Structural changes of cholesterol (above) to bile acid (below).

1.2.2. Biological Significance of Bile Salt Aggregates

The solubilization of dietary lipids in the intestinal lumen requires a large quantity of bile acids, which is maintained by the enterohepatic recirculation of a small pool of endogenous bile acids. The physiology of the enterohepatic circulation is indicated schematically in Figure 1.7.

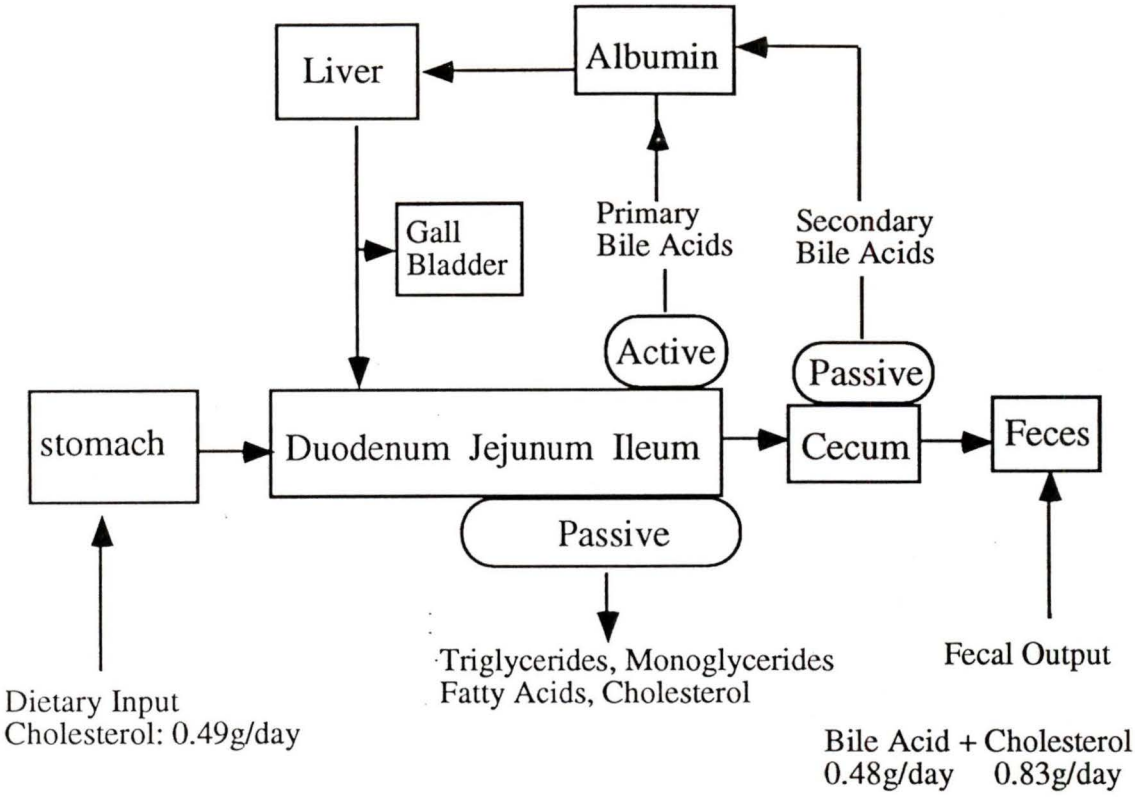

Figure 1.7: Physiology of the enterohepatic circulation of bile salts (Adapted from reference17).

The primary bile acids, cholic and chenodeoxycholic acids are synthesized from cholesterol in the liver. Prior to hepatic secretion, the primary bile acids are conjugated through an amide linkage with taurine or glycine in an approximate ratio of 1:3.[17] The conjugated bile acids are then secreted in bile and stored in the gallbladder. After ingestion of a meal, they are expelled from the gallbladder into the duodenum where they facilitate absorption of dietary lipids in the jejunum and ileum. Subsequently, the bile salts are resorbed, primarily by an active transport system in the terminal ileum, and are returned to the liver via the portal vein. The total pool of bile in humans circulates 6-10 times per day and contains 3-5 g of bile and 0.25 g of cholesterol. The daily loss of bile

acids and cholesterol normally is balanced by the hepatic de novo synthesis of cholesterol and of bile acids from cholesterol.

Elevated concentrations of total cholesterol and low-density lipoprotein cholesterol are major risk factors for coronary heart disease.[17] Lipid lowering agents are used with the purpose of ameliorating hyperlipoproteinemias, in order to prevent arterial disease. Lipid lowering drugs can be classified into systemic and non-systemic agents. The latter act within the gastrointestinal lumen which interrupt the recirculation of bile acids or reduce the absorption of cholesterol. The major non-systemic antihypercholesterolemic agents are anion-exchange resins which bind bile acids in the intestine, thus favoring their fecal excretion. Treatment with this kind of agents, such as cholestyramine or colestipol, increases the normal daily loss of bile acids which leads to a reduction of the body pools of cholesterol.

1.2.3. Structures of bile salts

The most commonly occurring bile salts are cholate (3α, 7α, 12α-trihydroxy-5β-cholan-24-oate), deoxycholate (3α, 12α-dihydroxy-5β-cholan-24-oate) and chenodeoxycholate (3α, 7α-dihydroxy-5β-cholan-24-oate). Their perspective structural formulae are shown in Figure 1.8.

In general, the molecules of a free bile acid are about 20 Å long. The cross section shows that the steroid nucleus is not flat, but nearly circular with a diameter of about 6 to 7 Å. Aside from the perspective structural formula shown in Figure 1.8, other ways of representing the cholate ion are shown in Figure 1.9.

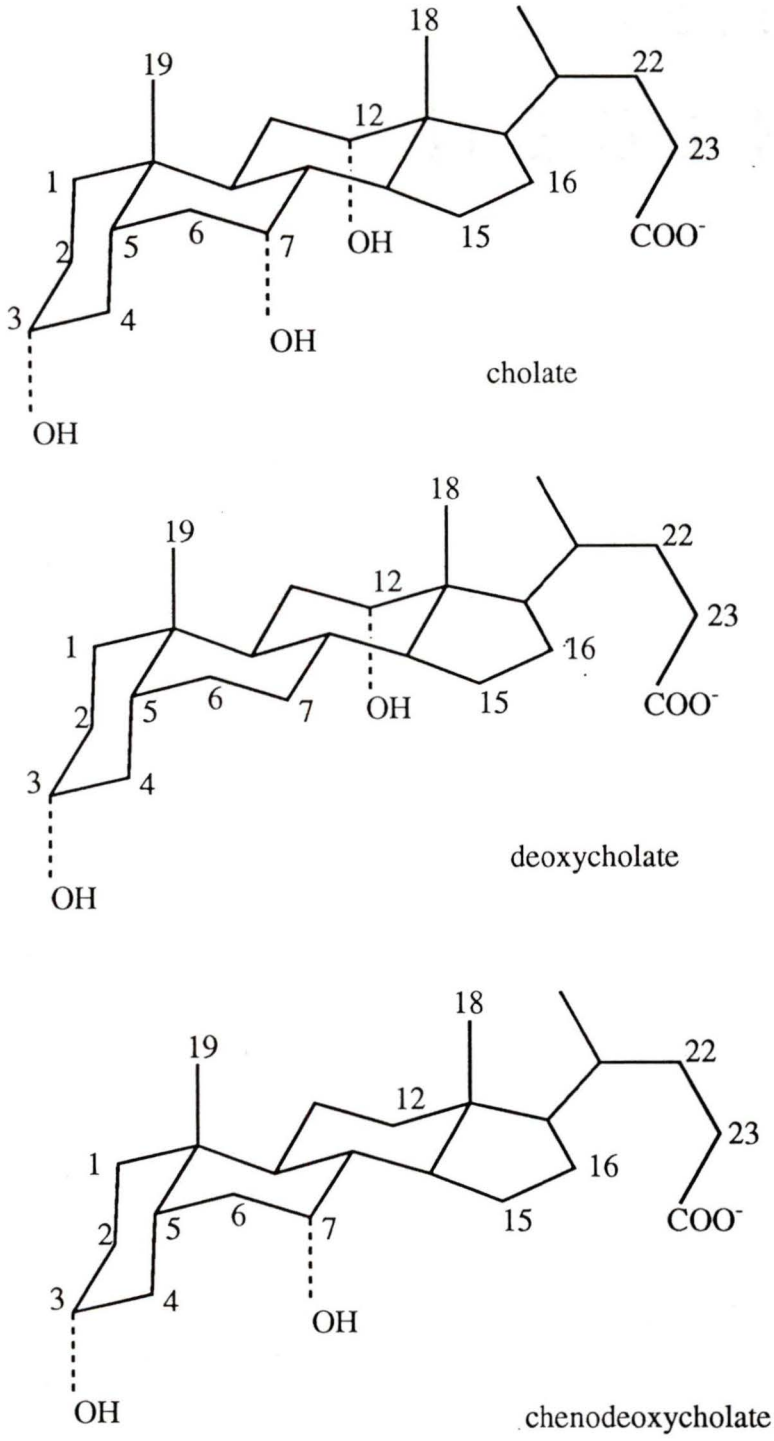

Figure 1.8: Structures of the three most commonly occurring bile salts: cholate, deoxycholate and chenodeoxycholate.

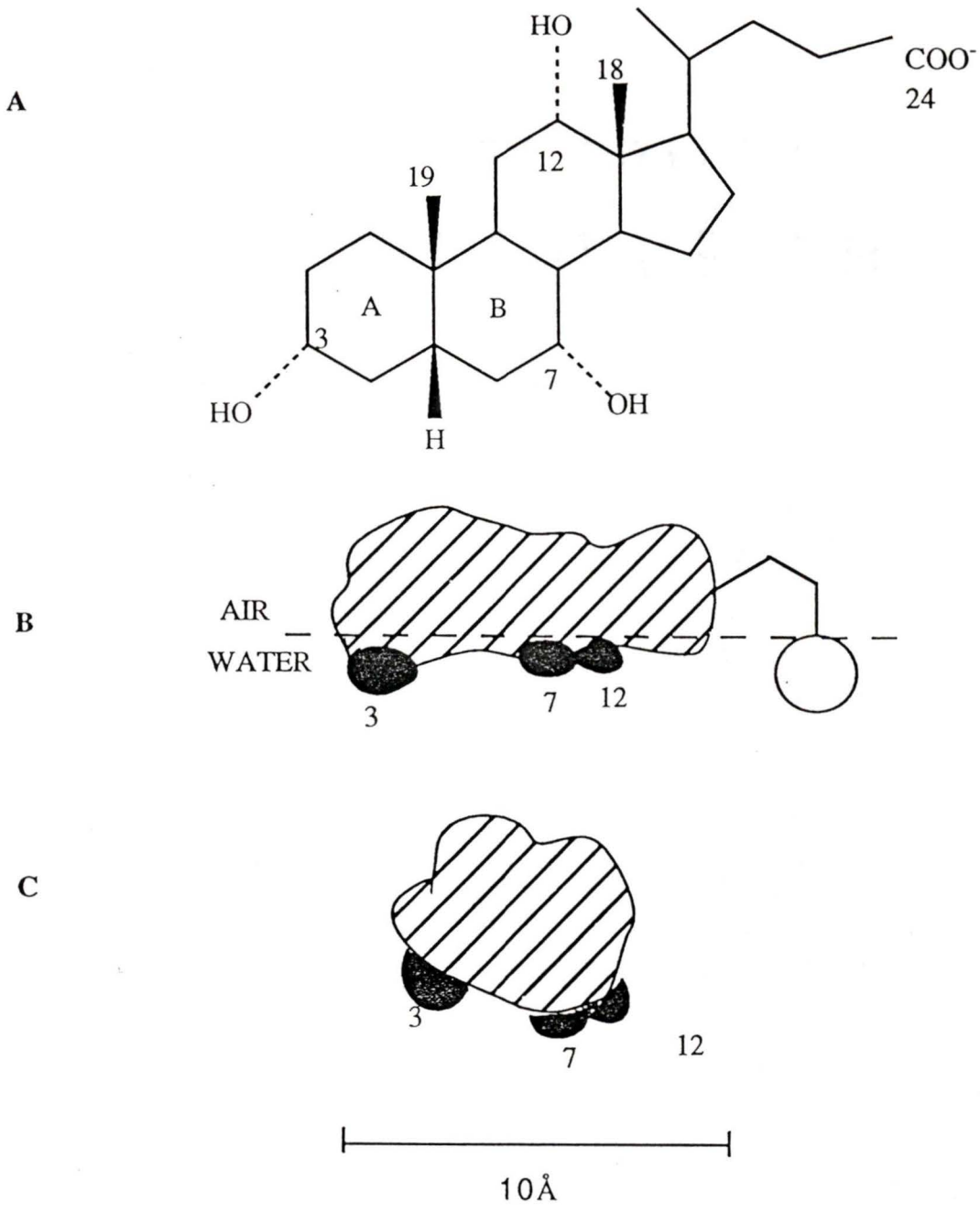

Figure 1.9: A: the conventional chemical representation; B: the longitudinal shorthand representation of the orientation at the air water interface (with the hydrophilic groups being oriented towards the aqueous phase); C: a transverse cross section. (Adapted from reference 18)

The perspective structural formula shows that the three hydroxyl groups of the cholate residue lie beneath the plane of the steroid-skeleton. The connection of the A and B rings is kinked, and the A ring is in the cis conformation with respect to the B ring. This interesting skeletal modification of the bile salt precursor, cholesterol, brings the hydroxyl groups at C_3 and C_7 closer together.[19] Thus, the steroid nucleus of the bile salt molecule exhibits planar polarity, with the hydrophilic groups being situated below the equator of the molecule and most of the steroid-skeleton with its protruding methyl groups lying above it. At one end of the steroid-nucleus a short branched aliphatic chain terminating into a hydrophilic carboxyl group (COO^-) exists. This side chain orients its polar group in the same plane as the hydroxyl groups, providing a major contribution to the polarity of the surface below the equator of the molecule. It is the planar polarity, caused by the particular positioning of the hydrophilic groups in relation to the hydrophobic steroidal nucleus, which gives the bile salts their surface activity and determines their ability to aggregate in water.

After their biosynthesis from cholesterol, bile acids are conjugated with glycine or taurine by peptide linkages in the liver before secretion into bile. The conjugation results in (a) elongation of the side chain; (b) an increase in polarity of the side chain because of the peptide bond; and (c) a lowering of the pK_a;[20] For instance, the pK_a of cholic acid is 6.4 while those of the glycine and the taurine ($NH_2CH_2CH_2SO_3H$) conjugates are 4.4 and 1.4 respectively.[19]

1.2.4. Bile salt aggregation

Bile salts in solution are known to form aggregates. Because the molecular structure of bile salts is very different from that of conventional detergents, bile salts exhibit an unique behavior with respect to self-association and molecular solubilization.[21-24] Contrary to the molecules of classical detergents where the hydrophilic and hydrophobic moieties are clearly separated, bile salt molecules have a

hydrophobic surface on the convex side of the steroid nucleus and a hydrophilic surface on the concave side of this nucleus.[18] The mechanism of bile salt aggregation is considerably more complex than that for conventional micelles. Conventional micelles are formed spontanously from monomers as soon as the critical micelle concentration (CMC) is reached. In the case of bile salt, stepwise association appears to take place over an extensive concentration range. At low bile salt concentrations, small aggregates , i.e. dimer, trimers are formed. These small aggregates eventually form primary aggregates. At higher bile salt concentrations the primary aggregates aggregate and form secondary aggregates (Figure 1.10). The term critical micelle concentration (CMC) for conventional micelles cannot be used rigorously on bile salt aggregates. "CMC" will be used to describe the critical aggregation range of bile salt aggregates. According to Small and co-workers,[25,26] the primary aggregates are stabilized through hydrophobic interactions, whereas the formation of secondary aggregates involves hydrogen bonding between the hydroxyl groups at the primary aggregates surfaces.

The size and structure of bile salt aggregates can be affected by: the type of bile salt with respect to the number and position of the hydroxyl groups, whether the bile salt is free or conjugated, the pH, temperature, and the nature and concentration of counterions.

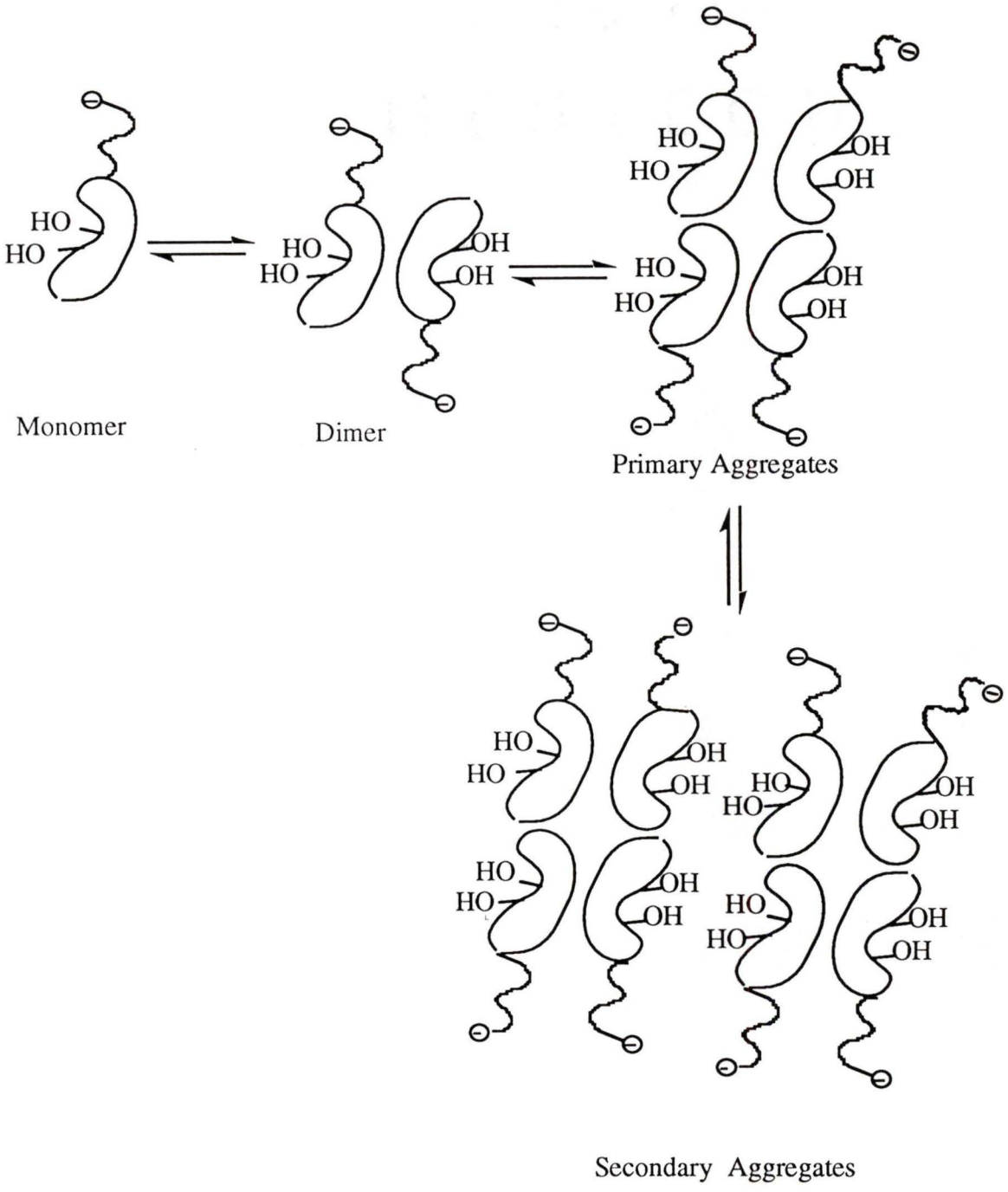

Figure 1.10: Cartoon for a mechanism of bile salt aggregation (Adapted from reference15)

1.2.4.1. Effect of Molecular Structure

Conjugated bile salts have much lower pK_a's than unconjugated bile salts, thus they are resistant to precipitation as protonated acids at the pH of the upper gut (pH = 6.5). As a result, conjugation allows bile salts to form aggregates over a much wider pH range than the free bile salts. The "CMC" of bile salt aggregates is strongly influenced by the number and position of the hydroxyl groups. The trihydroxy bile salts display greater aqueous solubilities and higher "CMC"s than the dihydroxy bile salts.[27] In the dihydroxy series, the chenodeoxycholate salts give slightly higher "CMC"s than the deoxycholate salts.[15] This may be due to the positioning of the C_7 and C_{12} hydroxyl groups.[18] In general, the water solubility of hydroxyl groups is improved when these groups are situated in close proximity in a molecule. As far as deoxycholate and chenodeoxylate are concerned, the 3α, 12α-hydroxyl groups in chenodeoxycholate are slightly further apart than the 3α, 7α-hydroxyl groups in deoxycholate. This may cause the difference in the "CMC" values. When the relative aqueous solubilities of the three hydroxyl groups are compared, the hydroxyl group at the C_3 position appears to be the most important. Artificial dihydroxy bile salts synthesized without a hydroxyl group at the C_3 position but with hydroxyl groups at the C_7 and C_{12} positions are only sparingly soluble in water at ambient temperatures.[20]

1.2.4.2. Effect of pH

In general, there is no influence of pH on the "CMC" if the pH is sufficiently above the pK_a of the bile salt so that virtually all the bile salt molecules are ionized.[20] At a pH near the pK_a, participation of ionized and unionized species in aggregates formation will decrease the "CMC". Variation of pH from 6 to 8 does not significantly influence the aggregation behavior of glycine and taurine conjugated bile salts.[20] However, pH is an important variable when an additive with an ionizable group, e. g., a fatty acid, is present.

1.2.4.3. Effect of Counterion Concentration

The effect of counterion on the "CMC"s and aggregation numbers of bile salt aggregates are mainly mediated by progressive neutralization of the ionic charges. Since the "CMC" is an index of the balance between the opposing forces of hydrophobic interactions and ionic repulsion, reduction of the latter allows aggregate formation to occur at a lower concentration. For trihydroxy bile salts, in the absence and presence of 0.15M sodium cation (Na^+), the "CMC" values are 12 mM and 3-8 mM, respectively. In the case of dihydroxy bile salts, the "CMC" value is 4-6 mM in the absence of counterions, but 2-4 mM in presence of 0.15M Na^+.[20]

1.2.4.4. Effect of Temperature

The effect of temperature on bile salt aggregation is obviously complex. In general, increases of temperature have the following effects: (a) The strength of hydrophobic interactions is increased. (b) The dielectric constant of water is reduced and thereby the ionic repulsion forces at the aggregate's surface are increased. (c) Dehydration of the nonionic polar groups of the bile salt molecules may occur.[15] The "CMC"s of taurocholate and taurodeoxycholate have been studied as a function of temperature (10 to 80 °C) by the spectral shift technique.[27] In general in water and at low counterion concentrations ([NaCl] ≤ 0.15 M), the "CMC" of both taurocholate and taurodeoxycholate falls slightly between 10 and 20 °C, remains at a minimum level between 20 and 30 °C and rises after 40 °C. This phenomenon can be explained by the hydrophobic effect dominating between 10 °C and 20 °C. A balance between the hydrophobic interaction and the ionic repulsion force is reached between 20 and 30 °C; and above this temperature, the repulsive forces predominate.[27]

1.2.4.5. Studies of fluorescence probes in bile salt aggregates

Many studies on determining the "CMC" values of bile salt aggregates have been carried out since Roepke and Mason.[28] Different physicochemical techniques have been used including solubilization of water-insoluble dyes and other large molecules,[29] surface tension measurements,[30] conductivity measurements[31] and light scattering.[30] Although the aggregation behavior of bile salts has been well-studied, considerable controversy still exists over the "CMC" values. Bile salt aggregation is quite different from that of conventional detergents: sharp, well-defined CMC's do not exist, and aggregation occurs over wide concentration ranges.[32] A comprehensive literature survey of the published "CMC" values of bile salts was undertaken by Small in 1971.[18] One can draw a conclusion from the survey that the "CMC" value for a particular bile salt varies, and is dependent upon both the method used for its determination and the experimental conditions employed.

Fluorescence probing technique has been widely used to study aqueous solutions of bile salts.[21-23,33-41] Fluorescence probes such as pyrene, which is nearly insoluble in water, are solubilized by bile salt aggregates. By studying the emission spectrum and the fluorescence decay of the aggregate-solubilized probe, one can obtain information on the nature and size of the aggregates, the fluidity of the aggregate's interior, and also the association mechanism of bile salt aggregates.

Zana et al[21] studied the fluorescence spectra and the fluorescence decay of pyrene solubilized in aqueous micellar solutions of sodium cholate, deoxycholate and taurochenodeoxycholate. The results showed that the micellar environment of the solubilized pyrene was much more apolar in the bile salt aggregates than in classical surfactant micelles. It was suggested that the solubilized pyrene molecule was probably squeezed between the hydrophobic sides of several steroid nuclei of the bile salts which shielded pyrene very effectively against water. The binding sites of polycyclic aromatic

hydrocarbon probes in sodium taurocholate and taurodeoxycholate aggregates were investigated by Meyerhoffer and McGown.[38] The fluorescence intensity ratios of the vibronic bands and fluorescence lifetimes of the probes were measured. The results showed that the bile salts are capable of providing rigid, apolar binding environments to solubilized probes. The microenvironments of the solubilized probes showed a much greater probe-to-probe diversity in taurocholate than in taurodeoxycholate aggregates. This was explained to be due to the smaller size of the taurocholate aggregates, in which the smaller probes were more easily isolated in the well-protected, apolar binding environments than larger probes.

Viscosity measurements have been shown to be useful in investigating the nature of the micellar interior. They give a measure of the rigidity of the environment holding the probe molecules. Chen et al[23] found that the interior viscosity of taurodeoxycholate aggregates was 675 cP by measuring the fluorescence depolarization of 2-methylanthracene. This value was greater than that of either sodium dodecyl sulfate or hexadecyl trimethyl ammonium bromide. Similarly, Fischer and Oakenfull[22] also found that the interior of cholate, deoxycholate and chenodeoxychoalte aggregates were all more rigid than that of the long chain sodium dodecyl sulfate surfactant.

1.3. Photophysical probe molecules used in studying bile salt aggregates

Photophysical probe molecules have been extensively used to characterize microheterogeneous systems.[42] Information about a variety of characteristics, such as polarity, microviscosity, partition coefficients, aggregation parameters, entry/exit dynamics and exchange rate constants, has been obtained. We will only describe the probe molecules that were employed in this work.

The basic idea behind the use of photophysical probes is that certain types of molecules display a selective affinity for a unique site in a supramolecular assembly and the structural and dynamic properties of the host system are reflected in the luminescence

properties of the probe (guest). The majority of photophysical probes that have been examined are organic molecules and there are two types of luminescence with different spectral and decay characteristics: fluorescence which results from the decay of the singlet excited state, and phosphorescence which is associated with the triplet excited state. Fluorescence is comparatively short-lived with lifetimes typically in the range of 10^{-6}-10^{-12} s. Phosphorescence occurs generally at longer time scales, with typical lifetimes between 10^{-6} and 10^{-1} s. Together, the two types of emission span a dynamic range of 10^{11} and allow monitoring of both the static and dynamic properties of the aggregates. On fluorescence time scales, most of the aggregates can be considered as rigid host systems carrying the solubilized probe molecules. Hence fluorescence techniques allow monitoring of static features of the host assemblies and/or related fast kinetic processes. Exit and reentry dynamics of the solutes with the host aggregates may be observed on longer phosphorescence time scales. Since most organic molecules do not phosphoresce, the triplet decay can be followed by triplet-triplet absorption.

1.3.1. Pyrene

Pyrene (Figure 1.11) is a popular fluorescence probe to study the properties of organized systems, such as surfactant micelles[42-44] and phospholipid vesicles.[42]

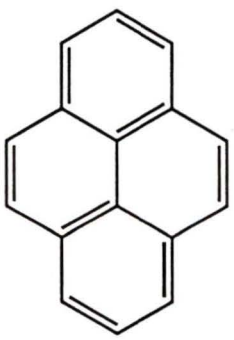

Figure 1.11: Structure of pyrene.

Pyrene has several interesting photophysical properties which make it suitable for use as an effective probe. Excited singlet pyrene has a very long lifetime with a high

fluorescence quantum yield. In non polar solvent, pyrene has a singlet lifetime of 650 ns with fluorescence quantum yield at ca. 0.65.[45] In polar solvent, the singlet lifetime of pyrene is 190 ns and the fluorescence quantum yield is 0.72.[46] An additional important characteristic of pyrene is that the shape of pyrene fluorescence spectrum is extremely sensitive to solvent polarity.

At room temperature, the pyrene fluorescence emission in solution shows five principal vibronic bands (Figure 1.12).

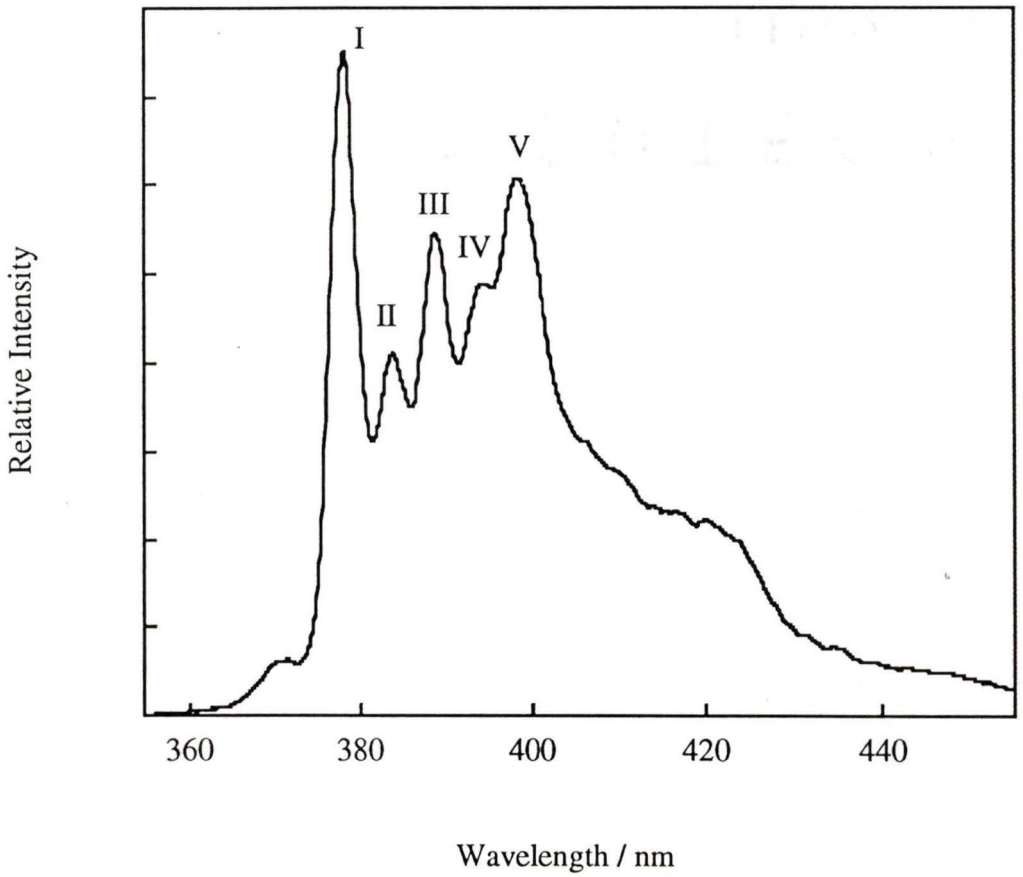

Figure 1.12: Pyrene (5×10^{-7} M) fluorescence emission spectrum in methanol.

The usual numbering of the vibronic bands (I-V) is shown in Figure 1.12. The first band (I) at 372.4 nm shows significant intensity enhancement in polar solvents, while the third band (III) located at 383.0 nm shows minimal variation of its intensity with the change of solvent polarity. Therefore, the ratio of intensities of the two bands, R(I/III), changes with solvent polarity. This "medium effect" on the pyrene fluorescence spectra is explained by the Ham effect.[44,47,48] In aromatic molecules such as benzene or pyrene with a minimum D_{2h} symmetry, the absorption and fluorescence spectra show mixed polarization owing to the vibronic coupling between the first (S_1) and second (S_2) singlet excited states. The transition corresponding to the first band (I) is symmetry forbidden. In polar solvent, band I shows marked intensity enhancement due to the stronger vibronic coupling between S_1 and S_2 singlet excited states.[49]

The strong dependence of the R(I/III) of pyrene emission spectrum makes it possible to use pyrene monomer fluorescence as an "indicator" of solvent polarity.[44,48] Table 1.1 provides some quantitative data on the R(I/III) in various neat solvents and micellar solutions.

Table 1.1: Variation in the R(I/III) of pyrene monomer fluorescence in homogeneous solvents and in aqueous micellar solutions.[44]

Solvent	R(I/III)
Homogeneous Solvents:	
Water	1.84
Acetonitrile	1.75
Ethanol	1.10
Hexane	0.61
Cyclohexane	0.57
Micellar Solutions:	
SDS	1.14
CTAB	1.30
Triton X-100	1.32
CTAC	1.35

The R(I/III) of pyrene fluorescence spectrum has been used as a probe to accurately determine the CMC of various classical micelles. Pyrene fluorescence undergoes significant changes above and below the CMC both in R(I/III) and the lifetime so that one can readily detect the CMC by monitoring either of these properties as a function of the surfactant concentration. The measured CMC values are in very good agreement with those determined by other physical methods. Pyrene was also the most widely used fluorescence probe molecule to characterize bile salt aggregates.[21,23,34,37,41] The results show that the micellar environment of the solubilized pyrene was much more apolar in the bile salt aggregates than in classical surfactant micelles.

1.3.2. Naphthalene

Naphthalene (Figure 1.13) is a small aromatic hydrocarbon.

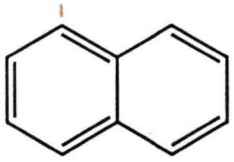

Figure 1.13: Structure of naphthalene.

The fluorescence lifetime of excited singlet naphthalene is ca. 96 ns and the fluorescence quantum yield is 0.19 in nonpolar solvents.[50] The intersystem crossing quantum yield of excited singlet naphthalene is 0.75 and the lifetime of excited triplet naphthalene is ca. 175 μs in nonpolar solvents.[50]

The solubilization of naphthalene was used to investigate the self-association patterns of sodium cholate (NaC).[29] The solubility of naphthalene in aqueous solutions of NaC was determined over the concentration range of 0-0.20 M at 25°C. The data show that the "CMC" for NaC is not well definded by using this probe. A complex pattern of association of NaC including the formation of dimers and one or more higher oligomers was suggested.

1.3.3. Anthracene

Anthracene (Figure 1.14) is a polycyclic aromatic hydrocarbon.

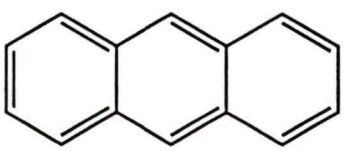

Figure 1.14: Structure of anthracene.

The fluorescence lifetime of excited singlet anthracene is ca. 5.3 ns in nonpolar solvents and 5.8 ns in polar solvents.[50] The fluorescence quantum yields are 0.30 and 0.27 in nonpolar and polar solvents, respectively. The intersystem crossing quantum yield of excited singlet anthracene in non polar and polar solvents are 0.71 and 0.66,

respectively.[50] The lifetimes of excited triplet anthracene in non polar and polar solvents are 670 μs and 3300 μs, respectively.[50]

The dynamics of excited triplet anthracene in sodium taurocholate aggregates (NaTC) was studied using laser photolysis. The exit rate constant of excited triplet anthracene from NaTC aggregates was estimated to be $\leq 3 \times 10^3$ s^{-1}.[23]

1.3.4. Xanthone

Xanthone (Figure 1.15) is a heterocyclic aromatic ketone. It is structurally quite similar to benzophenone, and its triplet energy is almost identical with that of acetophenone (310 kJ/mol).[50]

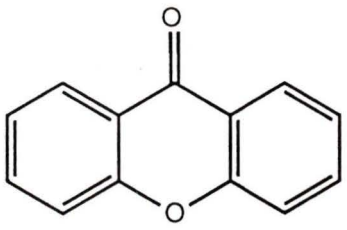

Figure 1.15: Structure of xanthone.

The nature of the low-lying triplet state of xanthone has a strong dependence on the polarity of the media: n,π* character in highly non-polar solvents and π,π* character in moderately polar and polar solvents.[51] The π,π* triplet xanthone has a relatively long lifetime as a result of the low reactivity associated with π,π* triplet state. The triplet-triplet absorption spectra of xanthone are strong and sensitive to the polarity of the media, and a marked red shift of the absorption maximum was observed with decreasing polarity. For example, λ_{max} = 580 nm in water, 602 nm in β-cyclodextrin (β-CD) and 655 nm in carbon tetrachloride.[51,52] All these properties of xanthone makes it an ideal probe to study the association and dissociation processes in organized systems.[52,53]

Xanthone was found to form 1:1 inclusion complexes with cyclodextrins (CD) and the microenvironment sensed in the CD cavity is sufficiently polar for xanthone to retain predominant π,π* character. It was also shown that xanthone triplets relocate from

the CD cavity into the aqueous phase due to the higher dipole moment of triplet state and ground state xanthone.[52,54]

1.4. Project proposal

Bile salt aggregation in aqueous solution has been an active area of research, with primary emphasis on the physiological role of bile salts in lipid solubilization.[18,19] More recently, bile salt media has attracted attention as an alternative to conventional micellar reagents for chemical analysis.[55] Because the molecular structure of bile salts is very different from that of conventional detergents, the bile salts exhibit unique behavior with respect to self-association and molecular solubilization.[21-24]

The primary objective of this work is to obtain a better understanding of bile salt aggregation, such as aggregation behavior at low bile salt concentrations and the correlation between the protection efficiency of the bile salts and the size of included molecules. The three probe molecules employed are naphthalene, anthracene and pyrene. They are all smaller than most polycyclic aromatic hydrocarbons previously used,[36-41] but naphthalene and pyrene are soluble enough in water for photophysical measurements in the absence and at very low bile salt concentrations to be performed.

The dynamics of association and dissociation of probe molecules with surfactant micelles has been widely studied for synthetic detergents.[56-58] However, dynamic studies on bile salt aggregate are very scarce. The second objective of this work is to determine the dynamics of association and dissociation of excited probe molecules in bile salt aggregates. The incorporation of excited triplet naphthalene and xanthone were investigated by quenching studies using nitrite and cupric ions.

2. Experimental

2.1. Materials

The bile salts used were obtained from Aldrich. Sodium deoxycholate (NaDC, 98%) and sodium taurocholate (NaTC, 97%) were used as received. Sodium cholate (NaC, 98%) was recrystallized twice from a methanol-ethyl acetate mixture for experiments involving fluorescence quenching studies. Melting point measurements (198-199°C) did not adequately detect the fluorescence impurity. The purity of the recrystallized NaC was check by single photon counting. A very weak emission with a fast decay lifetime which was dur to the impurities still persisted. The pre-exponential factor for this fast decay was less than 5% of the total amplitude.

Pyrene (Py) was purchased from Aldrich (99%, recrystallized at least twice from 95% ethanol).[59] The pyrene fluorescence decay in deaerated water was monoexponential ($\tau \geq 190$ ns). Xanthone obtained from Aldrich (97%) was recrystallized at least twice from 95% ethanol. The purity was checked by gas chromatography and no impurities were observed.[60] Naphthalene (Np, 99+% Aldrich), anthracene (Anc, 99+% Aldrich), sodium iodide (NaI, 98% Aldrich), sodium nitrite ($NaNO_2$, 97+% Aldrich), sodium chloride (NaCl, BDH), cupric sulphate ($CuSO_4 \cdot 5H_2O$, 98% BDH), methanol (MeOH, 99.9% Aldrich) ethanol (EtOH, 95% BDH) and acetonitrile (ACN, 99.9% Aldrich) were used as received. The water used was deionized and was free of organic impurities. Distilled water was first passed through a SYBRON Barnstead system for deionization and was further irradiated with UV light for ca. 0.5 hour. All glassware was soaked in acid bath overnight and rinsed with methanol (99.9%) before using in sample preparation.

2.2. Sample preparation

2.2.1. Samples of Pyrene/bile salt aggregates for fluorescence and singlet quenching studies

The aqueous solution of pyrene (≤ 0.5 μM) was prepared by injecting a pyrene methanolic stock solution (3-4 mM) into water containing 0.2 M NaCl. Pyrene in bile salt samples were prepared by adding the appropriate amount of bile salts to the pyrene aqueous solution.

2.2.2. Samples of Naphthalene/bile salt aggregates for fluorescence studies

The aqueous solution of naphthalene and solutions containing naphthalene (≤ 10 μM) and various bile salt concentrations were prepared as described above for the samples of Pyrene/bile salt aggregates. The concentration of naphthalene methanolic stock solution was ≈ 20 mM.

2.2.3. Anthracene/bile salt aggregates for fluorescence studies

The aqueous solutions of anthracene containing various bile salt concentrations were prepared by injecting a anthracene methanolic stock solution (≈ 3 mM) into water containing 0.2 M NaCl with appropriate amount of bile salts (≥ 20 mM). Anthracene was not soluble enough for fluorescence measurements in water. For this reason, anthracene in ethanol / water (45 / 55, v / v) was used as homogeneous solution to compare the quenching behavior of anthracene to that in bile salt aggregates.

2.2.4. Samples of xanthone/bile salt aggregates for triplet quenching studies

A saturated aqueous solution of xanthone was prepared by stirring an excess of solid xanthone in organic pure water for over 4 hours, followed by filtration of the remaining solid ([xanthone] $\approx 2.0\times10^{-5}$ M).[60] Xanthone in bile salt aggregates was

prepared by adding the appropriately weighed amount of bile salts to the xanthone aqueous solution containing 0.2M NaCl.

2.2.5. Samples of Naphthalene/bile salt aggregates for triplet quenching studies

Solutions containing naphthalene (≈ 100 μM) and different bile salts were prepared as described above for Np/bile salt aggregate systems for fluorescence studies.

2.3. Fluorescence measurements

Steady-state fluorescence. Steady-state fluorescence studies were completed using a Perkin Elmer MPF 66 fluorescence spectrometer. A standard cell containing a pyrene/cyclohexane solution was used to correct for drifting in the excitation light intensity. The temperature in the sample chamber was maintained at 20.0 ± 0.1 °C with a Haake F 3 circulating bath. The excitation and emission slits were set at 2.0 nm for pyrene samples and 5.0 nm for naphthalene and anthracene samples. When necessary, the fluorescence emission intensity was decreased by attenuating the excitation beam with neutral density filters. The excitation wavelengths were set at 336 nm, 290 nm and 317 nm for pyrene, naphthalene and anthracene, respectively. All samples were contained in 10 mm × 10 mm quartz fluorescence cells. Solutions were not deaerated prior to measurements.

Time-correlated single photon counting (SPC). Fluorescence lifetime measurements were made with a PTI LS-1 time-correlated single photon counter. A temperature of 20.0 ± 0.1 °C in the sample chamber was kept constant by a RM6 Lauda circulating bath for all the samples. The flashlamp is operated by a Thryratron-gated discharge between two tungsten electrodes in an atmosphere of hydrogen. The repetition rate of the lamp is about 22-25 KHz. The nanosecond lamp is run using hydrogen as the plasma gas. The photon emitted by a lamp pulse is detected by a R928 photomultiplier (PMT). The time difference between excitation of the sample and detection of an emitted

photon is converted to a voltage reading by a Ortec 457 time to amplitude converter (TAC). The analog signals from TAC is converted to digital voltages by a nucleus PCAII computer card multichannel analyzer (MCA).

The excitation wavelengths were set at 336 nm, 290 nm and 380 nm for pyrene, naphthalene and anthracene, respectively. The fluorescence emissions were monitored at 380 nm, 420 nm and 400 nm for pyrene, naphthalene and anthracene, respectively. A 10,000 maximum count was used for all experiments. Visual analysis of residuals and the autocorrelation, χ^2 values and DW (Durbin-Watson) parameters were used as criteria for fitting and to differentiate single, double exponential decays. Typical χ^2 values were between 1.0 and 1.3, and DW values were bigger than 1.70 and 1.75 for single and double exponential fits, respectively.[6]

2.4. Laser flash photolysis (LFP)

The excitation source is a Spectra Physics YAG laser model GCR-12 (266nm, ≤40mJ/pulse; 355nm, ≤70mJ/pulse). The laser fires at a maximum repetition rate of 1Hz. The laser pulse energies are normally adjusted to less than 20mJ/pulse. The YAG laser beam is directly aligned onto the sample holder (Figure 2.1).

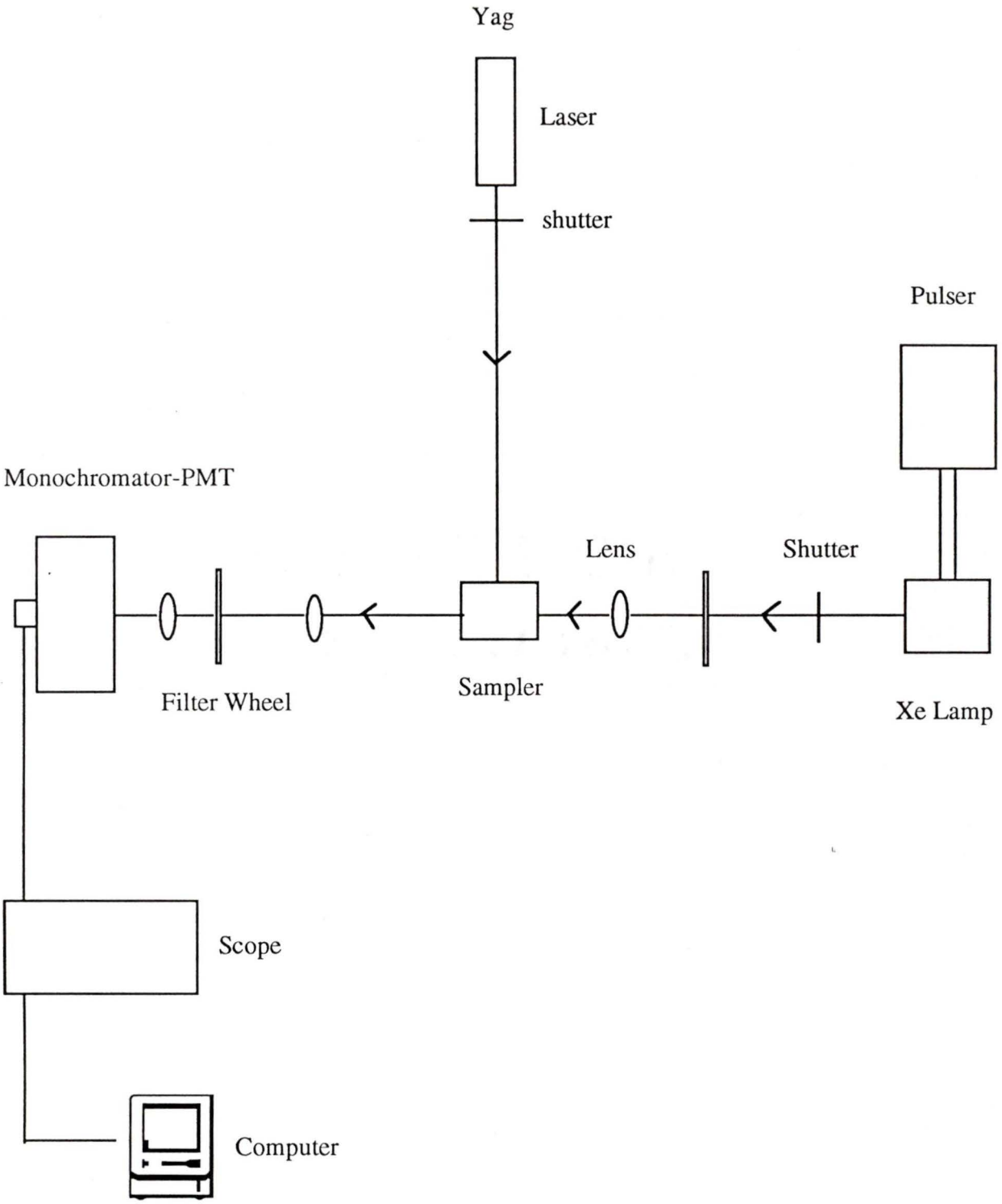

Figure 2.1: Simplified diagram of a laser flash photolysis apparatus.

The intensity of the YAG is set by adjusting the high voltage for the lamp flash. The analyzing beam is set at right angles to the laser beam. The analyzing light consists of a pulsed 150W xenon lamp (Oriel housing model 66057, PTI power supply model LPS-220). The pulser is custom made and upon triggering, the output of the xenon lamp is increased significantly for 4 ms in a wavelength dependent manner. For detecting light intensities at fixed wavelengths, a photomultiplier (PMT), Hamamatsu R446, 5 dynodes)/monochromator (CVI Digikrom 240) system is used. Signals from the PMT are sent into a baseline compensation circuit that incorporates a sample and hold amplifier with a digital memory. On receiving a trigger pulse, the circuit holds constant the value of the background intensity (V_0) and provides a DC output proportional to its magnitude. The transient signal which remains can then be measured with high precision using a Tektronix TDS 520 digital oscilloscope.

Timing for laser pulsing, lamp pulsing, track and hold on the baseline compensation unit and acquisition on the oscilloscope are set by a custom built pulse generator (millisecond delays) driving a Stanford Research System delay generator model DG535 (nanosecond delays). The timing is set so that the "flat' portion of the 4 ms lamp pulse is used, which in our system occurs about 2.2 ms after the start of the lamp pulse.

The oscilloscope, monochromator and Stanford delay generator are interfaced to a GPIB bus (National Instruments GPIB NI-488.2 board) attached to a Macintosh IIci computer. All settings on these units are controlled directly by the computer program. Digital outputs on an I/O data acquisition board (National Instruments Lab-NB) are employed to set logic levels (*and*, *nand* and *or* gates) to configure different experiments. These logic settings are employed to open or close shutters and to set filter wheels, as well as triggering the lasers, oscilloscopes and baseline compensation unit. Depending on the experimental conditions, the transient absorption signal may have to be corrected for fluorescence from the sample or for slope in the baseline. The baseline correction is introduced by subtracting a signal for which only the analyzing beam (laser blocked) was

recorded from the signal obtained where the laser and the analyzing beam are on. This correction is usually employed when the total time scale is larger than 20 μs. The fluorescence correction is made by recording the signal with the analyzing beam on and off while the laser is firing. The shot without the analyzing beam includes fluorescence from the sample.

Two filter wheels with cut-off filters at different wavelength (no filter, 320, 375, 435 and 590 nm) are set between the Xe lamp and the monochromator; one before and the second after the sample holder. The computer program sets both wheels to the first cut-off filter with wavelength smaller than the monochromator setting. The filter wheel in between the Xe lamp and sample is employed to avoid irradiation at short wavelength that could lead to degradation of the sample. The second filter ensures that the detection of overtones of emission that occurs at half the wavelength are not being monitored.

The computer program to control the experiment was written using Labview 3.1.1 (National Instruments). The program subtracted correction shots, transforms the data collected (V_t) on the oscilloscope into absorbance values (ΔA=-log(1-Corrected V_t/V_0)), averages sets of measurements and saves the data into disk files.

The absorbance value is equal to the negative logarithm of the ratio of light intensities being detected on the PMT in the absence and presence of a chromophore. This relationship assumes a linear response of the signal measured at the PMT with light intensity irradiating the detector. But the response of PMTs is not linear. For this reason, only small changes of light intensities ($\Delta A < 0.2$) are measured. In addition, an algorithm was incorporated into the program to acquire the data at a constant target V_0 value (default value of 250 mV). At wavelengths where the Xe lamp has a high light intensity output, the high voltage on the PMT is initially kept at 800V and the slit on the monochromator is adjusted according to an experimentally determined calibration curve.

A program including several different fitting routines (developed by Dr. A.D. Kirk) for different kinetic mechanisms was employed to evaluate the data. Kaleidagraph software (Synergy Software, version 3.0) was also used to fit the data.

Samples in 7 mm × 7 mm Suprasil cells (static or flow) were deareated by bubbling with nitrogen for 15 minute before laser experiments. The absorption due to the solvated electrons was checked and the laser power was attenuated until the signal for solvated electrons disappeared. The total amount of laser shots that do not lead to destruction of the sample was established by comparing the UV-Vis spectrum before and after irradiation. The number of laser shots given to naphthalene and xanthone that do not lead to deterioration of samples are 200 and 50 shots, respectively. All experiments were performed at room temperature (20 ± 2°C).

2.5. UV-Vis spectra

UV-Vis spectra were recorded on a Varian Cary 5 or Cary 1 at room temperature. Typical scan rate and slits were set at 100 nm/min and 2 nm, respectively. Baseline correction was always employed.

3. Incorporation of singlet excited probe molecules with bile salt aggregates

3.1. Incorporation of pyrene in bile salt aggregates

As addressed in Chapter 1, the intensities of the vibronic bands in the pyrene emission spectrum are dependent on the solvent polarity. The ratio between bands I and III (I/III, see Figure 1.12) is used as a measure for the polarity of the environment where pyrene resides.[6,42,44,48] This property of pyrene has been employed earlier to characterize bile salt aggregates.[21,34,39,41] The aggregation pattern of bile salts has been shown to be dependent on the ionic strength, pH and temperature at which the experiments were performed.[19] For this reason we first determined the experimental conditions for which we could obtain reproducible results. The temperature was kept at 20°C, the ionic strength was kept between 0.2 and 0.25 M and the pH was 7.0 ± 0.2. These experimental conditions were established by measuring the R(I/III) for pyrene fluorescence.

3.1.1 Effect of ionic strength

When the ionic strength was changed by adding different amounts of sodium chloride (NaCl), a variation of R(I/III) ratio of pyrene fluorescence emission was observed. Table 3.1 shows the R(I/III) values of pyrene fluorescence in the presence of 10 mM sodium cholate (NaC) at various concentrations of NaCl. In the absence of NaCl, R(I/III) was 1.75 and it decreased to 1.01 at 0.4 M of NaCl. This indicated that the formation of bile salt aggregates was affected by ionic strength and pyrene was in a less polar environment at higher ionic strength.

Table 3.1: R(I/III) of pyrene in 10 mM of NaC at various ionic strengths

[NaCl] mM	0.0	1.0	5.0	9.8	19.2	39.2	83.3	436
I/III	1.75	1.75	1.72	1.71	1.66	1.55	1.31	1.01

[a] The error for each measurement of R(I/III) is within ± 0.02.

Figure 3.1 shows the R(I/III) values of pyrene fluorescence as a function of NaC concentration in the presence (0.2 and 1.0 M) and in the absence of NaCl. In the presence of 1.0 M NaCl, the sudden transition of the R(I/III) in the concentration range from 5 to 10 mM suggested spontaneous aggregate formation. In the presence of 0.2 M NaCl, the transition of R(I/III) was not as sharp, and in the absence of NaCl the decrease of R(I/III) value was much slower and did not appear to reach the plateau until a concentration of 30 mM NaC. From the R(I/III) of pyrene fluorescence, it was apparent that in the presence of NaCl, the system provided a more hydrophobic medium for pyrene. We chose an ionic strength of 0.2 M NaCl for the remaining experiments so that our results can bear a resemblance to bile salt aggregates in biological systems ($[Na^+] \approx 0.15$ M in biological systems).

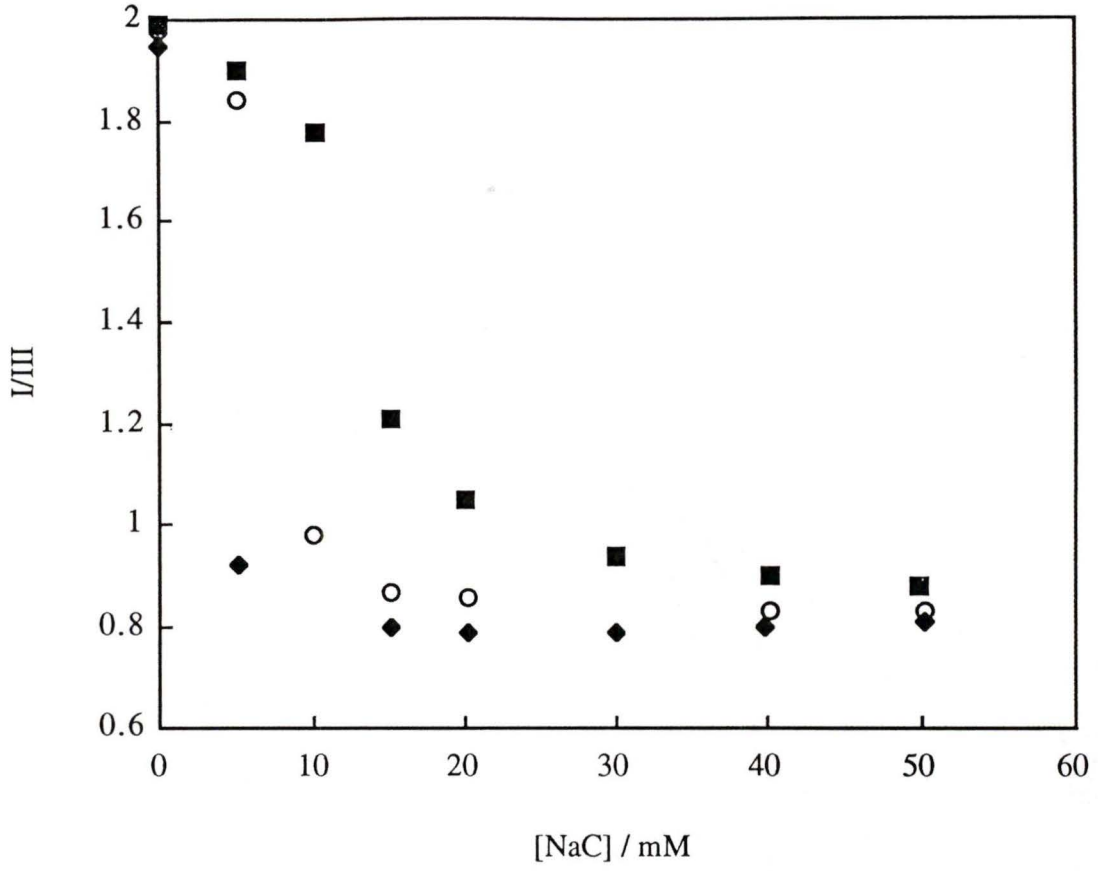

Figure 3.1: R(I/III) of pyrene at various concentrations of NaC in the presence of 0.2M NaCl (O), 1.0M NaCl (u) and in absence of NaCl (n).

3.1.2. UV-Vis spectra of pyrene in sodium cholate solutions

The UV-Vis absorption spectra of pyrene in the presence of sodium cholate shifted to the red with increasing NaC concentration. Figure 3.2 shows the UV-Vis absorption spectra of pyrene at various bile salt concentrations. The baseline was always corrected by subtracting the absorption of bile salts at the same concentration as the sample.

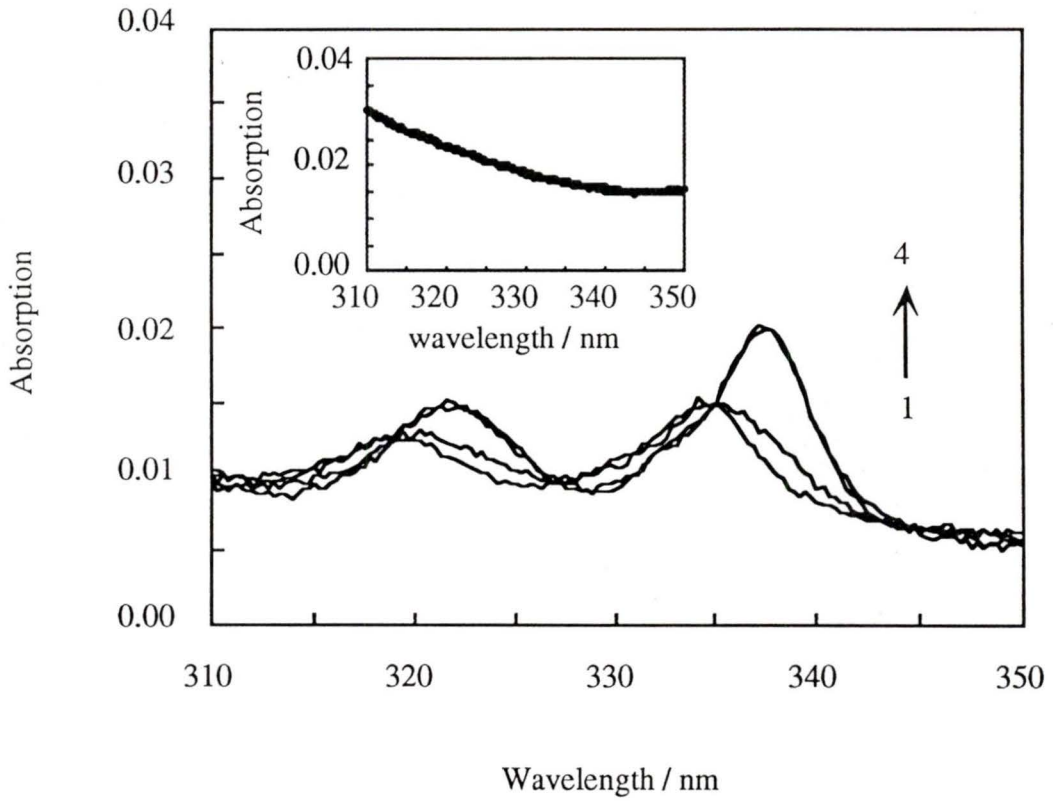

Figure 3.2: UV-Vis absorption spectra of pyrene (5×10^{-7} M) in the absence (1) of NaC and in the presence of 5.0 mM (2), 30 mM (3) and 40 mM (4) NaC. The inset shows the UV-Vis absorption spectrum of 20 mM NaC.

The red shift in the pyrene absorption spectrum was not mentioned in previously published work for bile salts. This result indicated that pyrene was located in a different environment at higher NaC concentrations compared to pyrene in water. The shift in the absorption spectrum may distort the R(I/III) values of pyrene fluorescence with increasing NaC concentrations if the excitation efficiencies for bound and free pyrene are very different at the excitation wavelength for fluorescence measurements. For this reason, the samples were excited at the isosbestic point (336 nm). At this wavelength, free pyrene in aqueous solution and pyrene inside the bile salt aggregates were excited with the same efficiency.

3.1.3. Fluorescence study of pyrene in NaC solutions

The R(I/III) of the pyrene fluorescence emission was studied at various bile salt concentrations ($[Na^+] = 0.2$ M). Increasing the concentration of NaC in the pyrene-NaC solution led to a decrease of the R(I/III) value. This indicated that the environment where most of the pyrene molecules were situated was less polar than at lower NaC concentrations. Above 15 to 20 mM NaC, the decrease of the R(I/III) was minimal (Figure 3.3) suggesting that the pyrene was located in an environment with approximately the same polarity.

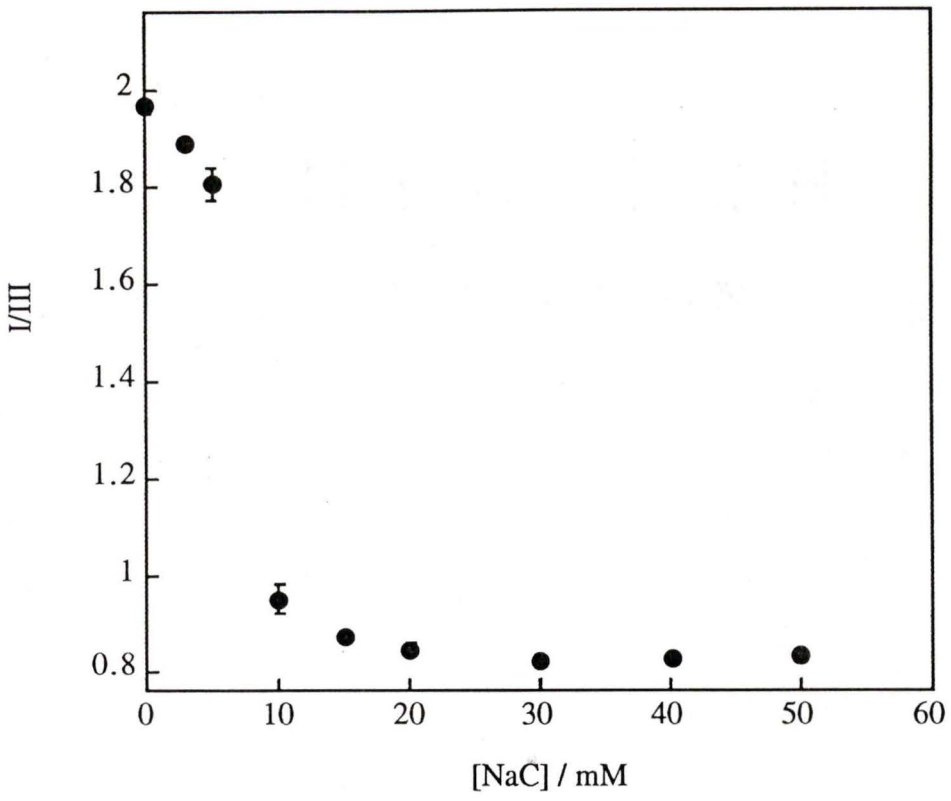

Figure 3.3: R(I/III) of pyrene at various concentrations of NaC

This observation was consistent with the results reported in the literature for sodium taurocholate aggregates (NaTC).[61] As addressed in the Introduction, changes in the R(I/III) value of pyrene fluorescence have previously been interpreted to be due to the formation of surfactant micelles. The breakpoint has been related to the critical micelle concentration (CMC) of surfactant micelles.[44] In the case of surfactant micelles, the R(I/III) values were constant at concentrations below and above the CMC and only at the CMC a drastic change (over a concentration range of 1 mM) of R(I/III) was observed. This indicated that below the CMC pyrene was in water and above the CMC most pyrene was solubilized inside the micelle. However, in the case of bile salts, a defined CMC value was not observed. The R(I/III) of pyrene fluorescence decreased continuously with increasing of NaC concentration, which was due to the stepwise formation of bile salt aggregates during a much broader concentration range. This phenomenon was consistent

with the mechanism of bile salt aggregate formation proposed by others.[18,61] Above 20 mM of sodium cholate the R(I/III) was almost constant which suggested that relatively big aggregates were formed and that most pyrene was bound into a hydrophobic environment.

3.1.4. Steady-state fluorescence quenching study

In order to study how well pyrene was incorporated into the NaC aggregates, iodide ion (I^-) was used to quench the pyrene fluorescence. The Stern-Volmer plots were linear (Figure 3.4) and the value of the Stern-Volmer constant (K_{SV}) decreased with increasing NaC concentration until a constant value was achieved at [NaC] ≥ 20 mM (Table 3.2).

The R(I/III) values at different quencher (I^-) concentrations were also determined in these experiments. At high bile salt concentration, this ratio was constant with increasing I^- concentrations, suggesting that pyrene was always in an environment with the same polarity (Figure 3.5). This indicated that I^- was quenching pyrene inside the aggregates. At intermediate NaC concentrations the K_{SV} values were higher indicating that some pyrene may be free in solution. The pyrene was initially quenched by I^- with a much higher efficiency. The decrease of R(I/III) with increasing I^- concentration at intermediate NaC concentrations reinforced the suggestion that before the aggregates were completely formed pyrene was partially bound to smaller aggregates (Figure 3.5).

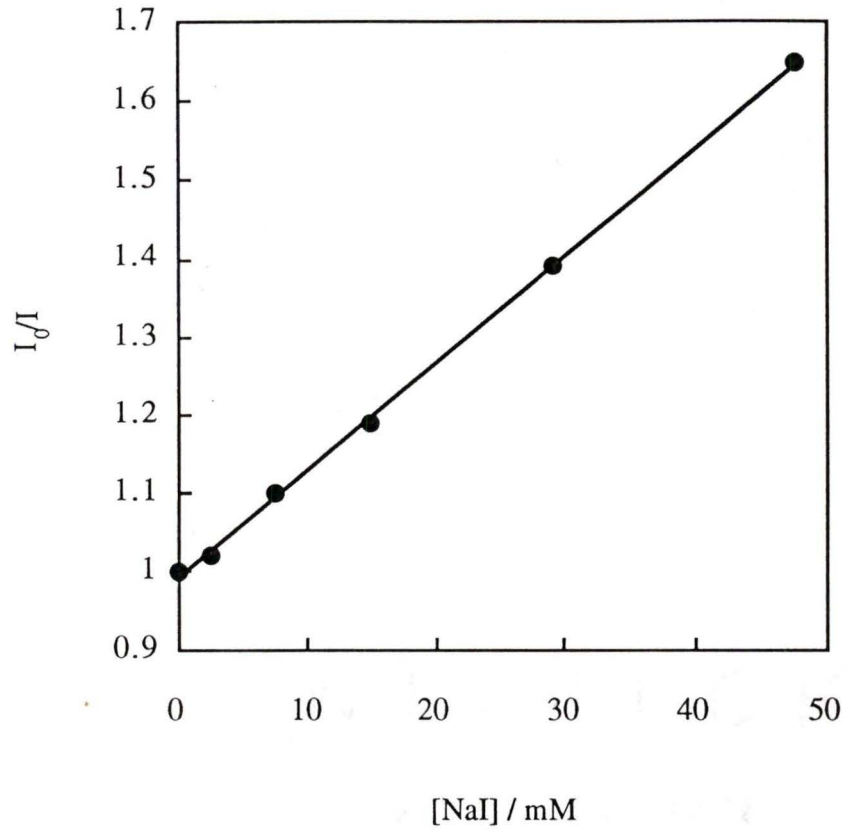

Figure 3.4: Stern-Volmer plot for pyrene quenching by NaI at [NaC] = 40mM

Table 3.2: Stern-Volmer constants for pyrene quenching by NaI at various concentrations of NaC.[a]

[NaC] / mM	K_{SV} / M^{-1}
0.0	141.0 ± 4.0 (2)
2.8	144.0 ± 1.0 (1)
5.0	123.1 ± 0.3 (2)
10.0	17.3 ± 1.3 (3)
20.0	14.8 ± 3.0 (3)
30.0	12.9 ± 0.3 (2)
40.0	13.7 ± 0.2 (2)

[a] The numbers in parentheses show the number of independent experiments. For the experiments performed only once, the errors were obtained from statistical fits of the data to the Stern-Volmer equation. For the experiments performed twice, the errors were calculated as average deviations, while for the experiments performed three times, the errors corresponded to standard deviations.

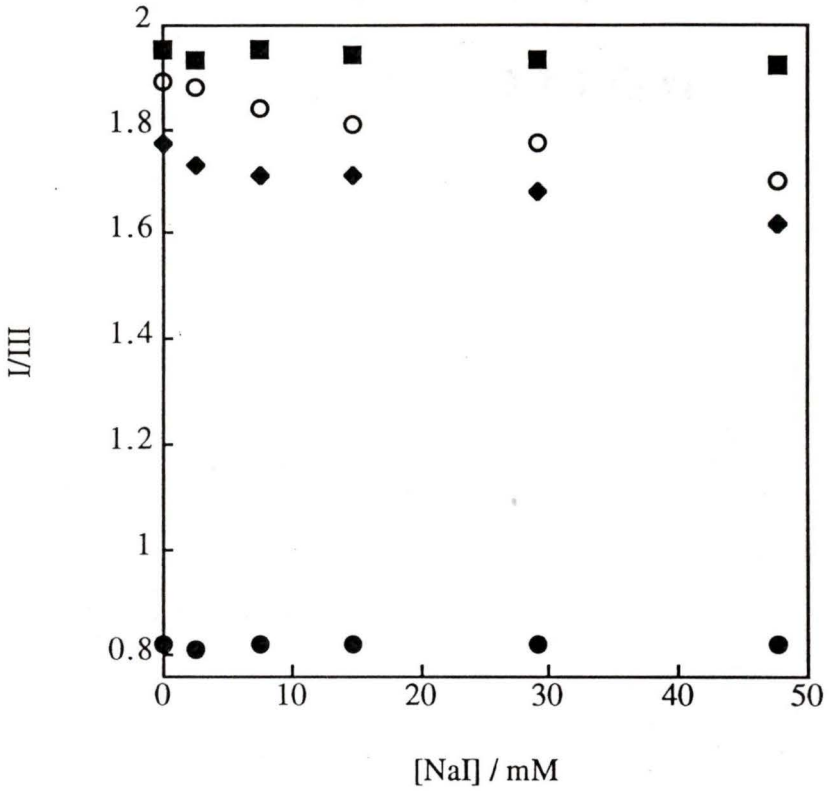

Figure 3.5: Changes of R(I/III) for pyrene fluorescence at various concentrations of NaI in the presence of 3 mM (O), 5 mM (u)and 30 mM (l) NaC and in the absence of NaC(n).

3.1.5. Lifetime measurements of pyrene in bile salt aggregates by single photon counting

Time-correlated single photon counting (SPC) experiments were performed. An increase of the pyrene lifetime from 131 ns in water to ca. 311 ns at 30 mM NaC was observed. The increase of the fluorescence lifetime of pyrene in micellar solutions was attributed to the increased structural rigidity in the micelle and reduction of collisional interactions with dissolved oxygen in the bulk solution.[62] In the SPC experiments, an initial fast component was observed when pyrene fluorescence decay was monitored at 380 nm (Figure 3.6). This fast decay was due to an impurity in NaC, however the pre-exponential factor of it was less than 5% of the total amplitude. This fast decay was not included in the fitting of the decay curves. Some traces were fitted including the fast decay and an extra exponential term, and the other exponential terms recovered were the same within the experimental uncertainty. The lifetimes of pyrene in various NaC concentrations are shown in Table 3.3.

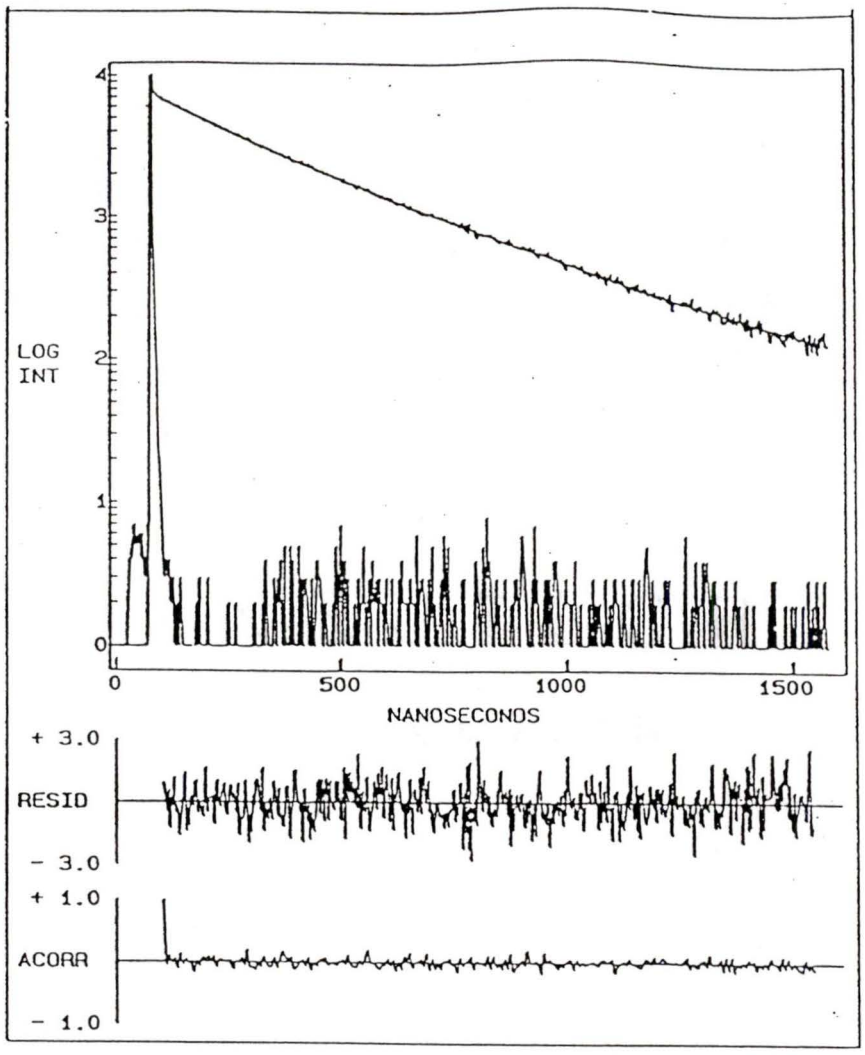

Figure 3.6: Pyrene (4.7×10^{-7} M) fluorescence decay curve in 10 mM NaC ($\lambda_{ex} = 336$ nm, $\lambda_{em} = 380$ nm). The fit to experimental data corresponds to a double exponential. The Chi squared (χ^2) value is 0.911. The lifetimes of the two species were: $\tau_1 = 111 \pm 14$ ns; $\tau_2 = 323 \pm 2$ ns. The pre-exponential factors were: $A_1 = 0.11 \pm 0.01$; $A_2 = 0.89 \pm 0.01$. The fractional intensity contributions were: $F_1 = 0.043$; $F_2 = 0.957$.

Table 3.3: Lifetimes of pyrene in the presence of various concentrations of NaC.[a]

[NaC] / mM	τ_1 / ns	τ_2 / ns
0.0	132.7 ± 1.3 (2)	
3.0	131.84 ± 0.04 (1)	
5.0	120.4 ± 7.6 (3)	190 ± 19 (3)
10.0	123 ± 11 (2)	324 ± 2 (2)
20.0		339.7 ± 0.2 (2)
30.0		347.0 ± 0.6 (1)

[a] The numbers in parentheses show the number of independent experiments. For the experiments performed only once, the errors were obtained from statistical fits of the data to single exponential decays. For the experiments performed twice, the errors were calculated as average deviations, while for the experiments performed three times, the errors corresponded to standard deviations.

The decay in solutions with NaC concentration above 20 mM NaC was first order indicating that all pyrene was incorporated into the bile salt aggregates. At intermediate NaC concentrations, the fluorescence decays were not first order. Due to the stepwise aggregation and polydispersity of bile salt aggregates,[29,34,40,61] more than two pyrene species may exist in the presence of bile salts. However, adequate fits were obtained when the fluorescence decays of pyrene were fitted to double exponentials in the presence of low concentrations of NaC. The short-lived species had a lifetime that was

the same as the lifetime of pyrene in water within experimental errors and the lifetime of the long-lived species was similar to that for pyrene at high NaC concentrations.

3.1.6. Fluorescence quenching studies by SPC

Time resolved fluorescence quenching studies by I^- were performed using SPC. The Stern-Volmer plots were linear (Figure 3.7). The relationship between the reciprocal of the lifetime of singlet pyrene and the quenching rate constant is given by:

$$\frac{1}{\tau_{obs}} = \frac{1}{\tau_0} + k_q[NaI] \qquad 3\text{-}1$$

Where τ_{obs} and τ_0 are lifetimes of pyrene in the presence and absence of NaI, respectively, and k_q is the quenching rate constant.

At intermediate NaC concentrations, quenching of both short-lived and long-lived pyrene species were independently fitted to Eq 3-1 and two quenching rate constants were obtained. For pyrene in the presence of 3 mM of NaC, a long-lived pyrene species was observed at higher quencher concentrations ([NaI] ≥ 7.44 mM). However, the pre-exponential factor of this component was so small (≤ 2%) that the quenching rate constant (k_q^2) of this long-lived species was not obtained. In the presence of low NaC concentrations, the quenching rate constant (k_q^1) of the short-lived pyrene species was only smaller than the quenching rate constant of pyrene in water by a factor of two. The quenching rate constant (k_q^2) of the long-lived pyrene species was similar to that at higher bile salt aggregates (Table 3.4). This suggested that at intermediate bile salt concentrations, pyrene was partially incorporated into bile salt aggregates and partially free in water or bound to small bile salt aggregates.

The quenching rate constant (k_q^2) in bile salt aggregates was constant at various NaC concentrations. The k_q^2 value obtained, ca. $(3.2 \pm 0.2) \times 10^7$ $M^{-1}s^{-1}$, was consistent with the value previously reported (3.6×10^7 $M^{-1}s^{-1}$).[23]

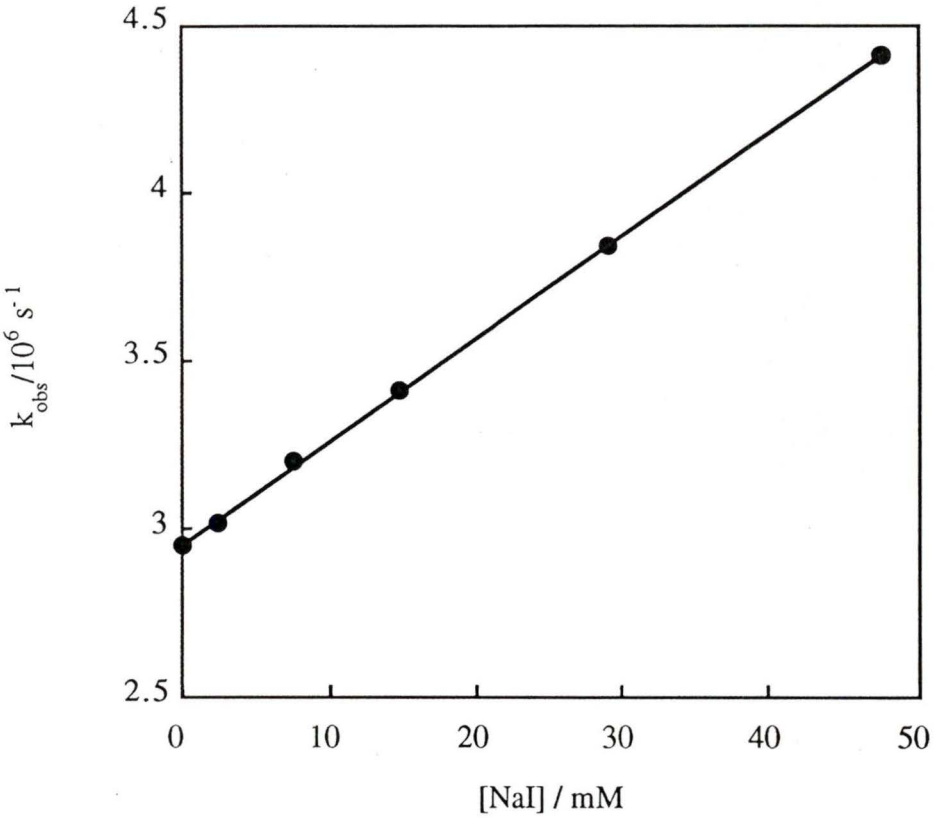

Figure 3.7: Quenching of pyrene in 20 mM NaC by NaI.

Table 3.4: Quenching rate constants of pyrene in the presence of various concentrations of NaC.[a]

[NaC] / mM	$k_q^1/10^8$ $M^{-1}s^{-1}$	$k_q^2/10^8$ $M^{-1}s^{-1}$
0.0	11.7 ± 1.3 (4)	
3.0	10.8 ± 0.4 (1)	
5.0	8.47 ± 0.05 (2)	0.357 ± 0.005 (2)
10.0	4.2 ± 0.4 (2)	0.31 ± 0.01 (2)
20.0		0.307 ± 0.001 (2)
30.0		0.32 ± 0.01 (1)

[a] k_q^1 is the quenching rate constant of the short-lived pyrene species; k_q^2 is the quenching rate constant of the long-lived pyrene species. The numbers in parentheses show the number of independent experiments. For the experiments performed only once, the errors were obtained from statistical fits of the data to Eq 3-1. For the experiments performed twice, the errors were calculated as average deviations, while for the experiments performed four times, the errors corresponded to standard deviations.

3.1.7. Comparison of fluorescence quenching studies by the SPC and steady-state fluorescence measurements

Two quenching mechanisms should be considered: dynamic quenching and static quenching. If only dynamic quenching occurs, quenching plots obtained by SPC (τ_0/τ vs [Q]) and steady-state fluorescence measurements (I_0/I vs [Q]) should be the same.

In order to understand the quenching mechanism of pyrene in bile salt aggregates by NaI, the values of I_0/I obtained directly from steady-state fluorescence studies, $(I_0/I)_{ss}$, were compared with the I_0/I values calculated from SPC results, $(I_0/I)_{dyn}$ (Figure 3.8).

The values of $(I_0/I)_{dyn}$ were calculated from Equation 3-2:

$$\left(\frac{I_0}{I}\right)_{dyn} = 1 + k_q \tau_0 [Q] \qquad (3\text{-}2)$$

where k_q is the quenching rate constant, τ_0 is the lifetime of pyrene in the absence of the quencher (Q).

At intermediate bile salt concentrations when there were two pyrene species, the value of $(I_0/I)_{dyn}$ was calculated for the short-lived pyrene species, $(I_0/I)_{dyn}{}^1$, and the long-lived pyrene species, $(I_0/I)_{dyn}{}^2$, separately.

The integrated fluorescence intensities in the absence of quencher for the short-lived species, $(I_0)_1$, and the long-lived species, $(I_0)_2$ are given by:

$$(I_0)_1 = F_1 (I_0)_t \qquad (3\text{-}3)$$

$$(I_0)_2 = F_2 (I_0)_t \qquad (3\text{-}4)$$

Where F_1 and F_2 are the fractional intensity contributions of the short-lived and the long-lived pyrene species, respectively. $(I_0)_t$ is the total fluorescence intensity.

The total $(I_0/I)_{dyn}$ was obtained by:

$$\left(\frac{I_0}{I}\right)_{dyn} = \frac{(I_0)_t}{\frac{(I_0)_1}{\left(\frac{I_0}{I}\right)^1_{dyn}} + \frac{(I_0)_2}{\left(\frac{I_0}{I}\right)^2_{dyn}}} \qquad (3\text{-}5)$$

Substituting Eq 3-3 and Eq 3-4 into Eq 3-5, the total $(I_0/I)_{dyn}$ can be given by:

$$\left(\frac{I_0}{I}\right)_{dyn} = \frac{1}{\frac{F_1}{\left(\frac{I_0}{I}\right)^1_{dyn}} + \frac{F_2}{\left(\frac{I_0}{I}\right)^2_{dyn}}} \qquad (3\text{-}6)$$

Figure 3.8 shows the difference between plotting $(I_0/I)_{ss}$ and $(I_0/I)_{dyn}$ against various concentrations of NaI. This suggested that both dynamic and static quenching were involved in the quenching of pyrene in NaC aggregates by NaI. The quenching mechanism can be described by Equation 3-7:

$$\left(\frac{I_0}{I}\right)_{ss} = 1 + (k_q\tau_0 + K_{eq})\,[Q] \qquad (3\text{-}7)$$

Where k_q is the quenching rate constant and K_{eq} is the equilibrium constant of the complex of NaI and NaC aggregates.

According to Eq 3-7, the slope for the plot $(I_0/I)_{ss}$ vs. [NaI] is $K_{eq} + k_q\tau_0$. Similarly, the slope for the plot $(I_0/I)_{dyn}$ vs. [NaI] is $k_q\tau_0$. At various NaC concentrations, the differences between $(I_0/I)_{ss}$ and $(I_0/I)_{dyn}$ were compared. The slopes for the plots of $(I_0/I)_{ss}$ vs. [NaI] and $(I_0/I)_{dyn}$ vs. [NaI], as well as the extent of static quenching are listed in Table 3.5.

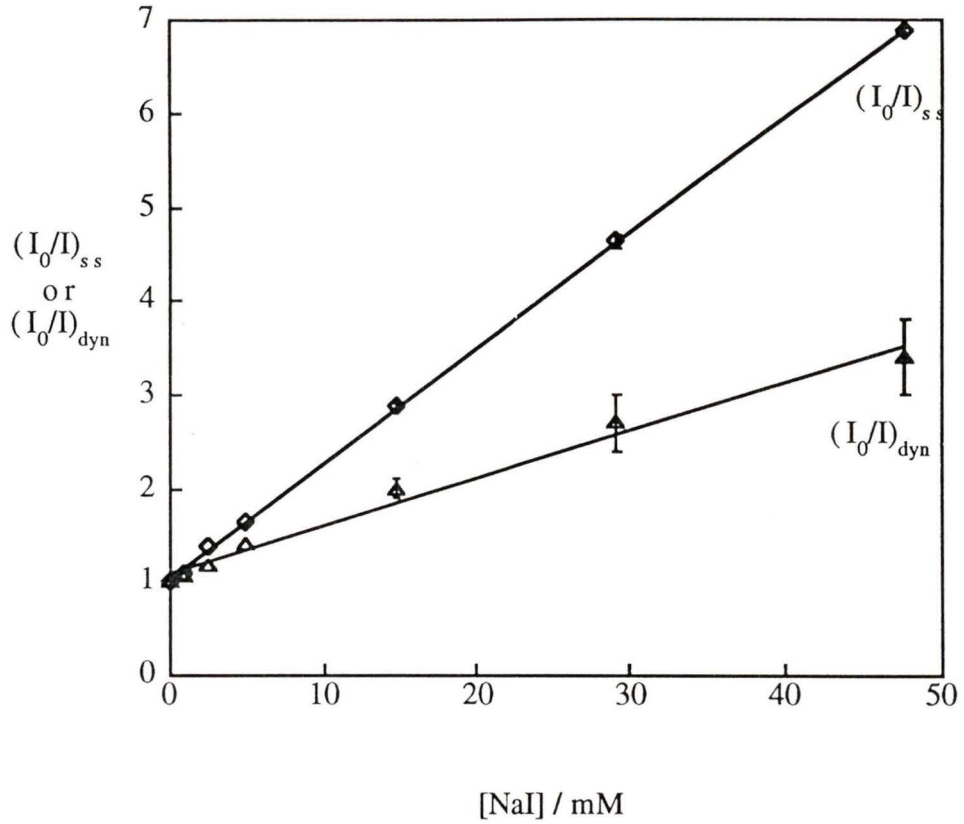

Figure 3.8: Comparison of $(I_0/I)_{ss}$ and $(I_0/I)_{dyn}$ of pyrene in 5 mM NaC.

Table 3.5: The slopes of the steady-state fluorescence quenching plot ($K_{eq} + k_q\tau_0$) and time-resolved quenching plot ($k_q\tau_0$) of pyrene at various NaC concentrations and extent of static quenching ($\frac{K_{eq}}{K_{eq} + k_q\tau_0} \times 100\%$).[a]

[NaC] / mM	$k_q\tau_0$ / M^{-1}	$(K_{eq} + k_q\tau_0)$ / M^{-1}	$\frac{K_{eq}}{K_{eq} + k_q\tau_0} \times 100\%$
0.0	133.7 ± 0.5 (1)	140.8 ± 4.5 (2)	5.0 ± 3.5
3.0	138 ± 4 (1)	144 ± 1 (1)	4.2 ± 3.5
5.0	53.5 ± 8.5 (2)	124 ± 1 (2)	56.9 ± 7.7
10.0	10.95 ± 0.15 (2)	16.7 ± 2.1 (2)	34 ± 14
20.0	10.8 ± 0.3 (2)	14.1 ± 0.5 (2)	23.4 ± 5.7
30.0	11.4 ± 0.2 (1)	13.2 ± 0.2 (1)	13.6 ± 3.0

[a] The numbers in parentheses show the number of independent experiments. For the experiments performed only once, the errors were obtained from statistical fits of the data to Eq 3-2 and Eq 3-7. For the experiments performed twice, the errors were calculated as average deviations.

As shown in Table 3.5, static quenching is negligible for pyrene in water and at 3 mM NaC. In the presence of bile salts (≥ 5 mM), the amount of static quenching of pyrene decreased with increasing of NaC concentrations.

3.2. Incorporation of naphthalene in bile salt aggregates

A much higher naphthalene concentration was solubilized in the presence of NaC than in water. This indicated that an interaction occurred with cholate aggregates. The intensities of the vibronic bands for naphthalene fluorescence spectrum do not show dependence on the solvent polarity, and the incorporation can only be tested by performing quenching studies and by monitoring changes in the fluorescence lifetime in the presence of bile salts.

3.2.1. Steady-state fluorescence quenching study

Sodium iodide was used to quench naphthalene in NaC aggregates. The Stern-Volmer plots were linear (Figure 3.9) and Stern-Volmer constant decreased with increasing NaC concentration until a constant value was achieved at [NaC] ≥ 20 mM (Table 3.6). This indicated that all naphthalene was bound to cholate aggregates above 20 mM cholate.

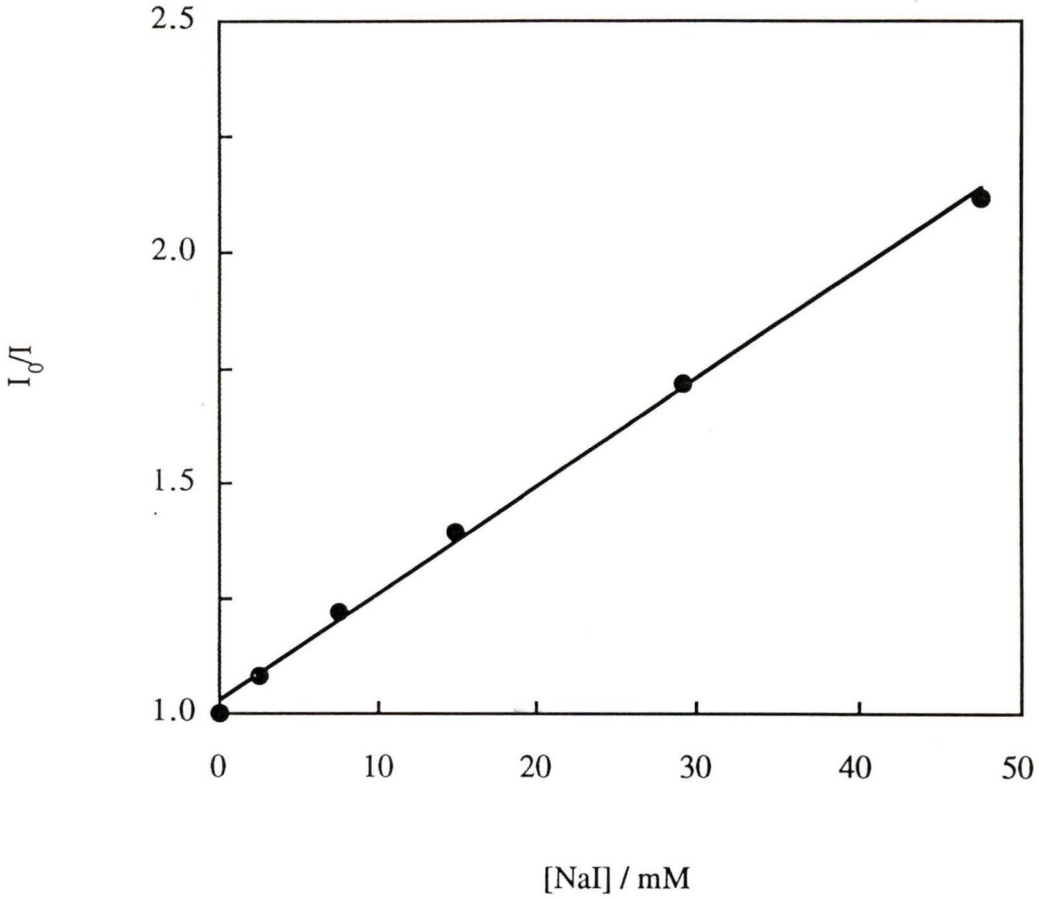

Figure 3.9: Stern-Volmer plot for naphthalene quenching by NaI in 40 mM NaC

Table 3.6: Stern-Volmer constants of naphthalene quenching by NaI at various concentrations of NaC.[a]

[NaC] / mM	K_{SV} / M^{-1}
0.0	269 ± 13 (2)
5.0	251 ± 39 (3)
10.0	105.0 ± 3.0 (1)
20.0	34.0 ± 3.4 (3)
30.0	40 ± 13 (2)
40.0	28.0 ± 2.0 (2)

[a] The numbers in parentheses show the number of independent experiments. For the experiments performed only once, the errors were obtained from statistical fits of the data to the Stern-Volmer equation. For the experiments performed twice, the errors were calculated as average deviations, while for the experiments performed three times, the errors correponded to standard deviations.

3.2.2. Fluorescence quenching studies by SPC

Time-correlated single photon counting experiments of naphthalene in NaC were performed. The lifetime of naphthalene increased from 34 ns in water to ca. 98 ns in 40 mM NaC which indicated an incorporation of singlet excited naphthalene into the NaC aggregates. A typical fluorescence decay trace obtained from SPC measurements is

shown in Figure 3.10. The lifetimes of naphthalene in various NaC concentrations are shown in Table 3.7.

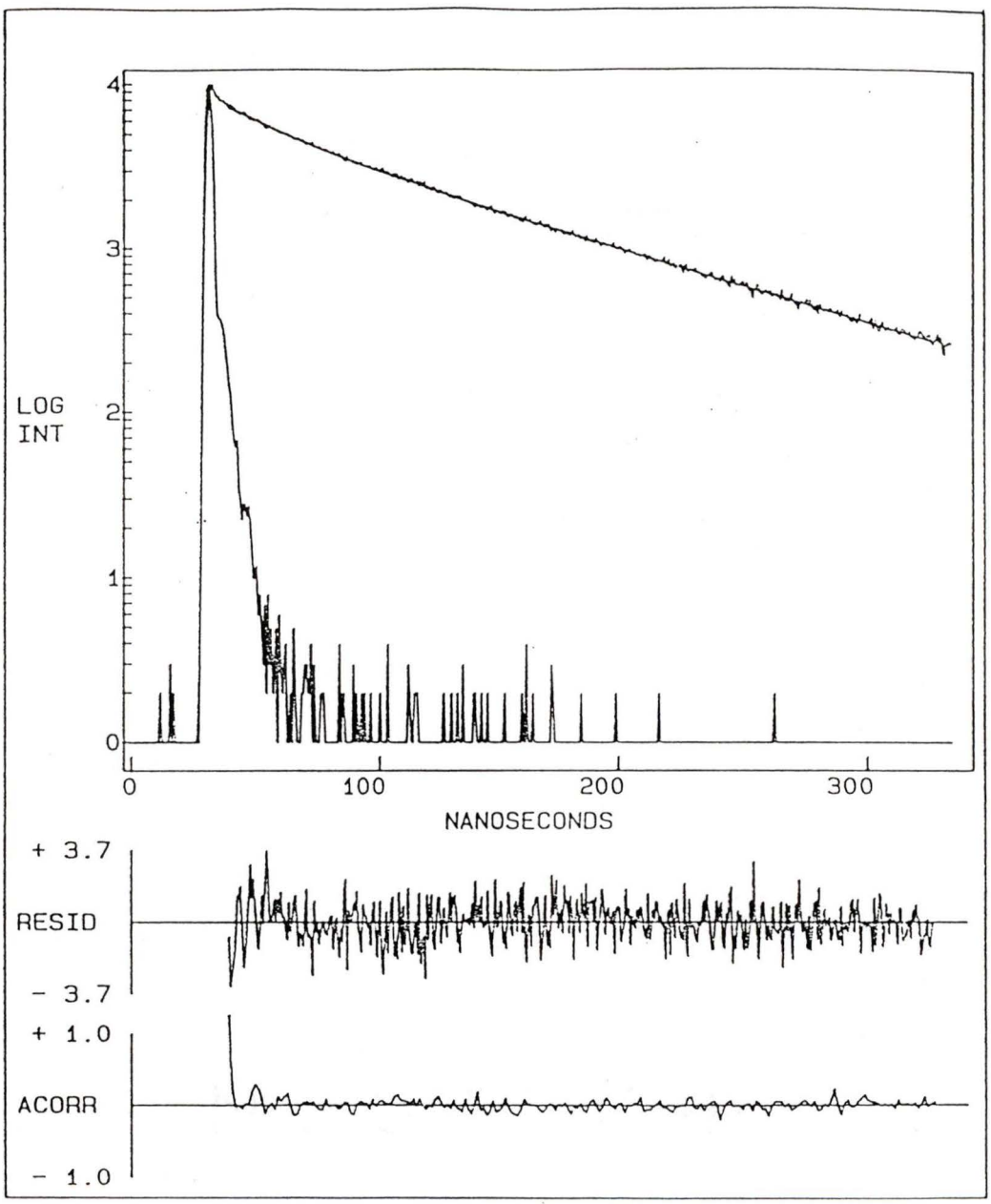

Figure 3.10: Naphthalene (1.0×10^{-5} M) fluorescence decay curve in 20 mM NaC (λ_{ex} = 290 nm, λ_{em} = 340 nm). The fit to experimental data corresponds to a double exponential. The Chi squared (χ^2) value is 1.23. The lifetimes of the two species were: $\tau_1 = 21.7 \pm 0.8$ ns; $\tau_2 = 93.0 \pm 0.4$ ns. The pre-exponential factors were: $A_1 = 0.291 \pm 0.006$; $A_2 = 0.709 \pm 0.005$. The fractional intensity contributions were: $F_1 = 0.088$; $F_2 = 0.912$.

Table 3.7: Lifetimes of naphthalene in the presence of various concentrations of NaC.[a]

[NaC] / mM	τ_1 / ns	τ_2 / ns
0.0	34.35 ± 0.04 (1)	
5.0	35.0 ± 0.3 (3)	
10.0	31.6 ± 0.5 (1)	84.4 ± 1.3 (1)
20.0	25.5 ± 3.1 (3)	94.0 ± 1.5 (3)
30.0	12.0 ± 1.6 (2)	95.7 ± 1.1 (2)
40.0	8.5 ± 0.5 (2)	97.8 ± 0.4 (2)

[a] The numbers in parentheses show the number of independent experiments. For the experiments performed only once, the errors were obtained from statistical fits of the data to the single exponential ([NaC] = 0.0 mM) or double exponential decays ([NaC] = 10.0 mM). For the experiments performed twice, the errors were calculated as average deviations, while for the experiments performed three times, the errors corresponded to standard deviations.

Due to the stepwise aggregation and polydispersity of bile salt aggregates,[29,34,40,61] more than two naphthalene species may exist in the presence of bile salts. However, adequate fits were obtained when the fluorescence decay traces of naphthalene above 5 mM of NaC were fitted to double exponentials. The lifetime of the short-lived species was similar to the lifetime of naphthalene in water. The lifetime of the long-lived species were fairly constant at different NaC concentrations. Due to the

interference of the impurity in NaC, the lifetimes of the short-lived naphthalene species could not be accurately determined at higher NaC concentrations. The values were smaller than that of naphthalene in water (Table 3.7). When the fluorescence decay traces were fitted from different starting points, the lifetimes of the long-lived component were always the same within experimental uncertainties, but the values for the short-lived species varied.

The time-resolved fluorescence quenching studies by I^- were performed by SPC. The quenching rate constants for the short-lived naphthalene species (k_q^1) and the long-lived species (k_q^2) were obtained by fitting to Eq 3-1 (Figure 3.11). The values of the quenching rate constants (k_q^1 and k_q^2) are listed in Table 3.8.

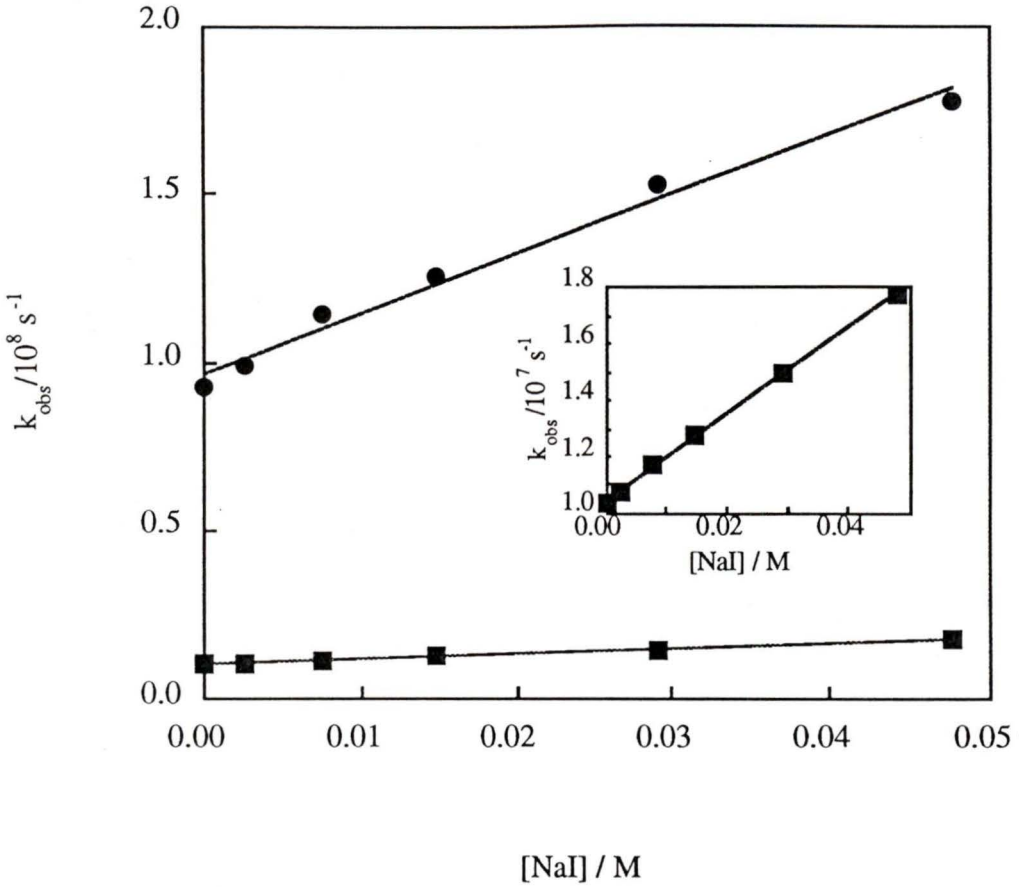

Figure 3.11: Time-resolved fluorescence quenching of the short-lived naphthalene species (l) and the long-lived naphthalene species (n) in the presence of 30 mM NaC. The inset is the expanded quenching plot of the long-lived naphthalene species.

Table 3.8: Quenching rate constants of naphthalene at various concentrations of NaC.[a]

[NaC] / mM	$k_q^1/10^8$ $M^{-1}s^{-1}$	$k_q^2/10^8$ $M^{-1}s^{-1}$
0.0	77.7 ± 0.7 (2)	
5.0	63.0 ± 4.0 (1)	
10.0	49.1 ± 3.1 (1)	2.07 ± 0.06 (1)
20.0	35.3 ± 4.5 (3)	1.5 ± 0.0 (3)
30.0	17.4 ± 0.4 (2)	1.53 ± 0.03 (2)
40.0	31 ± 21 (2)	1.5 ± 0.1 (2)

[a] k_q^1 is the quenching rate constant of the short-lived naphthalene species; k_q^2 is the quenching rate constant of the long-lived naphthalene species. The numbers in parentheses show the number of independent experiments. For the experiments performed only once, the errors were obtained from statistical fits of the data to Eq 3-1. For the experiments performed twice, the errors were calculated as average deviations, While for the experiments performed three times, the errors corresponded standard deviations.

At high NaC concentrations, the quenching rate constant (k_q^1) of the short-lived naphthalene species were smaller than the quenching rate constant of naphthalene in water by a factor of two. The quenching rate constants (k_q^2) of the long-lived naphthalene species were the same for naphthalene at above 20 mM NaC, and the value

was $(1.5 \pm 0.1) \times 10^8$ $M^{-1}s^{-1}$, which was ca. 50 times smaller than that of naphthalene in water, $(7.8 \pm 0.1) \times 10^9$ $M^{-1}s^{-1}$. This suggested that above 20 mM NaC, naphthalene was incorporated into NaC aggregates and was well protected from the aqueous quencher. For naphthalene in 5.0 mM of NaC, a long-lived naphthalene species was observed at higher quencher concentrations ([NaC] $\geq$ 7.44 mM). However, the pre-exponential factor of this component was so small ($\leq$ 5%) that the quenching rate constant (k_q^2) of this long-lived species was not obtained.

3.2.3. Comparison of fluorescence quenching studies by SPC and steady-state fluorescence measurements

In the case of naphthalene, the steady-state fluorescence quenching studies were compared with time-resolved quenching studies by SPC (Figure 3.12). The values of $(I_0/I)_{ss}$ were determined directly from steady-state fluorescence measurements. The values of $(I_0/I)_{dyn}$ were calculated from Eq 3-2 and Eq 3-3. A different relationship between I_0/I and τ_0/τ against the quencher concentrations was observed for naphthalene as in the case for pyrene. The differences between $(I_0/I)_{ss}$ and $(I_0/I)_{dyn}$ were obtained at various NaC concentrations (Table 3.9).

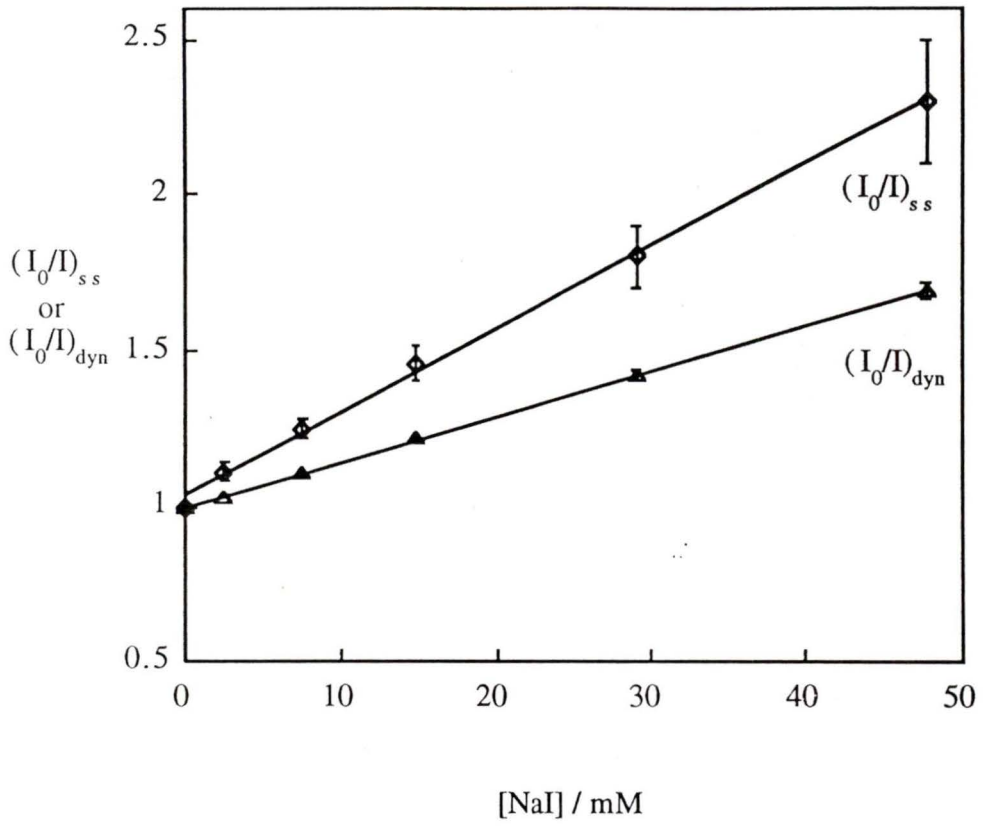

Figure 3.12: Comparison of $(I_0/I)_{ss}$ and $(I_0/I)_{dyn}$ of naphthalene in 40 mM NaC.

Table 3.9: The slopes of the steady-state fluorescence quenching plot ($K_{eq} + k_q\tau_0$) and time-resolved quenching plot ($k_q\tau_0$) of naphthalene at various NaC concentrations and extent of static quenching ($\frac{K_{eq}}{K_{eq} + k_q\tau_0} \times 100\%$).[a]

[NaC] / mM	$k_q\tau_0$ / M^{-1}	$(K_{eq} + k_q\tau_0)$ / M^{-1}	$\frac{K_{eq}}{K_{eq} + k_q\tau_0} \times 100\%$
0.0	253.2 ± 5.3 (1)	258.0 ± 2.4 (1)	1.9 ± 3.0
5.0	164 ± 24 (1)	199.8 ± 4.6 (1)	18 ± 14
10.0	46.7 ± 2.9 (1)	104.9 ± 4.2 (1)	55.5 ± 7.1
20.0	16.8 ± 0.7 (2)	36.2 ± 3.5 (2)	54 ± 13
30.0	14.7 ± 0.3 (2)	52.8 ± 0.2 (2)	72.2 ± 1.0
40.0	14.5 ± 0.7 (2)	27.6 ± 3.4 (2)	47 ± 16

[a] The numbers in parentheses show the number of independent experiments. For the experiments performed only once, the errors were obtained from statistical fits of the data to Eq 3-2 and Eq 3-7. For the experiments performed twice, the errors were calculated as average deviations.

3.3. Incorporation of anthracene in bile salt aggregates

The solubilization of anthracene was studied by fluorescence quenching using iodide ion (I^-). The aqueous solubility of anthracene is smaller than pyrene.[63] Anthracene is not soluble enough in water for the fluorescence to be measured in the absence and presence of low bile salt concentrations. Thus the fluorescence studies of anthracene in homogeneous solution was carried out in ethanol / water (45 / 55, v / v).

3.3.1. Steady-state fluorescence quenching of anthracene in homogeneous solution and NaC aggregates

Anthracene fluorescence was quenched by I^-. The Stern-Volmer plots are shown in Figure 3.13 and the Stern-Volmer constants are listed in Table 3.10.

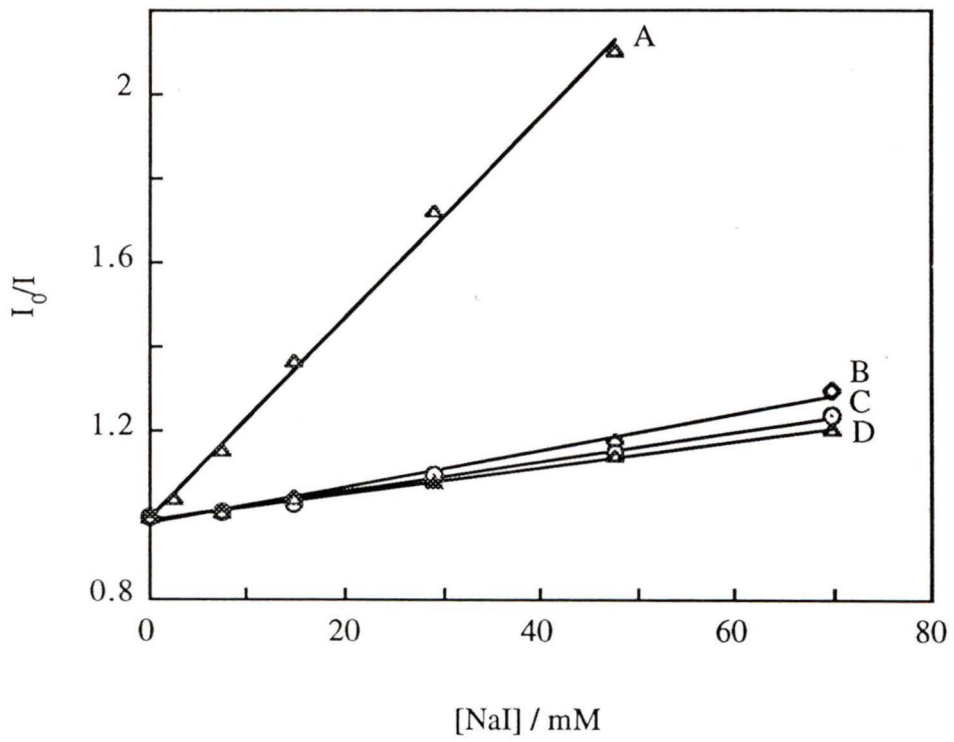

Figure 3.13: Stern-Volmer plot of anthracene quenching by NaI in A: ethanol / water (45 / 55, v / v), B: 20 mM NaC, C: 30 mM NaC and D: 40 mM NaC.

Table 3.10: Stern-Volmer constants of anthracene determined by fluorescence quenching with NaI in ethanol / water (45 /55, v /v) and at various concentrations of NaC[a].

[NaC] / M	K_{SV} / M^{-1}
0.0	23.2 ± 0.5 (1)
20.0	4.3 ± 0.3 (1)
30.0	3.6 ± 0.1 (2)
40.0	3.1 ± 0.4 (2)

[a] The numbers in parentheses show the number of independent experiments. For the experiments performed only once, the errors were obtained from statistical fits of the data to the Stern-Volmer equation. For the experiments performed twice, the errors were calculated as average deviations.

The Stern-Volmer plots are linear for anthracene in ethanol / water (45 / 55, v / v) and in the presence of various NaC concentrations. The Stern-Volmer constants are similar for anthracene in different NaC concentrations and the value is ca. 5-7 times smaller than that of anthracene in ethanol / water (45 / 55, v / v). This indicated that anthracene was incorporated into NaC aggregates above 20 mM of NaC and was protected from aqueous quencher.

3.3.2. Time-resolved fluorescence quenching of anthracene by SPC

The fluorescence lifetime of anthracene in ethanol / water (45 / 55, v / v) and in bile salt aggregates were measurement by SPC technique. The lifetimes of anthracene in the presence of NaC were only slightly higher than the lifetime of anthracene in ethanol / water (45 / 55, v / v). A typical decay trace is shown in Figure 3.14. Due to the stepwise aggregation and polydispersity of bile salt aggregates, more than one anthracene species may exist. However, the lifetimes of more than one species were difficult to determine since the fluorescence lifetime of anthracene is short (≈ 4.4 ns).

Time-resolved fluorescence quenching studies of anthracene in ethanol / water (45 / 55, v / v) and in the presence of various NaC concentrations by I^- were performed by SPC. The quenching plots were linear and the data were fitted to Eq 3-1. The quenching rate constants (k_q) are shown in Table 3.11.

The quenching rate constants were similar for various NaC concentrations and ca. 20 times smaller than that of anthracene in ethanol / water (45 / 55, v / v). This suggested that anthracene was equally protected from aqueous quencher at above 20 mM of NaC.

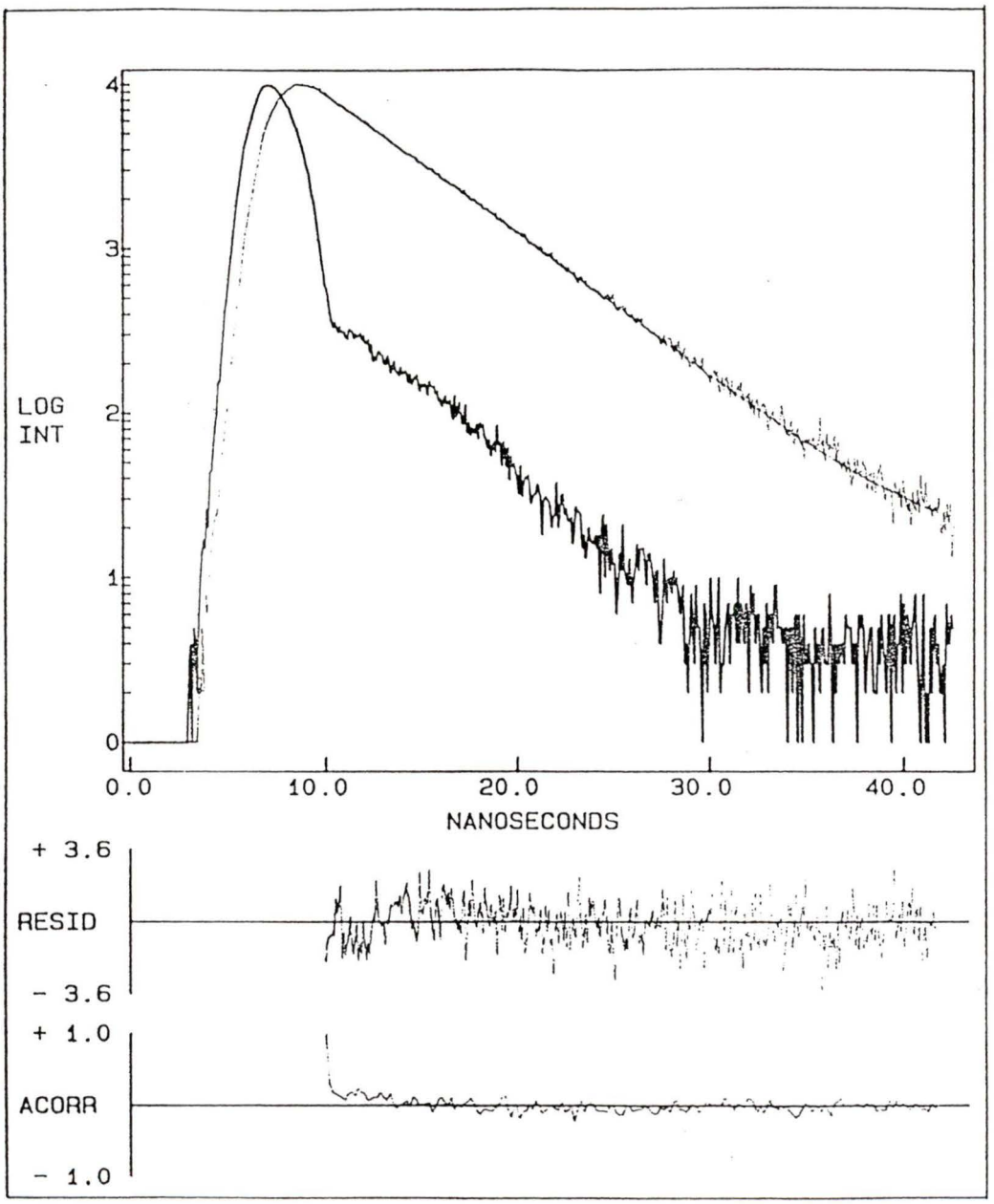

Figure 3.14: Anthracene (3.3×10^{-5} M) fluorescence decay curve in 40 mM NaC (λ_{ex} = 380 nm, λ_{em} = 400 nm). The fit to experimental data corresponds to a single exponential. The Chi squared (χ^2) value is 1.14. The lifetime was 4.61 ± 0.01 ns.

Table 3.11: Quenching rate constants of anthracene by NaI in ethanol / water (45 / 55, v / v) and various NaC concentrations[a].

[NaC] / mM	$k_q/10^8$ $M^{-1}s^{-1}$
0.0	52.7 ± 1.7 (1)
20.0	2.6 ± 0.6 (2)
30.0	2.65 ± 0.05 (2)
40.0	2.15 ± 0.05 (2)

[a] The numbers in parentheses show the number of independent experiments. For the experiments performed only once, the errors were obtained from statistical fits of the data to Eq 3-1. For the experiments performed twice, the errors were calculated as average deviations.

3.3.3. Comparison of fluorescence quenching studies by SPC and steady-state fluorescence measurements

For anthracene, the steady-state fluorescence quenching studies were compared with time-resolved quenching studies in order to understand the quenching mechanism. A difference between the two quenching experiments was observed. Figure 3.15 compares the steady-state fluorescence quenching plot of $(I_0/I)_{ss}$ vs. [NaI] with the time-resolved quenching plot of $(I_0/I)_{dyn}$ vs. [NaI] of anthracene at 30 mM NaC. Table 3.12 shows the comparison of the two quenching experiments for anthracene at various NaC concentrations.

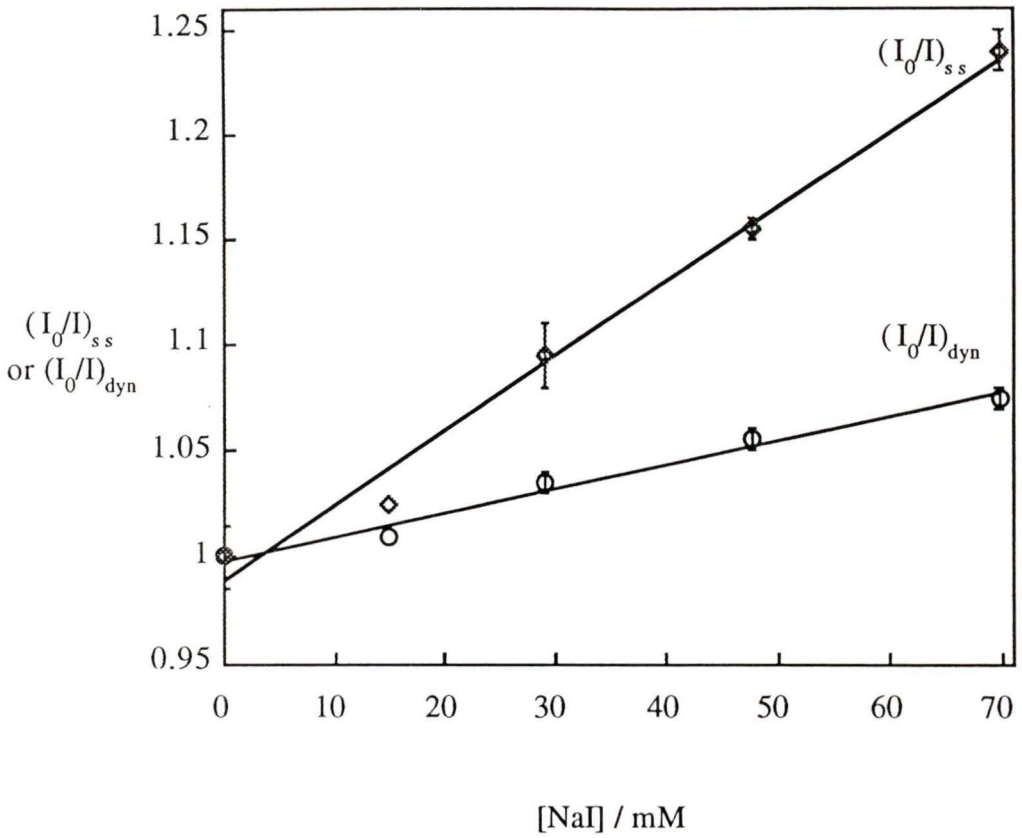

Figure 3.15: Comparison of I_0/I and τ_0/τ of anthracene in 30 mM NaC.

Table 3.12: The slopes of the steady-state fluorescence quenching plot ($K_{eq} + k_q\tau_0$) and time-resolved quenching plot ($k_q\tau_0$) of anthracene at various NaC concentrations and extent of static quenching ($\frac{K_{eq}}{K_{eq} + k_q\tau_0} \times 100\%$).[a]

[NaC], mM	$k_q\tau_0$, M^{-1}	$(K_{eq} + k_q\tau_0)$, M^{-1}	$\frac{K_{eq}}{K_{eq} + k_q\tau_0} \times 100\%$
20.0	1.5 ± 0.2 (1)	4.3 ± 0.3 (1)	65 ± 12
30.0	1.13 ± 0.04 (2)	3.59 ± 0.09 (2)	68.5 ± 4.0
40.0	0.98 ± 0.06 (2)	3.07 ± 0.36 (2)	68 ± 16

[a] The numbers in parentheses show the number of independent experiments. For the experiments performed only once, the errors were obtained from statistical fits of the data to Eq 3-2 and Eq 3-7. For the experiments performed twice, the errors were calculated as average deviations.

3.4. Preliminary studies with other bile salt aggregates

3.4.1. Sodium Deoxycholate

The UV-Vis absorption spectrum of pyrene in sodium deoxycholate (NaDC) system shifted to longer wavelength with increasing NaDC concentration (Figure 3.16).

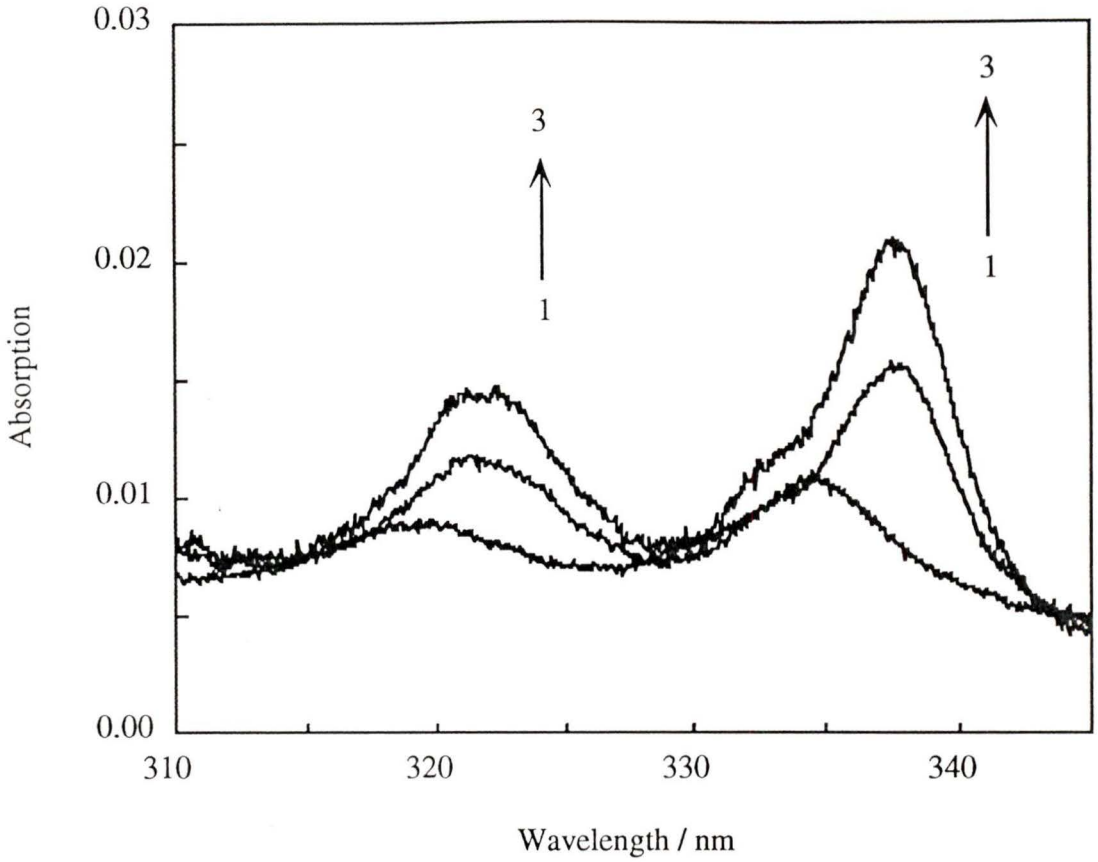

Figure 3.16: UV-Vis absorption spectra of pyrene (5×10^{-7} M) in the presence of 0.5 mM (1), 4.0 mM (2) and 20.0 mM (3) NaDC.

The red shift was observed above 3.0-4.0 mM NaDC. This result indicated that above ca. 3.0 mM to 4.0 mM of NaDC, pyrene was incorporated into the aggregate media with the same hydrophobicity.

The pyrene fluorescence emission spectra were taken at various concentrations of NaDC ([NaCl] = 0.2 M). A decrease of the R(I/III) was observed with increasing of NaDC concentration. Above 3.0 mM to 4.0 mM of NaDC the decrease of R(I/III) was minimal (Figure 3.17).

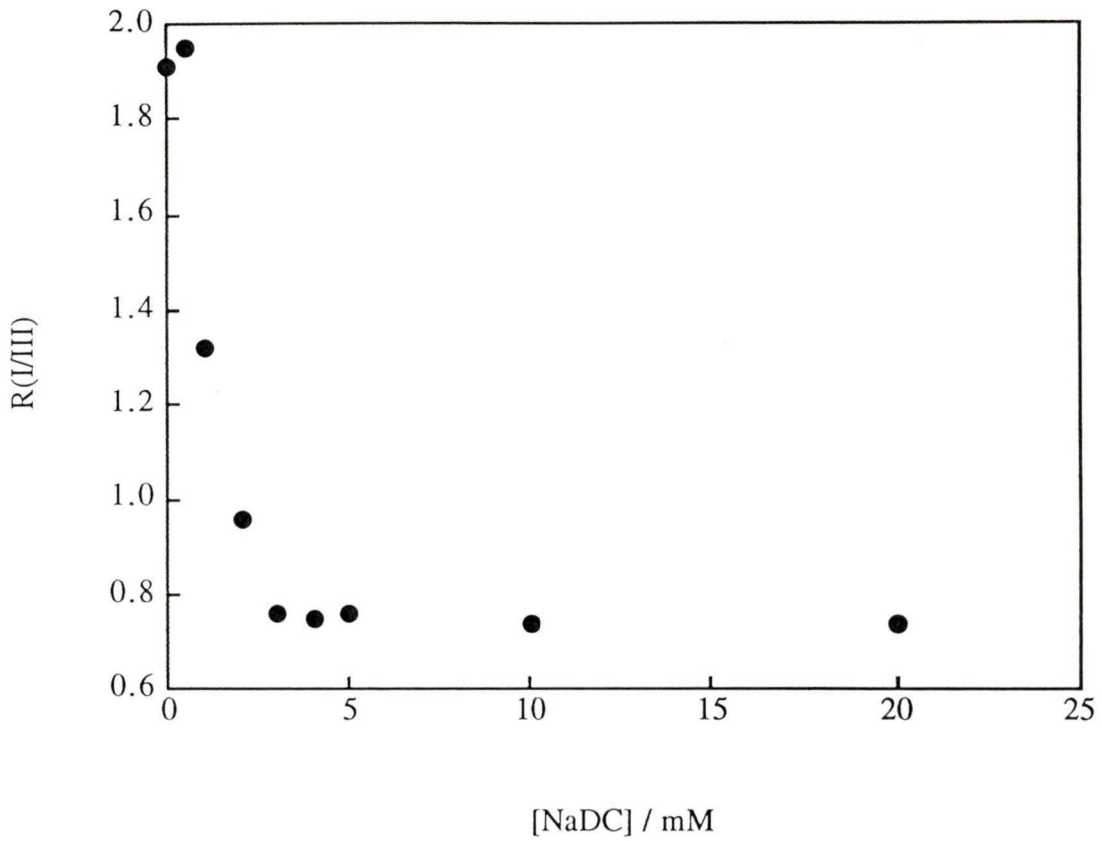

Figure 3.17: R(I/III) of pyrene in various concentrations of NaDC

The R(I/III) of pyrene in NaDC became constant at a much lower concentration (3-4 mM) than in the case of NaC (15-20 mM). This suggested that NaDC formed aggregates more readily than NaC. This may be due to the structural difference between NaDC and NaC.[27] In the case of NaDC, it is the lack of a hydroxyl group at C_7 which makes the molecule more hydrophobic and leads the aggregation to occur at lower concentrations.

3.4.2. Sodium Taurocholate

Increasing the concentration of sodium taurocholate (NaTC) in the aqueous pyrene solution led to a decrease of the R(I/III) of pyrene fluorescence ([NaCl] = 0.2 M). This suggested that the average environment around pyrene was less polar (Figure 3.18).

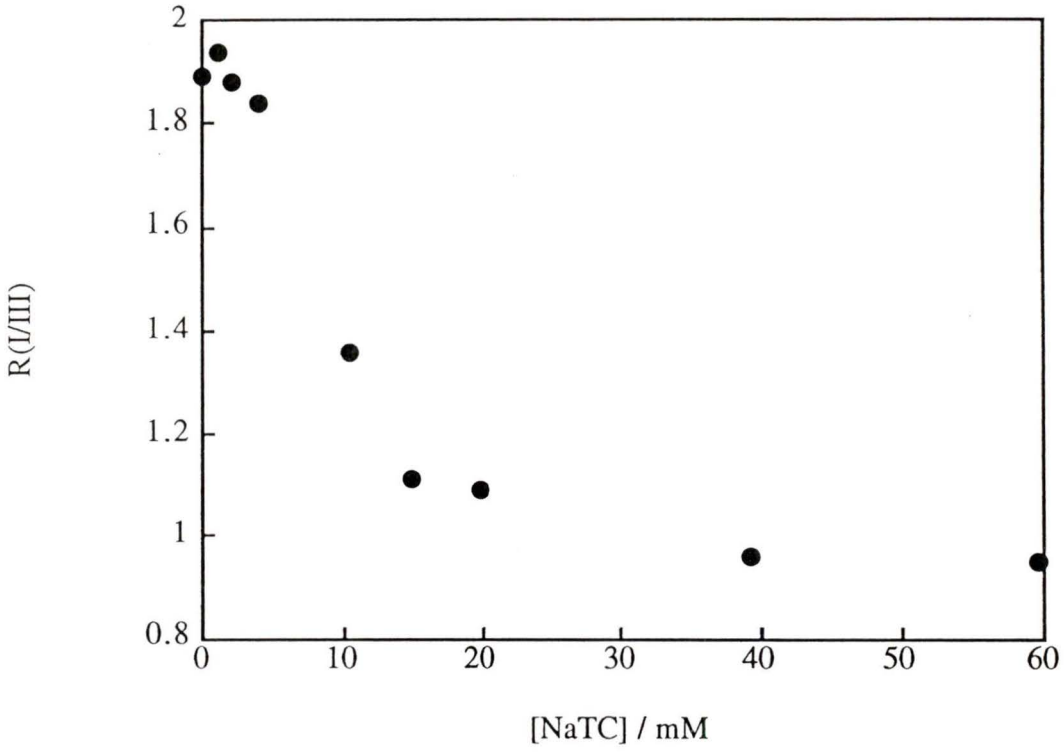

Figure 3.18: R(I/III) of pyrene in various concentrations of NaTC

The intersection of the two linear regions in Figure 3.18 occurs at ca. 20 mM. This indicated that above 20 mM of NaTC, the pyrene was incorporated in an environment with roughly the same polarity. This observation was similar to pyrene in NaC aggregates.

In order to understand the behavior of NaTC aggregates and the extent of pyrene incorporation, iodide ion (I^-) was used to quench pyrene and naphthalene fluorescence in NaTC system. The Stern-Volmer constant (K_{SV})decreased with increasing NaTC concentration for both pyrene and naphthalene until a constant value was achieved (Table 3.13 and Table 3.14). For pyrene, the value of K_{SV} was ca. 30 M^{-1} above 20 mM of NaTC and for naphthalene the K_{SV} was ca. 50 M^{-1} above 30 mM of NaTC.

Table 3.13: Stern-Volmer constants of pyrene quenching by NaI at various concentrations of NaTC[a].

[NaTC] / mM	K_{SV} / M^{-1}
0.0	135 ± 1
5.0	75 ± 2
10.0	40.9 ± 0.4
20.0	30.1 ± 0.2
30.0	31 ± 1
40.0	29.6 ± 0.3

[a] The errors were obtained from fitting the data to Stern-Volmer equation.

Table 3.14: Stern-Volmer constants of naphthalene quenching by NaI at various concentrations of NaTC[a].

[NaTC] / mM	K_{SV} / M^{-1}
0.0	256 ± 2
5.0	235 ± 2
10.0	156 ± 1
15.0	74 ± 1
20.0	70 ± 1
30.0	58 ± 1
40.0	50 ± 1
50.0	46 ± 1

[a] The errors were obtained from fitting the data to Stern-Volmer equation.

3.6. Discussion

Although the aggregation behavior of bile salts has been well-studied,[18,19,64,65] considerable controversy still exists over the significance of values for the "CMC" and aggregation numbers (N). The values for these parameters varied when different methods were used for the determination at different experimental conditions.[18]

Pyrene was the most widely used fluorescence probe molecule to characterize bile salt aggregates,[21,23,34,36,37,39,41] since the ratio of the different vibronic bands (I and III) of its emission spectrum is dependent on solvent polarity.[44,48] Bile salt aggregate incorporating excited singlet pyrene was protected from aqueous quenchers, since the quenching rate constants measured when pyrene was incorporated were smaller than that for free pyrene in aqueous solution.[23,34] Polycyclic aromatic hydrocarbons other than pyrene have also been employed to characterize the environment in bile salt aggregates.[37,39] The polydispersity of bile salt aggregates was investigated by the

fluorescence anisotropy of perylene[40] and by solubilization of several polycyclic aromatic hydrocarbons at different bile salt concentrations.[41] These studies were complemented by molecular modeling and it was proposed that primary aggregation occurs due to the hydrophobic interaction between the probes and the hydrophobic faces of the bile salt molecules. The number of bile salt molecules necessary to solubilize each hydrocarbon was suggested to be dependent on the size of the probe molecules.[41]

The objective of this work was to obtain a more detailed understanding of bile salt aggregation, specifically at low bile salt concentrations and the correlation between the protection efficiency of the bile salts and the size of the included probe molecules.

The three fluorescence probe molecules employed in this study were naphthalene, anthracene and pyrene. They are all smaller than most polycyclic aromatic hydrocarbons previously used, but naphthalene and pyrene are soluble enough in water for photophysical measurements to be performed in the absence of bile salt or at very low bile salt concentrations. The bile salt employed was sodium cholate (NaC). Steady-state and time-resolved quenching studies were employed to measure the protection efficacy when the probes were incorporated into bile salt aggregates. In order to compare the extent of incorporation of the probes into bile salt aggregates, the ratios of the quenching rate constants of the probes in homogeneous solutions (k_q^0) to the quenching rate constants of the probes inside of NaC aggregates (k_q) were plotted against various concentrations of NaC (Figure 3.19). The greater value of the ratio, the better the probe was protected from aqueous quencher (NaI). All the quenching rate constants involved in Figure 3.19 were obtained from dynamic quenching studies by SPC. Figure 3.19 only compared the long-lived species of each of the probes which corresponded to molecules incorporated into the hydrophobic region in bile salt aggregates.

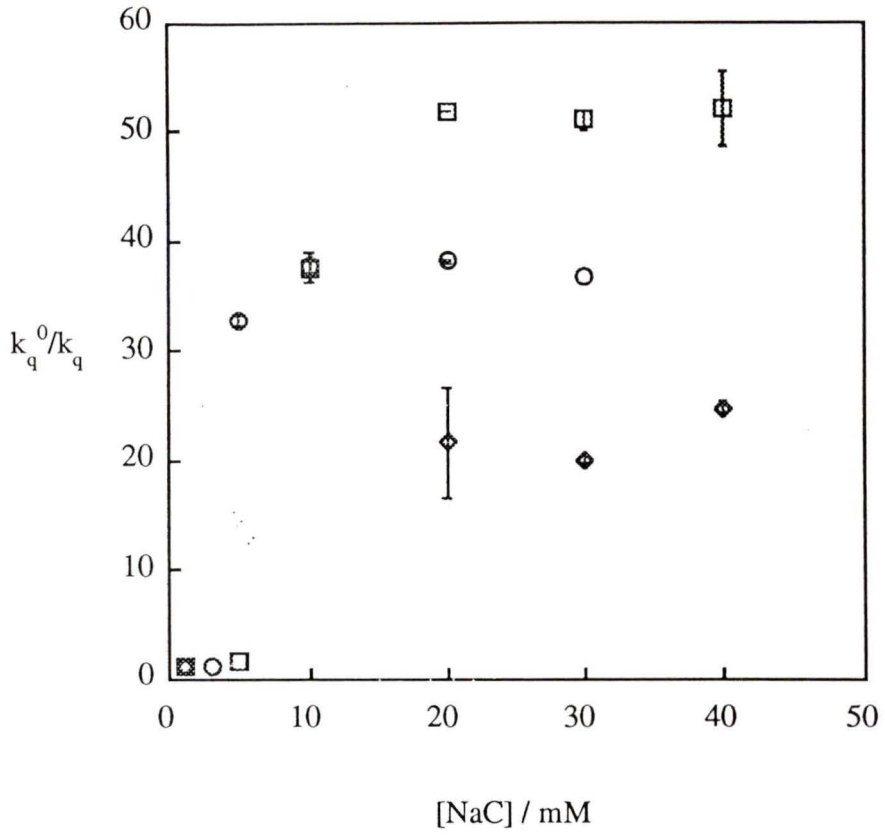

Figure 3.19: Comparison of the ratio of the quenching rate constants in homogeneous solution (k_q^0) to the quenching rate constants (k_q) at various NaC concentrations for naphthalene(o), pyrene (O) and anthracene (◊) .

In the case of naphthalene, all the values of the quenching rate constants (k_q) used in Figure 3.19 were the values of k_q^2 in Table 3.8, except for naphthalene in 5 mM NaC the value of k_q^1 in Table 3.8 was used. For pyrene, all the values of k_q used in Figure 3.19 corresponded to the values of k_q^2 in Table 3.4 except for pyrene in 3 mM of NaC where the value of k_q^1 was used. Figure 3.19 shows that for naphthalene the ratio of the quenching rate constants (k_q^0/k_q) in the absence and presence of bile salt remained constant until a concentration of 5 mM NaC was reached. In the case of pyrene, the ratio

(k_q^0/k_q) already increased at above 5 mM of NaC. This indicated that pre-aggregation between the hydrocarbon probe and sodium cholate occurred at lower concentrations in the case of pyrene than naphthalene. This could be due to the stronger hydrophobic interaction between bile salt molecules and pyrene. This result implied that the aggregation patterns of the bile salts were different for probe molecules with different structures. The same comparison for anthracene could not be made because the aqueous solubility of anthracene in the absence and the presence of very low bile salt concentrations was not great enough for photophysical measurements to be performed.

At high NaC concentrations ($\geq$ 20 mM), the ratio became constant for each of the probes, suggesting that they were located in a constant environment in the bile salt aggregates. However, the values of the ratio for the three probes were different indicating different degrees of protection from the aqueous quencher (I^-). Naphthalene had the largest value for the k_q^0/k_q ratio, which suggested that at high NaC concentrations, naphthalene was the most protected excited state probe. On the other hand, anthracene was the least protected from iodide quenching with the smallest value for the k_q^0/k_q ratio. The quenching rate constant (k_q^0) of anthracene in homogeneous solution used in Figure 3.19 was the quenching rate constant of anthracene in ethanol / water (45 / 55, v / v) (5.3×10^9 $M^{-1}s^{-1}$). Since the viscosity of ethanol (1.2×10^{-3} Pa·s) is slightly larger than that of water (1.0×10^{-3} Pa·s), the actual value of quenching rate constant for anthracene in water will be somewhat larger than the quenching rate constant in ethanol / water (45 / 55, v / v), which in turn would lead to a greater value of the ratio (k_q^0/k_q) than those shown in Figure 3.19. The quenching rate constant of anthracene in acetonitrile / water (1:1) was determined to be 7.8×10^9 $M^{-1}s^{-1}$. This value is expected to be higher than the quenching rate constant in water, since the viscosity of acetonitrile (0.35×10^{-3} Pa·s) is much smaller than the viscosity of water. However, we believe that the true quenching rate constant of anthracene in water is much closer to that in ethanol / water (45 / 55, v / v) than in acetonitrile / water (1:1). When the quenching rate constant of anthracene in

acetonitrile / water (1:1) was used as k_q^0 in Figure 3.19, the ratio (k_q^0/k_q) of anthracene was ca. 32 for NaC concentrations above 20 mM NaC, which was still smaller than that measured for pyrene, suggesting that although there is some uncertainty as to the k_q^0 value of anthracene the qualitative picture described is correct.

The quenching result suggested that the three probes were incorporated into sodium cholate aggregates to a different extent. This different protection pattern could be related to how bile salt molecules were oriented around the probe molecules, in order to achieve the maximum shielding for the probes from the aqueous phase. Naphthalene, being the smallest of the three probes, was able to fit into the very hydrophobic core of the bile salt aggregates. In the case of pyrene and anthracene, the sizes of these molecules are similar and both molecules are larger than naphthalene. However, the molecular shape of pyrene is different from anthracene. Pyrene is more symmetrical than anthracene when comparing the longest and shortest axes of these molecules to their longest axis. For this reason, pyrene was able to have the maximum hydrophobic interaction with the hydrophobic faces of the bile salt molecules, which in turn, can be better shielded from quenching in the aqueous phase. In the case of anthracene, due to its molecular shape, the aggregation pattern of bile salt molecules around anthracene was distorted, and a maximum "contact" between anthracene and the hydrophobic faces of the bile salt molecules was not as readily achieved as pyrene.

Comparing the steady-state fluorescence and the time-resolved quenching studies of all three probes, static quenching was observed in addition to dynamic quenching. Table 3.5, Table 3.9 and Table 3.12 listed the extent of static quenching for naphthalene, pyrene and anthracene, respectively. In this study, the short-lived and the long-lived species were both taken into account. The occurrence of static quenching indicated that iodide had to be located in close proximity to the probes.

It was observed by quenching studies that the short-lived species of the probes was quenched by NaI more efficiently than the long-lived species which was incorporated

inside of the hydrophobic region of the bile salt aggregates. This indicated that the two species were located at different sites in the bile salt aggregates. The short-lived species may be residing in the region where the hydroxyl groups of the bile salt molecules are and is less protected. The side chain of the bile salt molecule carries a negative charge. At high ionic strength, these negative charges were shielded by positive charges (Na^+) diminishing the repulsion between I- and the carboxylate anion on sodium cholate.

At low concentrations of NaC, the extents of static quenching involved in the iodide quenching were similar for all three probes. At higher concentrations of NaC, the extent of static quenching for pyrene was smaller than both naphthalene and anthracene. At high NaC concentrations, only the long-lived species of pyrene was detected and it was well protected in the hydrophobic region of bile salt aggregates, the static quenching was not likely to happen.

In summary, three singlet excited probes of different size, chemical structure and molecular shape were employed to study the bile salt aggregation of NaC in more detail. Both steady-state fluorescence quenching and time-resolved fluorescence quenching were performed to investigate the extent of incorporation of the probe molecules into bile salt aggregates. It was observed that the three probes were protected to different degrees from the aqueous quencher due to the size and the shape of the molecules. The highest protection was observed for naphthalene followed by pyrene and anthracene. At intermediate bile salt concentrations, different patterns of pre-aggregation between the probe and the bile salt molecules were observed. Pyrene formed the pre-aggregation with bile salt molecules more readily than naphthalene. In the quenching studies by NaI, static quenching was surprisingly observed for all three probes in bile salt aggregates. This observation has not been reported in the literature. We suggest that it is necessary to employ both steady-state and time-resolved fluorescence studies to investigate the incorporation of excited singlet probes in bile salt aggregates.

4. Dynamics of triplet excited probe molecules in bile salt aggregates

In principle, studies of excited triplet states can yield similar information to that of excited singlet probes. However, studies of excited triplet states usually yield information about dynamic processes that are not easily accessible when studying excited singlet states. The primary difference between excited singlet and triplet states is their lifetimes. Typically, complex mathematical fitting procedures have to be employed to obtain quantitative information about processes that are much slower than the lifetime of the transient. As a result of their short lifetime, singlet states only explore a small portion of the environment and are normally considered not to change locations before decaying to the ground state. Thus, the study of singlet states tends to give information about the location site of the probe molecule in a microheterogeneous system. In the case of triplet states, the lifetime (nanoseconds to hundreds of microseconds) can be of the same order of magnitude as the time required for excited state probe relocation between environments. Excited triplet xanthone and naphthalene were employed to establish the dynamics of association and dissociation of these probes with bile salt aggregates.

4.1. Dynamics of triplet naphthalene in bile salt aggregates

It was observed from fluorescence studies that excited singlet naphthalene incorporated readily into NaC and NaTC aggregates above a concentration of 20 mM. The fluorescence lifetime of singlet naphthalene increased and naphthalene was well protected from quenching by iodide (I^-). It was also observed that the degree of protection did not increase when the NaC concentration was increased from 20 mM up to 40 mM. In order to establish the dynamics of association and dissociation of the excited probe molecules, the behavior of the excited triplet naphthalene was studied in three

kinds of bile salts: sodium cholate (NaC), sodium taurocholate (NaTC) and sodium deoxycholate (NaDC).

4.1.1. Triplet-triplet absorption spectra of naphthalene in different solvents and in NaC aggregates

The triplet-triplet absorption spectra of triplet naphthalene in water, cyclohexane and 40 mM NaC are shown in Figure 4.1. The triplet-triplet absorption maximum for naphthalene was observed at 412 nm in water and cyclohexane indicating that there is no dependence on solvent polarity. The maximum observed in cyclohexane agreed well with that previously reported.[66] The spectrum was broader in water than in cyclohexane. When comparing the triplet-triplet absorption spectrum of triplet naphthalene in water to that in the presence of 40 mM NaC a narrowing and a red shift of 4 nm in the absorption maximum was observed (Figure 4.1). The narrowing of the spectrum indicated that triplet naphthalene was in a non polar environment. A red shift of the absorption spectrum could be due to the rigidity of the bile salt aggregates which brings the triplet electronic states closer together ($T_1 \rightarrow T_n$). These marked changes in the triplet-triplet absorption spectrum of naphthalene indicated that triplet naphthalene was incorporated into the bile salt aggregates. This was in agreement with what was observed for excited singlet naphthalene (see Chapter 3).

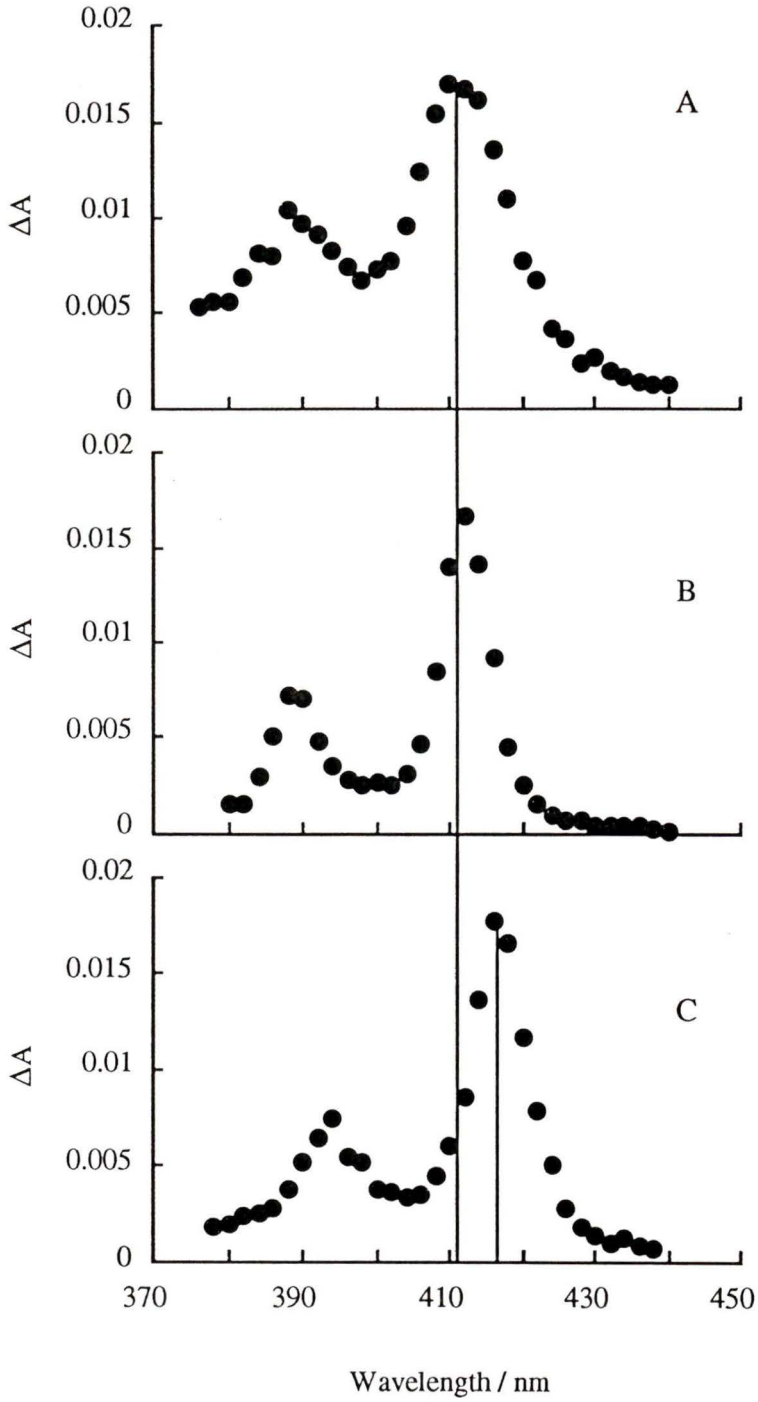

Figure 4.1: Triplet-triplet absorption spectra of triplet naphthalene in water (A), cyclohexane (B) and 40 mM NaC (C).

4.1.2. Quenching of excited triplet naphthalene by nitrite ions in bile salt aggregates

Quenching of excited triplet state molecules leads to an increase in the rate of decay. This process is suitable to obtain information about the dynamics of the association and dissociation of the probe molecule with organized systems.

Naphthalene was excited by a YAG laser at 266 nm. The decay of triplet naphthalene was monitored at 420 nm. The lifetime of triplet naphthalene was consistently longer than 30 μs and was primarily determined by the residual amount of oxygen present after deaeration. There was little change in the triplet lifetime when bile salts were added. In order to obtain information about the association dynamics, quenching studies by nitrite ions (NO_2^-) were employed to quench triplet naphthalene incorporated into three kinds of bile salt aggregates. The maximum number of laser shots given to naphthalene that do not lead to deterioration of the sample was 200. In the quenching experiments of naphthalene at each bile salt concentration, three or four samples were employed. The triplet lifetimes were similar for all samples after deaeration. Each sample was given less than 60 shots. At some quencher concentrations, the measurement was repeated for different samples and the triplet lifetimes were the same for each sample.

In aqueous solution, the relationship between the observed rate constant of triplet naphthalene and the quenching rate constant was given by:

$$k_{obs} = k_w + k_q[Q] \qquad (4\text{-}1)$$

where k_{obs} is the observed rate constant, k_q is the quenching rate constant and k_w is the triplet decay rate constant in water measured in the absence of quencher (Q) (Figure 4.2).

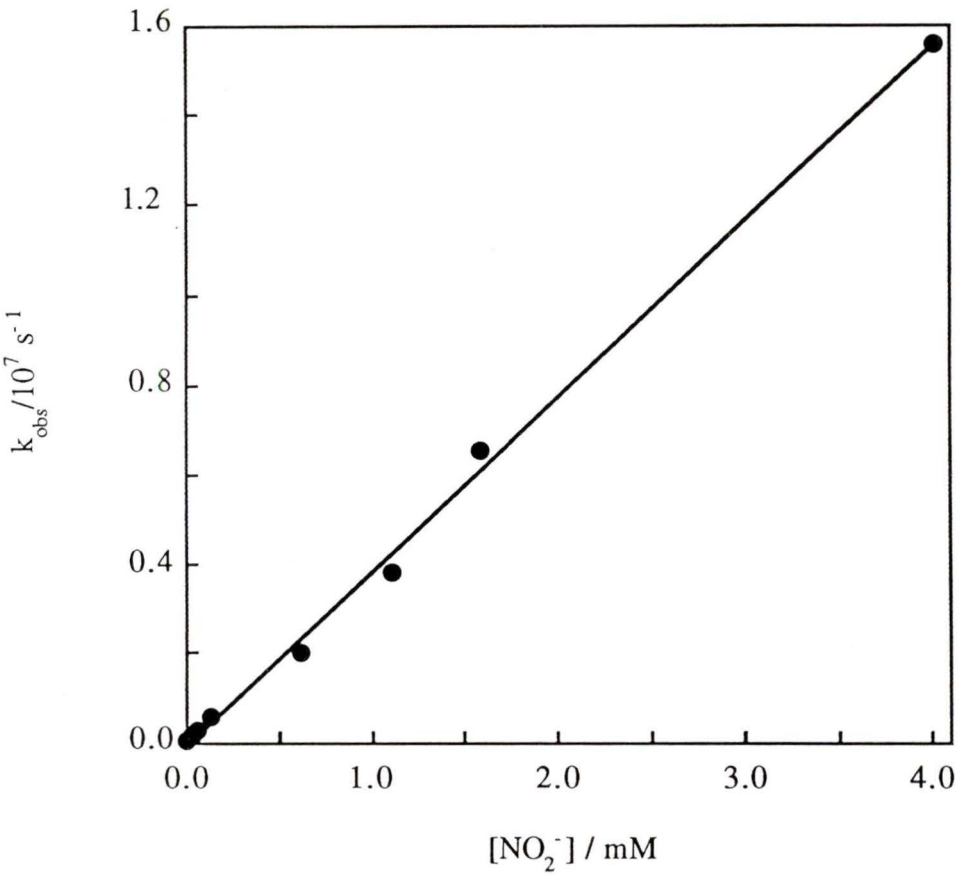

Figure 4.2: Quenching of triplet naphthalene by NO_2^- in aqueous solution. The solid line corresponds to the fitting of the data to Equation 4-1.

The dynamic processes to be considered for naphthalene in bile salt aggregates after excitation are shown in Scheme 4.1. This kinetic scheme has been previously applied to the study of association dynamics of probes in organized systems.[57,67]

$$^3P^* \xrightarrow{k_w} P \qquad (4\text{-}2)$$

$$^3P^* + Q \xrightarrow{k_q} P + Q \qquad (4\text{-}3)$$

$$^3P^* + (BaS)_N \underset{k_-}{\overset{k_+}{\rightleftharpoons}} {}^3P^*\cdot(BaS)_N \qquad (4\text{-}4)$$

$$^3P^*\cdot(BaS)_N \xrightarrow{k_B} P\cdot(BaS)_N \qquad (4\text{-}5)$$

$$^3P^*\cdot(BaS)_N + Q \xrightarrow{k_q'} P\cdot(BaS)_N + Q \qquad (4\text{-}6)$$

Scheme 4.1: Dynamic processes of excited triplet probes in bile salt aggregates in the presence of quencher. $(BaS)_N$ represents bile salt aggregates, and N indicates the aggregation number of the bile salt aggregates. P and Q represent the probe molecule and the quencher, respectively, and k_+ and k_- are the association and dissociation rate constants of excited triplet probe with bile salt aggregates. k_W and k_B are the triplet decay rate constants in the absence of quencher for the triplet probe in aqueous solution and in bile salt aggregates, respectively. k_q and k_q' are the quenching rate constants for the triplet probe in water and in bile salt aggregates, respectively.

Based on Scheme 4.1, the observed decay rate constant k_{obs} is given by Equation 4-7.[57,67]

$$k_{obs} = k_- + k_B + k_q'[Q] - \frac{k_+ k_-[(BaS)_N]}{k_+[(BaS)_N] + k_w + k_q[Q]} \qquad (4\text{-}7)$$

The assumption of this equation is that the probe molecule must be far more soluble in the aggregates than in water so that $[^3P^*(BaS)_N] \gg [^3P^*]$ is true. It furnishes the situation which allows the application of the steady-sate approximation of $^3P^*$.[57]

The values for k_w and k_q in the equation can be determined independently in aqueous solution; k_B is the decay rate constant of the triplet probe in the presence of bile salts and in the absence of the quencher. In Eq 4-7, $[(BaS)_N]$ indicates the concentration of bile salt aggregates. However, the aggregation number of bile salt aggregates cannot be easily defined since bile salt aggregates were shown to be quite polydisperse[29,40] and the number of bile salt molecules necessary to form primary aggregates was dependent on the probe's size[41]. For this reason, $k_+(app)$ will be used to express the association rate constant.

The quenching plots of triplet naphthalene in the presence of the different bile salts are shown in Figure 4.3, Figure 4.4 and Figure 4.5.

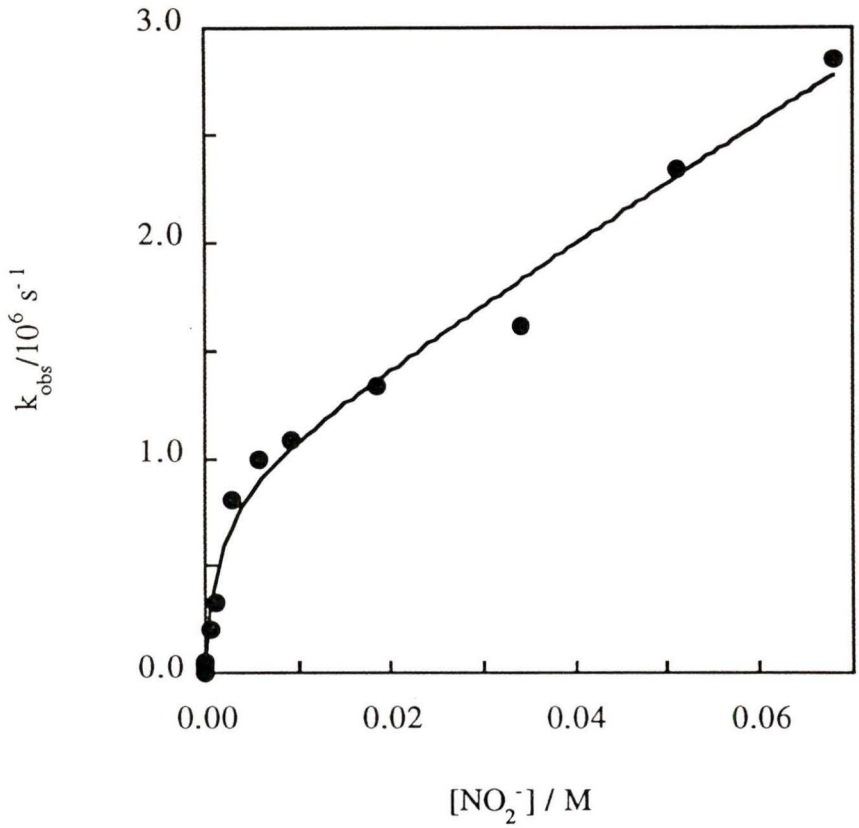

Figure 4.3: Quenching of triplet naphthalene by NO_2^- in 40 mM NaC. The solid line corresponds to the fitting of the data to Eq 4-7 (see text). The values for k_w and k_q were fixed ($k_w = 3.88 \times 10^4\ s^{-1}$, $k_q = 3.8 \times 10^9\ M^{-1}s^{-1}$). The value of k_B ($1.06 \times 10^4\ s^{-1}$) was determined directly from the experiment, when the quencher concentration was zero.

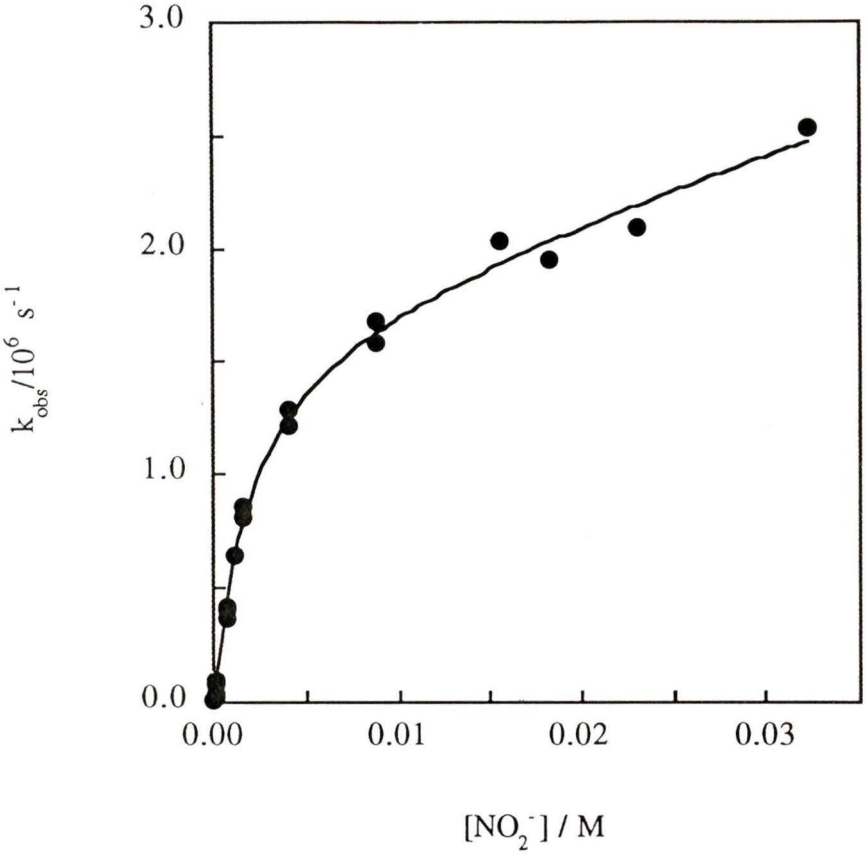

Figure 4.4: Quenching of triplet naphthalene by NO_2^- in 40 mM NaTC. The solid line corresponds to the fitting of the data to Eq 4-7. The values for k_w and k_q were fixed ($k_w = 3.88 \times 10^4\ s^{-1}$, $k_q = 3.8 \times 10^9\ M^{-1}s^{-1}$). The value of k_B ($1.38\times 10^4\ s^{-1}$) was determined directly from the experiment, when the quencher concentration was zero.

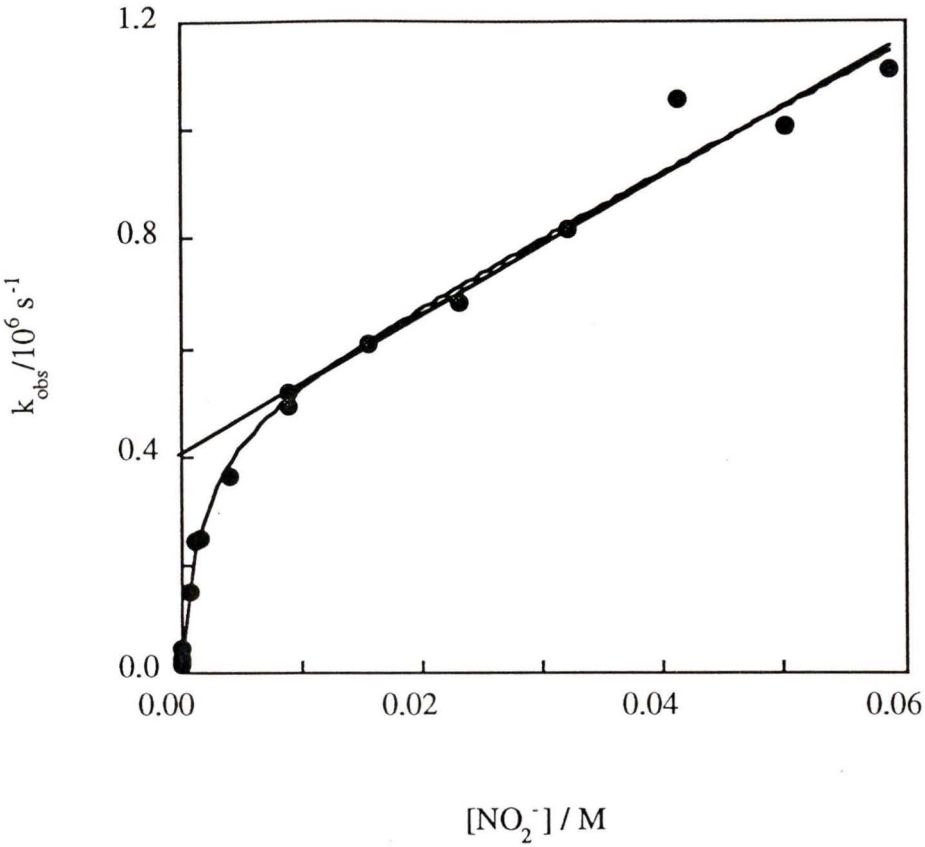

Figure 4.5: Quenching of triplet naphthalene by NO_2^- in 30 mM NaDC. The non-linear solid line corresponds to the fitting of the data to Eq 4-7. The values for k_w and k_q were fixed ($k_w = 3.88 \times 10^4\ s^{-1}$, $k_q = 3.8 \times 10^9\ M^{-1}s^{-1}$). The value of k_B ($1.34\times 10^4\ s^{-1}$) was determined directly from the experiment, when the quencher concentration was zero. The solid straight line corresponds to the fitting to Eq 4-8 (see text in the Discussion).

The quenching plots were curved at high concentrations of NO_2^-, but they did not approach a plateau, which suggested that NO_2^- was able to quench the triplet naphthalene located inside of bile salt aggregates. The data of Figure 4.3, Figure 4.4 and Figure 4.5 were fitted to Eq. 4-7. In Eq 4-7, k_w and k_q were fixed to the values which were determined independently in aqueous solution. k_B was determined two or three times for each experiment and the average was taken. $k_+(app)$, k_- and k_q' were floated and the values were obtained from the fitting. The kinetic parameters and quenching rate

constants of triplet naphthalene in the presence of various concentrations of NaC, NaTC and NaDC are shown in Table 4.1, Table 4.2 and Table 4.3, respectively. It was observed that the NaDC solution was not very stable. It became a gel-like solution after 2 or 3 hours of preparation. The results shown here were obtained from quenching experiments completed shortly after preparation of the sample (less than 2 hours).

Table 4.1: The association ($k_+(app)$) and dissociation (k_-) rate constants of triplet naphthalene in NaC aggregates and the quenching rate constant (k_q') of naphthalene in NaC aggregates quenching by NO_2^-.[a]

[NaC] / mM	$k_+(app)/10^8$ $M^{-1}s^{-1}$	$k_-/10^6$ s^{-1}	$k_q'/10^7$ $M^{-1}s^{-1}$
20.0 ± 0.2	1.5 ± 0.2 (1)	0.99 ± 0.05 (1)	2.5 ± 0.2 (1)
40.0 ± 0.2	1.0 ± 0.8 (3)	1.0 ± 0.4 (3)	2.2 ± 0.4 (3)

[a] [Naphthalene] = $(1.0 \pm 0.1) \times 10^{-4}$ M. The numbers in parentheses show the number of independent experiments. For the experiments performed only once, the errors were calculated from statistical fits of the data to Eq 4-7. For the experiments performed three times, the errors were calculated as standard deviations.

Table 4.2: The association ($k_+(app)$) and dissociation (k_-) rate constants of triplet naphthalene in NaTC aggregates and the quenching rate constant (k_q') of naphthalene in NaTC aggregates quenching by NO_2^-.[a]

[NaTC] / mM	$k_+(app)$ /10^8 $M^{-1}s^{-1}$	k_- /10^6 s^{-1}	k_q' /10^7 $M^{-1}s^{-1}$
20.0 ± 0.2	2.2 ± 0.8 (2)	1.55 ± 0.25 (2)	3.9 ± 1.2 (2)
40.0 ± 0.2	4.5 ± 2.6 (2)	2.22 ± 0.45 (2)	2.85 ± 0.15 (2)

[a] [Naphthalene] = (1.0 ± 0.1) × 10^{-4} M. The numbers in parentheses show the number of independent experiments. The errors were calculated as average deviations.

Table 4.3: The association (k_+(app)) and dissociation (k_-) rate constants of triplet naphthalene in NaDC aggregates and the quenching rate constant (k_q') of naphthalene in NaDC aggregates quenching by NO_2^-.[a]

[NaDC] / mM	k_+(app) /10^8 $M^{-1}s^{-1}$	k_- /10^6 $M^{-1}s^{-1}$	k_q' /10^7 $M^{-1}s^{-1}$
5.0 ± 0.2	6 ± 2 (2)	0.80 ± 0.08 (2)	1.2 ± 0.7 (2)
10.0 ± 0.2	2.7 ± 0.5 (1)	0.53 ± 0.03 (1)	1.8 ± 0.1 (1)
30.0±0.2	2.35±0.25 (2)	0.49±0.03 (2)	1.4±0.2 (2)

[a] [Naphthalene] = (1.0 ± 0.1) × 10^{-4} M. The numbers in parentheses show the number of independent experiments. For the experiments performed only once, the errors were calculated from statistical fits of the data to Eq 4-7. For the experiments performed twice, the errors were calculated as average deviations.

4.2. Interaction of triplet xanthone with bile salt aggregates

Triplet xanthone has been shown to be an ideal probe molecule to establish the complexation dynamics in microheterogeneous systems. The triplet-triplet absorption spectrum of xanthone shows dependence on solvent polarity and its relocation between media with different polarities can be directly followed.[52,53]

4.2.1. Fluorescence spectra of xanthone in NaC aggregates

Although all the experiments were performed with saturated aqueous xanthone solutions, it was observed that when solid xanthone was left in contact with an aqueous NaC solution an increased amount of xanthone (by a factor of 5) could be solubilized. The association of xanthone with NaC was investigated by fluorescence studies. When increasing concentrations of NaC were added to a saturated aqueous xanthone solution, the fluorescence intensity of excited singlet xanthone decreased (Figure 4.6). The fluorescence quantum yield of excited singlet xanthone has been shown to be dependent on the solvent polarity.[52] The decrease in fluorescence intensity of singlet xanthone in NaC aggregates indicated that xanthone was located in a less polar environment of NaC aggregates than in water. The same behavior was observed when the fluorescence of xanthone was studied in sodium taurocholate (NaTC) aggregates.

4.2.2: Triplet-triplet absorption spectrum of xanthone in NaC aggregates

The triplet-triplet absorption spectrum of excited triplet xanthone is known to be dependent on the polarity of the environment where excited triplet xanthone resides.[52,53] The triplet-triplet absorption spectrum of xanthone was taken in the presence of 40 mM NaC using a flow system to prevent deterioration of the sample by laser shots. The absorption due to the solvated electrons was monitored above 650 nm, and the laser power was attenuated until the signal for solvated electrons disappeared. The spectrum of xanthone in NaC aggregates was compared with the triplet-triplet absorption spectrum of xanthone in water (Figure 4.7). It is known that the absorption maximum shifted to longer wavelength when triplet xanthone is located in a non polar environment. For instance, the absorption maximum of triplet xanthone in water was found at 580 nm and it shifted to 602 nm in β-cyclodextrin aqueous solution when xanthone was excited at 355 nm (see Chapter 1)[51,52].

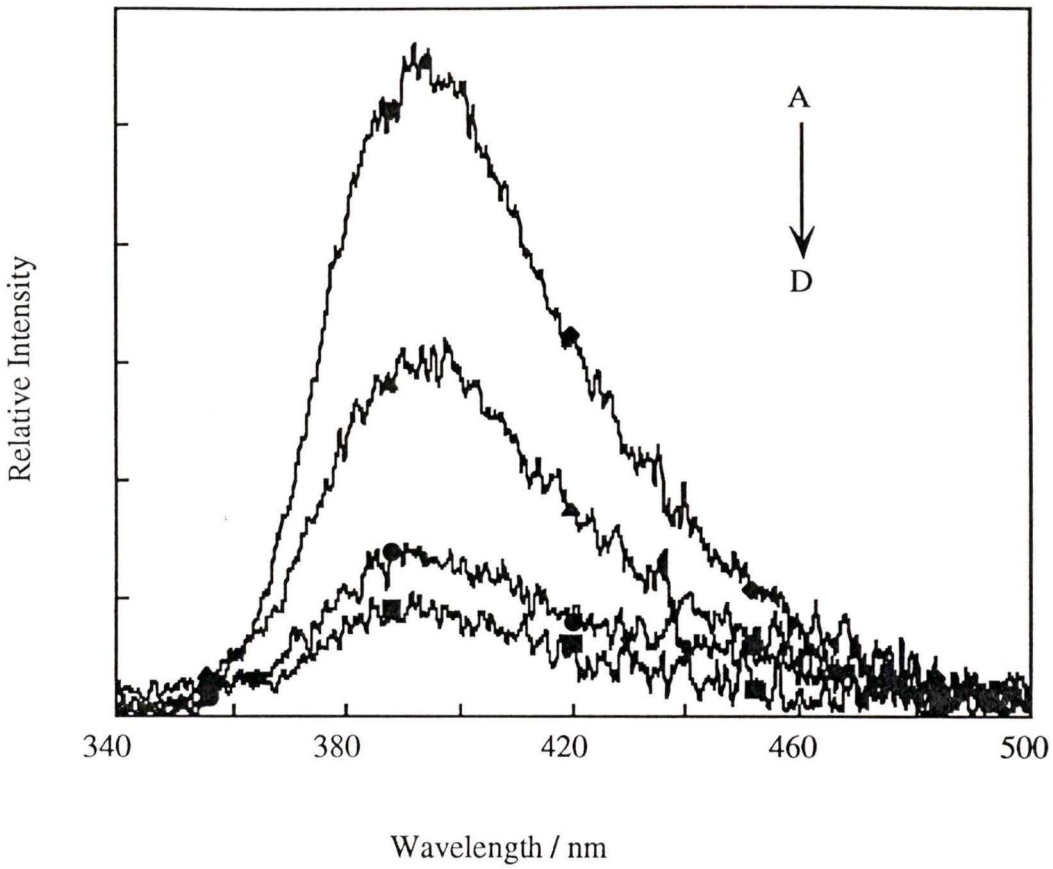

Figure 4.6: Fluorescence spectra of xanthone (λ_{ex} = 320 nm) in the absence of NaC (A) and in the presence of 2 mM (B), 10 mM (C) and 20 mM (D) of NaC.

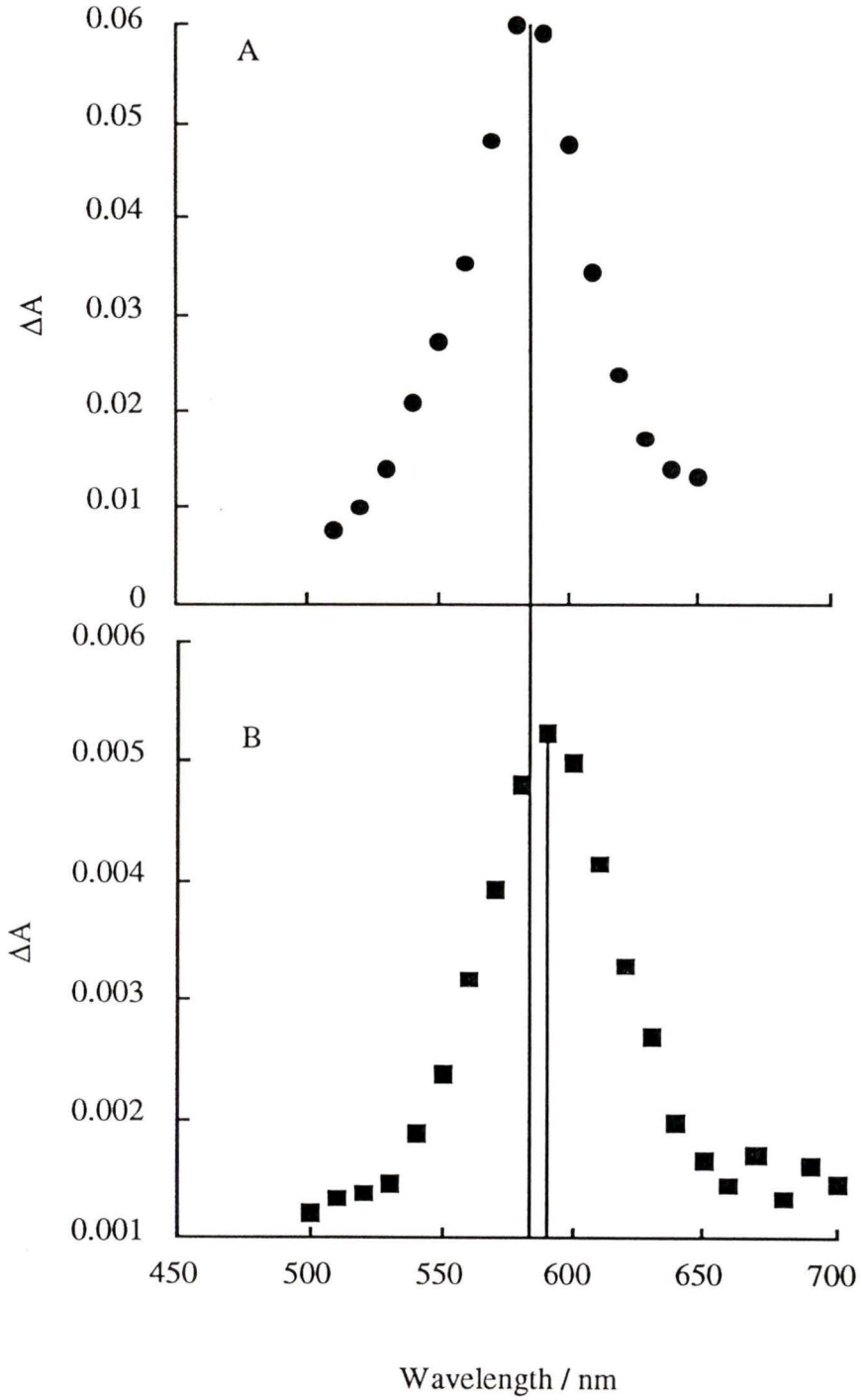

Figure 4.7: Triplet-triplet absorption spectra of triplet xanthone in water (A) and in the presence of 40 mM NaC (B).

The absorption maximum of excited triplet xanthone shifted from 580 nm in water to 590 nm at 40 mM NaC. This red shift was not sufficient to suggest that triplet xanthone was incorporated into the very hydrophobic core of the NaC aggregate as in the case of pyrene and naphthalene. The excited triplet xanthone may reside in the region of hydroxyl groups through hydrogen bonding so that it was more exposed to the aqueous phase. To test this hypothesis, the quenching of triplet xanthone by cupric and nitrite ions was studied.

4.2.3. Quenching of triplet xanthone in NaTC aggregates by cupric ion

Quenching of excited triplet xanthone in bile salt aggregates by cupric ions (Cu^{2+}) was studied in NaTC aggregates instead of NaC aggregates, because NaTC is much less sensitive to precipitation from solutions by divalent cations.[20]

Cupric ion (Cu^{2+}) quenching experiments have been used to establish the dissociation rate constant of excited triplet xanthone from the cyclodextrin cavity (CD).[52,60] It has been previously indicated that Cu^{2+} did not have easy access to molecules inside the CD cavity.[68] Increasing the concentration of Cu^{2+} led to a decrease in the lifetime of triplet xanthone. At sufficiently high concentrations of Cu^{2+}, the quenching plot approached a plateau level and the rate constant measured was equal to the exit rate constant of the excited triplet xanthone from the CD cavity. Further increase of Cu^{2+} concentration did not affect the lifetime of triplet xanthone, since Cu^{2+} was unable to access the interior of the host where the excited probe was located.

In xanthone aqueous solutions, the quenching of triplet xanthone by Cu^{2+} followed a linear relationship (Figure 4.8). The quenching rate constant obtained was $5.7\times 10^{7}\ M^{-1}s^{-1}$, which was consistent with the value obtained in previous work.[60]

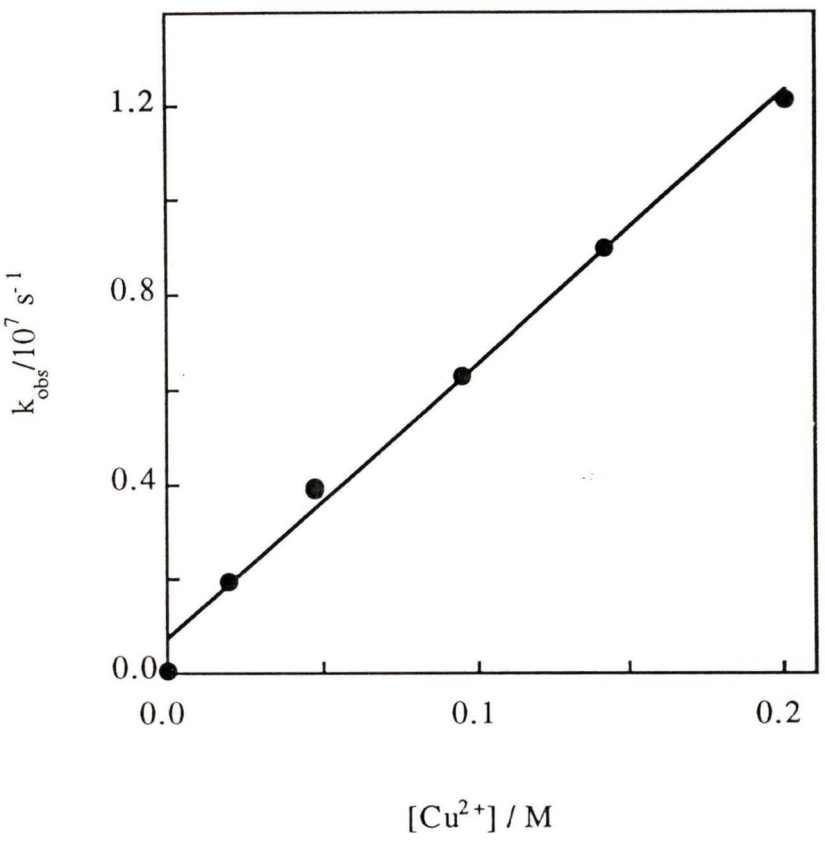

Figure 4.8: Quenching of triplet xanthone by Cu^{2+} in aqueous solution. The solid line corresponds to the fitting of the data to Equation 4-1.

The quenching plot for triplet xanthone in NaTC aggregates in the presence of Cu^{2+} was nonlinear, and it did not approach a plateau at high concentrations of Cu^{2+} (Figure 4.9). This result suggested that Cu^{2+} could quench the triplet xanthone which was incorporated into NaTC aggregates as well as free xanthone in water although the quenching efficiency was different. The mechanism can be described by Scheme 4.1.

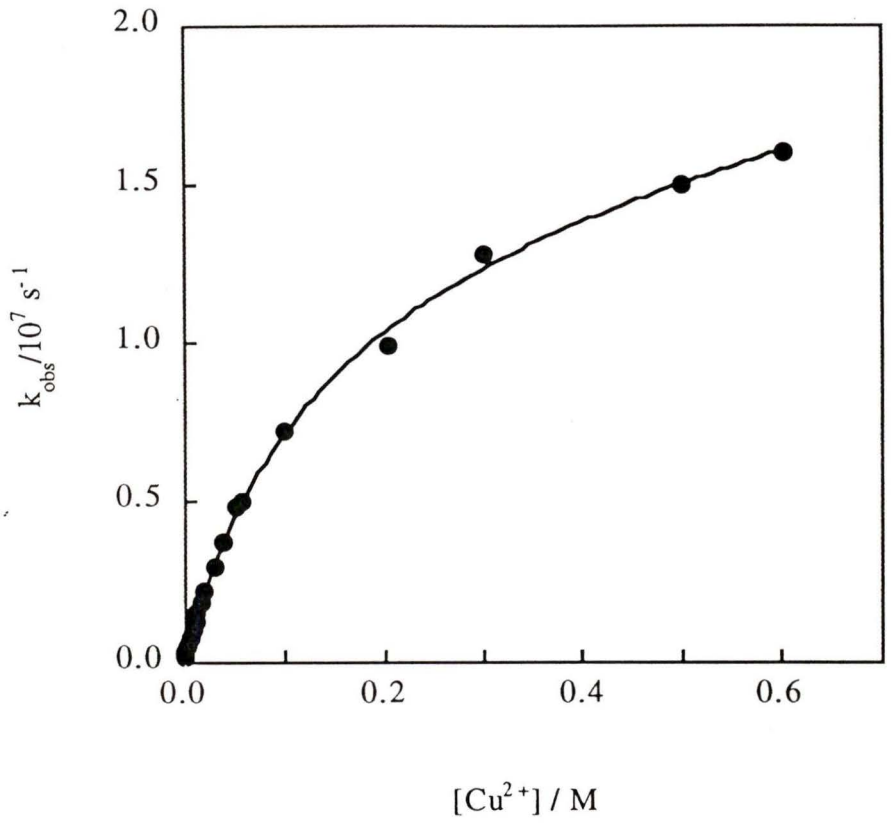

Figure 4.9: Quenching of excited triplet xanthone by Cu^{2+} in the presence of 40 mM NaTC. The solid line corresponds to the fitting of the data to Eq 4-7. The values for k_w and k_q were fixed ($k_w = 5.0 \times 10^4\ s^{-1}$, $k_q = 5.7 \times 10^7\ M^{-1}s^{-1}$). The value of k_B ($1.48 \times 10^5\ s^{-1}$) was determined directly from the experiment when the quencher concentration was zero.

Based on Scheme 4.1, the quenching of triplet xanthone by Cu^{2+} in NaTC aggregates was fitted to Eq 4-7. The results are given in Table 4.4.

Table 4.4: The association (k_+(app)) and dissociation (k_-) rate constants of excited triplet xanthone in 40 mM NaTC and the quenching rate constant (k_q') of xanthone in 40 mM NaTC quenching by Cu^{2+}.[a]

[NaTC] / mM	k_+(app) / 10^8 $M^{-1}s^{-1}$	k_- /10^6 s^{-1}	k_q' /10^7 $M^{-1}s^{-1}$
40.0 ± 0.1	2.5 ± 0.8 (2)	18 ± 3 (2)	0.5 ± 0.1 (2)

[a] [Xanthone] = 2×10^{-5} M. The numbers in parentheses show the number of independent experiments. The errors were calculated as average deviations.

4.2.4. Quenching of excited triplet xanthone in NaC and NaTC aggregates by nitrite ions

Quenching of triplet xanthone by nitrite ions (NO_2^-) was studied in NaC and NaTC aggregates. The NO_2^- ion has a triplet energy of 53 ± 2 kcal/mol,[69] and it efficiently quenched triplet xanthone in water with a rate constant of 5.9×10^9 $M^{-1}s^{-1}$. Again, in the presence of bile salts the quenching plots were curved at high concentrations of NO_2^- but no leveling off was observed (Figure 4.10). The data were fitted to Eq 4-7 and the results are shown in Table 4.5. In this quenching experiment, NO_2^- ion quenched xanthone very efficiently, the triplet lifetime of xanthone decreased rapidly with increasing quencher concentrations. Thus, we were not able to perform measurements at higher concentrations of the quencher. For this reason, the errors for the parameters fitted by Eq 4-7 were large.

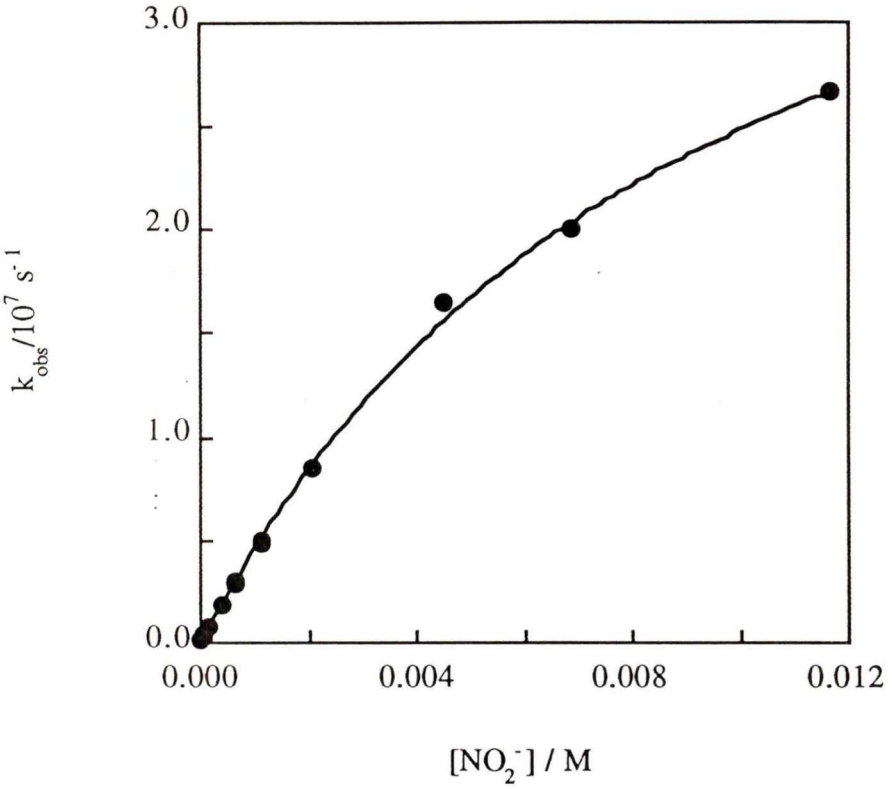

Figure 4.10: Quenching of excited triplet xanthone by NO_2^- in the presence of 40 mM NaTC. The solid line corresponds to the fitting of the data to Eq 4-7. The values for k_w and k_q were fixed ($k_w = 5.0 \times 10^4\ s^{-1}$, $k_q = 5.9 \times 10^9\ M^{-1}s^{-1}$). The value of k_B ($1.33 \times 10^5\ s^{-1}$) was determined directly from the experiment when the quencher concentration was zero.

Table 4.5: The association ($k_+(app)$) and dissociation (k_-) rate constants of triplet xanthone in bile salt aggregates (40 mM NaC and 40 mM NaTC)and the quenching rate constant (k_q') of triplet xanthone in the bile salt aggregates.[a]

	$k_+(app) / 10^8$ $M^{-1}s^{-1}$	$k_- / 10^6$ s^{-1}	$k_q' / 10^7$ $M^{-1}s^{-1}$
NaC	2 ± 2	5 ± 4	120 ± 50
NaTC	8 ± 3	25 ± 8	80 ± 40

[a] [Xanthone] = 2×10^{-5} M. The experiments were performed once, the errors were calculated from statistical fits of the data to Eq 4-7.

4.3. Discussion

Solubilization of organic molecules in micellar media generally leads to a dynamic equilibrium where a solute exchange takes place between micelles and the bulk phase.[58] The dynamics of association and dissociation of probe molecules with surfactant micelles has been widely studied for synthetic detergents, i.e. sodium dodecyl sulfate (NaDS) and cetyltrimethylammonium bromide (CTAB).[56-58] The bile salts, which are generated from cholesterol metabolism in the liver of mammals, can be considered as natural detergents.[15,19] Photophysical investigations in aqueous solutions of bile salts could be considered as a further step in bringing the studies in simple heterogeneous system closer to biological reality. Surprisingly, studies of this kind are very scarce and, to our knowledge, have mostly been limited to the ground and first excited singlet state of hydrophobic chromophores.[23,34,36-38,61]

Dynamics of excited triplet probes in bile salt aggregates have been investigated by a few research groups.[23,70] Rose Bengal was employed as a probe for NaTC aggregates by Seret et al.[70] Triplet and other transients were monitored by flash photolysis. Excited triplet rose bengal was shown to be solubilized both in the aqueous phase and in the NaTC aggregates. A lower limit of the corresponding association and dissociation rate constants k_+ and k_- have been estimated to be $k_+(app) \geq 5 \times 10^6\ M^{-1}s^{-1}$ and $k_- \geq 10^5\ s^{-1}$, respectively. The exit rate of excited triplet anthracene from NaTC aggregates was estimated by Chen et al.[23] The excited triplet anthracene left the aggregates and was destroyed by reaction with another triplet anthracene molecule. This triplet-triplet annihilation can only occur if the triplet anthracene diffuses from the aggregates into the aqueous solution where reaction occurs. At low concentrations of triplets ($\approx 10^{-5}$ M) the rate-determining step was therefore the rate of exit of the triplet anthracene from the aggregates. The exit rate constant was estimated to be $k_- \leq 3 \times 10^3\ s^{-1}$.

This work was undertaken with the aim of determining the dynamics of association and dissociation of excited probe molecules in bile salt aggregates. Triplet naphthalene and xanthone were employed as probe molecules to establish the dynamics of complexation with bile salt aggregates. Our fluorescence studies of excited singlet naphthalene, anthracene and pyrene have shown that the extent of incorporation of these molecules into the bile salt aggregates was different. Naphthalene was observed to be the most protected probe in bile salt aggregates from the quencher in aqueous solution.

To establish the association dynamics of the probe molecule in bile salt aggregates, triplet naphthalene was studied in three kinds of bile salts, NaC, NaTC and NaDC. The triplet-triplet absorption of naphthalene in the presence of 40 mM NaC was compared to that in water (Figure 4.1). A narrowing of the absorption band and a red shift of 4 nm of the absorption maximum was observed. These changes indicated that triplet naphthalene was incorporated into the hydrophobic region of the bile salt

aggregates. This was consistent with our fluorescence results which have shown that naphthalene was incorporated into the very hydrophobic core of the aggregates.

In order to understand the extent of incorporation of triplet naphthalene in bile salt aggregates and to establish the dynamics of the association and dissociation of naphthalene bile salt aggregates, quenching studies by NO_2^- were performed. The dynamic processes of triplet naphthalene can be described by Scheme 4.1 and the quenching plots were fitted to Eq 4-7. At high quencher concentrations, Eq 4-7 can be simplified to:

$$k_{obs} = k_- + k_B + k_q'[Q] \qquad (4\text{-}8)$$

The quenching plots of naphthalene in three kinds of bile salt aggregates were fitted to Eq 4-8 at higher concentrations of NO_2^-. The intercepts corresponds to (k_- + k_B). Since $k_B << k_-$, the contribution of k_B to the intercept is negligible. Within statistical errors, the values of the intercepts were the same as the values of k_- obtained from fitting to Eq 4-7. This treatment of the quenching plots is shown in Figure 4-5 as an example. The intercept by fitting the data at higher quencher concentrations to Eq 4-8 was determined to be $(4.1 \pm 0.4) \times 10^5$ s^{-1}, and the value of k_- obtained from fitting to Eq 4-7 was $(4.6 \pm 0.4) \times 10^5$ s^{-1}. The consistency of the values of k_- obtained by the two different data treatments showed that Eq 4-7 was reliable for fitting the data of quenching experiments.

The results of the quenching studies have shown that the association rate constants (k_+(app)) for the three kinds of bile salt aggregates were similar. The values were ca. 2×10^8 $M^{-1}s^{-1}$. The quenching rate constants of naphthalene incorporated into bile salt aggregates were different for the three kinds of bile salt aggregates by a factor of 1.5-2. The quenching rate constants in bile salt aggregates were at least 100 times smaller than that of naphthalene in water (4×10^9 $M^{-1}s^{-1}$) indicating that naphthalene was very efficiently incorporated into sodium cholate aggregates so that the aqueous

quencher cannot access it easily. Comparing the exit rate constants of naphthalene from the three different bile salt aggregates, this value was smaller for NaDC [$(0.6 \pm 0.1) \times 10^6$ s^{-1}] than for NaC [$(1.0 \pm 0.1) \times 10^6$ s^{-1}] and NaTC [$(1.9 \pm 0.3) \times 10^6$ s^{-1})]. This result suggested a stronger interaction between naphthalene and NaDC aggregates than NaC and NaTC aggregates. From steady-state fluorescence studies, it was observed that NaDC formed aggregates much more readily than the other two bile salts (see Chapter 3).[27] NaDC had a sharp "CMC" value, ca. 3-4 mM of NaDC (Figure 3.17), whereas in the case of NaC and NaTC, the aggregates were formed over a much broader concentration range (Figure 3.3 and Figure 3.18) and the complete aggregation was not observed until a concentration of 20 mM of bile salt. NaDC has two hydroxyl groups when compared to NaC and NaTC which have three hydroxyl groups. The unique structure of NaDC determines its greater hydrophobicity which can be attributed to the stronger interaction between naphthalene and NaDC aggregates.

Triplet xanthone is a popular probe molecule used to establish the complexation dynamics in microheterogeneous systems. The triplet-triplet absorption of xanthone is dependent on the polarity of the environment and the triplet state has a higher dipole moment than the ground state. These properties have been employed to directly study the association dynamics in host-guest complexes.[52-54]

Our fluorescence studies of excited singlet xanthone in NaC aggregates have shown that the fluorescence intensity of xanthone decreased with increasing of NaC aggregates. This result suggested that singlet xanthone was solubilized in a less polar environment than that for the aqueous phase, which in turn implied that xanthone was incorporated into bile salt aggregates. However, the triplet-triplet absorption spectrum of triplet xanthone in NaC aggregates did not show an appreciable red shift when compared to triplet xanthone in aqueous solution (Figure 4.7). This implied that triplet xanthone did not reside in the very hydrophobic core inside of bile salt aggregates. This observation seemed to be contradictory to our fluorescence results which indicated that

triplet xanthone was incorporated into bile salt aggregates. This controversy was suggested to be due to the interaction between triplet xanthone and the hydroxyl groups of the bile salts through hydrogen bonding which made the probe molecule more exposed to the aqueous phase. Our hypothesis was proven to be correct by quenching studies of triplet xanthone in bile salt aggregates using cupric and nitrite ions. For both quenchers similar association ($k_+(app)$) and dissociation (k_-) rate constants ($k_+(app) \approx 3\times 10^8$ $M^{-1}s^{-1}$, $k_- \approx 2\times 10^7$ s^{-1}) of xanthone with NaTC aggregates were obtained (Table 4.4 and Table 4.5). The dynamics of association for xanthone was ca. twice as fast as that for naphthalene, and the dissociation rate constant was ca. 5-10 times larger for xanthone than for naphthalene (Table 4.1, Table 4.2 and Table 4.5). These results indicated that triplet xanthone and naphthalene were located in very different environments of the bile salt aggregates.

Comparing quenching studies of xanthone by Cu^{2+} and NO_2^- (Table 4.4 and Table 4.5), the ratios of the quenching rate constant of xanthone in water and xanthone in bile salt aggregates (i.e. NaTC) were 11.4 and 7.4 for Cu^{2+} quenching and NO_2^- quenching, respectively. The similarity of these values indicated the consistency of the quenching studies by two different quenchers. Comparing the quenching efficiencies of xanthone and naphthalene by NO_2^- (Table 4.1, Table 4.2 and Table 4.5), one notices that the quenching rate constant (k_q') of xanthone in bile salt aggregates was ca. 20 times larger than that for naphthalene. This suggested that the quencher had an easier access to xanthone in bile salt aggregates than for naphthalene.

In summary, the dynamics of association and dissociation of excited triplet naphthalene and xanthone in bile salt aggregates was established. Quenching studies by cupric and nitrite ions were employed to obtain the kinetic parameters ($k_+(app)$ and k_-) and the quenching rate constants of the probes in bile salt aggregates. This is the first time the kinetic parameters of the excited triplet probes are accurately determined in bile salt aggregates. The association and dissociation rate constants of xanthone in bile salt

aggregates were greater than that for naphthalene. It was also observed that excited triplet xanthone was quenched much more efficiently in bile salt aggregates than excited triplet naphthalene.

5. Conclusion

Both steady-state and time-resolved fluorescence quenching of excited singlet naphthalene, anthracene and pyrene in bile salt aggregates were studied. The degree of protection of the three probes from the aqueous quencher was different. Naphthalene was the most protected followed by pyrene and anthracene. At intermediate bile salt concentrations, excited singlet pyrene was observed to form pre-aggregates with bile salt molecules more readily than naphthalene. By comparing steady-state fluorescence quenching and time-resolved quenching studies, we observed the involment of static quenching. These results suggested that the bile salt aggregation is probe dependent. The number of bile salt molecules required to solubilize different probes and the pattern of bile salt aggregation are dependent on the size and the shape of the probe molecule.

The dynamics of association and dissociation of excited triplet naphthalene and xanthone in bile salt aggregates were established. Quenching studies by cupric and nitrite ions were obtained. The association and dissociation rate constants of xanthone in bile salt aggregates were found to be greater than that of naphthalene. It was also observed that excited triplet xanthone was quenched much more efficiently by nitrite ion than naphthalene. This is the first time the kinetic parameters of the excited triplet probes are accurately determined for bile salt aggregates. The dynamic study of excited triplet probes also suggested that different probes are incorporated at different sites in bile salt aggregates.

6. References

(1) Jablonski, A. Z. *Phys.* **1935**, *94*, 38-46.

(2) Gilbert, A.; Baggott, J. *Essentials of Molecular Photochemistry*; CRC Press, Inc.: Boca Raton, 1991.

(3) Lakowicz, J. R. *Topics in Fluorescence Spectroscopy*; Plenum Press: New York, 1991; Vol. 1.

(4) Love, L. C.; Shaver, L. A. *Anal. Chem.* **1976**, *48*, 364A-371A.

(5) Eaton, D. F. *Pure Appl. Chem.* **1991**, *63*, 1631-1648.

(6) Bohne, C.; Redmond, R. W.; Scaiano, J. C. In *Photochemistry in Organized and Constrained Media*; V. Ramamurthy, Ed.; VCH Publishers, Inc.: New York, 1991.

(7) Boens, N. In *In Luminescence Techniques in Chmical and Biochemical Analysis*; W. R. G. Baeyens, D. D. Keukeleire and K. Korkidis, Ed.; Marcel Dekker, Inc.: New York, 1991.

(8) Novak, J. R.; Windsor, M. W. *Proc. R. Soc. London, Ser. A* **1968**, *95*, 308-314.

(9) Turro, N. J. *Pure Appl. Chem.* **1977**, *49*, 405-420.

(10) Lakowicz, J. R. *Principles of Fluorescence Spectroscopy*; Plenum Press: New York, 1983.

(11) Kopecky, J. *Organic Photochemistry*; VCH Publishers, Inc.: New York, 1992.

(12) Balzani, V.; Scandola, F. *Supramolecular Photochemistry*; Ellis Horwood: New York, 1991.

(13) Murphy, C. J.; Arkin, M. R.; Jenkins, Y.; Ghatlia, N. D.; Bossmann, S. H.; Turro, N. J.; Barton, J. K. *Science* **1993**, *262*, 1025-1029.

(14) Fox, M. A.; Jones Jr, W. E.; Watkins, D. M. *C & EN* **1993**, *March 15*, 38-48.

(15) Carey, M. C.; Small, D. M. *Arch. Intern. Med.* **1972**, *130*, 506-527.

(16) Hofmann, A. F.; Mysels, K. J. *Coll. Surf.* **1988**, *30*, 145-173.

(17) Stedronsky, E. R. *Biochim. Biophys. Acta* **1994**, *1210*, 255-287.

(18) Small, D. M. *The Physical Chemistry of the Cholanic Acids*; Plenum Press: New York, 1971; Vol. 1.

(19) O'Connor, C. J.; Wallace, R. G. *Adv. Coll. Inter. Sci.* **1985**, *22*, 1-111.

(20) Hofmann, A. F.; Small, D. M. *Ann. Rev. Med.* **1967**, *18*, 333-376.

(21) Zana, R.; Guveli, D. *J. Phys. Chem.* **1985**, *89*, 1687-1690.

(22) Fisher, L.; Oakenfull, D. *Aust. J. Chem.* **1979**, *32*, 31-39.

(23) Chen, M.; Gratzel, M.; Thomas, J. K. *J. Am. Chem. Soc.* **1975**, *97*, 2052-2057.

(24) Sugihara, G.; Yamakawa, K.; Murata, Y.; Tanaka, M. *J. Phys. Chem.* **1982**, *86*, 2784-2788.

(25) Carey, M. C.; Small, D. M. *Am. J. Med.* **1970**, *49*, 590-608.

(26) Small, D. M.; Penkett, S. A.; Chapman, D. *Biochim. Biophys. Acta* **1969**, *176*, 178-189.

(27) Carey, M. C.; Small, D. M. *J. Colloid Interface Sci.* **1969**, *31*, 382-396.

(28) Roepke, R. R.; Mason, H. L. *J. Biol. Chem.* **1940**, *133*, 103-120.

(29) Muckerjee, P.; Cardinal, J. R. *J. Pharm. Sci.* **1976**, *65*, 882-898.

(30) Carey, M. C.; Montet, J. C.; Phillips, M. C.; Armstrong, J. M.; Mazer, N. A. *Biochemistry* **1981**, *20*, 3647-3664.

(31) Oakenfull, D. G.; Fisher, L. R. *J. Phys. Chem.* **1977**, *81*, 1838-1841.

(32) Kratohvil, J. P.; Hsu, W. P.; Jacobs, M. A.; Aminabhavi, T. M.; Mukunoki, Y. *Coll. Polym. Sci.* **1983**, *261*, 781-785.

(33) Chen, M.; Gratzel, M.; Thomas, J. K. *Chem. Phys. Lett.* **1974**, *24*, 65-68.

(34) Hashimoto, S.; Thomas, J. K. *J. Colloid Interface Sci.* **1984**, *102*, 152-163.

(35) Nithipatikom, K.; McGown, L. B. *Anal. Chem.* **1988**, *60*, 1043-1048.

(36) Nithipatikom, K.; McGown, L. B. *Photochem. Photobio.* **1988**, *47*, 797-802.

(37) Nithipatikom, K.; McGown, L. B. *Anal. Chem.* **1989**, *61*, 1405-1410.

(38) Meyerhoffer, S. M.; McGown, L. B. *J. Am. Chem. Soc.* **1991**, *113*, 2146-2149.

(39) Meyerhoffer, S. M.; McGown, L. B. *Anal. Chem.* **1991**, *63*, 2082-2086.

(40) Li, G.; McGown, L. B. *J. Phys. Chem.* **1993**, *97*, 6745-6752.

(41) Li, G.; McGown, L. B. *J. Phys. Chem.* **1994**, *98*, 13711-13719.

(42) Kalyanasundaram, K. *Photochemistry in Microheterogeneous Systems*; Academic Press, Inc.: New York, 1987.

(43) Grieser, F.; Drummond, C. J. *J. Phys. Chem.* **1988**, *92*, 5580-5591.

(44) Kalyanasundaram, K.; Thomas, J. K. *J. Am. Chem. Soc.* **1977**, *99*, 2039-2044.

(45) Delouis, J. F.; Delaire, J. A.; Ivanoff, N. *Chem. Phys. Lett.* **1979**, *61*, 343-346.

(46) Bright, F. V. *Appl. Spectrosc.* **1988**, *42*, 1531-1537.

(47) Nakajima, A. *Bull. Chem. Soc. Jpn.* **1971**, *44*, 3272-3277.

(48) Dong, D. C.; Winnik, M. A. *Photochem. Photobiol.* **1982**, *35*, 17-21.

(49) Karpovich, D. S.; Blanchard, G. J. *J. Phys. Chem.* **1995**, *99*, 3951-3958.

(50) Murov, S. L.; Carmichael, I.; Hug, G. L. *Handbook of Photochemistry*; Marcel Dekker, Inc.: New York, 1993.

(51) Scaiano, J. C. *J. Am. Chem. Soc.* **1980**, *102*, 7747-7753.

(52) Barra, M.; Bohne, C.; Scaiano, J. C. *J. Am. Chem. Soc.* **1990**, *112*, 8075-8090.

(53) Abuin, E. B.; Scaiano, J. C. *J. Am. Chem. Soc.* **1984**, *106*, 6274-6280.

(54) Liao, Y.; Frank, J.; Holzwarth, J. F.; Bohne, C. *J. Chem. Soc., Chem. Comm.* **1995**, 199-200.

(55) Buckley, J. J.; Wetlaufer, D. B. *J. of Chromatography* **1989**, *464*, 61-71.

(56) Infelta, P. P.; Grätzel, M.; Thomas, J. K. *J. Phys. Chem.* **1974**, *78*, 190-195.

(57) Almgren, M.; Grieser, F.; Thomas, J. K. *J. Am. Chem. Soc.* **1979**, *101*, 279-291.

(58) Thomas, J. K. *Chem. Rev.* **1980**, *80*, 283-299.

(59) Yang, H. M.Sc. Thesis, University of Victoria, 1994.

(60) Liao, Y. M.Sc. Thesis, University of Victoria, 1995.

(61) Meyerhoffer, S. M.; McGown, L. B. *Langmuir* **1990**, *6*, 187-191.

(62) Grätzel, M.; Thomas, J. K. *In Modern Fluorescence Spectroscopy*; Plenum Press: New York, 1976; Vol. 2.

(63) Pearlman, R. S.; Yalkowsky, S. H.; Banerjee, S. *J. Phys. Chem. Ref. Data* **1984**, *13*, 555-562.

(64) Kratohvil, J. P. *Adv. Coll. Inter. Sci.* **1986**, *26*, 131-154.

(65) Kratohvil, J. P.; Hsu, W. P.; Kwok, D. I. *Langmuir* **1986**, *2*, 256-258.

(66) Hoffman, M. Z.; Porter, G. *Proc. R. Soc. London* **1962**, *268*, 46-56.

(67) Turro, N. J.; Bolt, J. D.; Kuroda, Y.; Tabushi, I. *Photochem. Photobiol.* **1982**, *35*, 69-72.

(68) Netto-Ferreira, J. C.; Scaiano, J. C. *J. Photochem. Photobiol. A:Chem.* **1988**, *45*, 109-116.

(69) Treinin, A.; Hayon, E. *J. Am. Chem. Soc.* **1976**, *98*, 3884-3891.

(70) Seret, A.; Van de Vorst, A. *J. Photochem. Photobiol. B:Biol.* **1993**, *17*, 47-56.

VITA

Surname: Ju Given Name: Changqing

Educational Institutions Attended:

University of Victoria	1993 to 1995
Peking University	1987 to 1991

Degree Awarded:

B. Sc.	Peking University	1991

Publication and Presentations:

1. C.Ju and C. Bohne, Characterization of Bile Salt Aggregates Using Excited Singlet and Triplet Probe Molecules (poster), The 78*th* CSC *Conference*, Guelph, Ontario, May, 1995.
2. C. Ju and C. Bohne, Dynamics of Probe Complexation to Bile Salt Aggregation, to be submitted.
3. C. Ju and C. Bohne, Probing Bile Salt Aggregates by Fluorescence Quenching, submitted.

Partial Copyright License

I hereby grant the right to lend my thesis to users of the University of Victoria Library, and make single copies only for such users or in response to a request from the Library of any other university, or similar institution, on its behalf or for one of its users. I further agree that permission for extensive copying of this thesis for scholarly purposes may be granted by me or a member of the University designated by me. It is understood that copying or publication of this thesis for financial gain shall not be allowed without my written permission.

Title of Thesis: Characterization of Bile Salt Aggregates Using Singlet and Triplet Excited Probe Molecules.

Author Changqing Ju

(Signature)

CHANGQING JU

(Name)

Sep. 1st, 95

(Date)